DOT/FAA/AR-08/50

Federal Aviation Administration
William J. Hughes Technical Center
Aviation Research Division
Atlantic City International Airport
New Jersey 08405

Statistical Loads Analysis of BE-1900D in Commuter Operation

February 2017

Final Report

U.S. Department of Transportation
Federal Aviation Administration

NOTICE

This report is available at the Federal Aviation Administration William J. Hughes Technical Center's Full-Text Technical Reports page: actlibrary.tc.faa.gov in Adobe Acrobat portable document format (PDF).

Technical Report Documentation Page

1. Report No.	2. Government Accession No.	3. Recipient's Catalog No.
DOT/FAA/AR-08/50		

4. Title and Subtitle:	1. Report Date
STATISTICAL LOADS ANALYSIS OF BE-1900D IN COMMUTER OPERATION	February 2017
	6. Performing Organization Code: AAR-480

7. Author(s)	8. Performing Organization Report No.
Kamran Rokhsaz[1], Linda K. Kliment[1], Richard B. Bramlette[1], and Thomas DeFiore[2]	

9. Performing Organization Name and Address	10. Work Unit No. (TRAIS)
National Institute for Aviation Research at Wichita State University 1840 Fairmount Street Wichita, KS 67260 Federal Aviation Administration William J. Hughes Technical Center Atlantic City, NJ 08405	11. Contract or Grant No.: 01-C-AW-WISU

12. Sponsoring Agency Name and Address	13. Type of Report and Period Covered
U.S. Department of Transportation FAA Central Regional Office 901 Locust St Kansas City, MO 64106	Final Report
	14. Sponsoring Agency Code: ANM-113

15. Supplementary Notes

The Federal Aviation Administration William J. Hughes Technical Center Aviation Research Division technical monitor for this report was Dr. Sohrob Mottaghi.

16. Abstract

The primary purpose of this research is to support the Federal Aviation Administration's (FAA) Operational Loads Measurement Program by acquiring typical in-service usage data, reduce these data, and develop improved methods and criteria for processing and presenting large amounts of data pertaining to the flight and ground loads usage for these aircraft. The scope of activities includes, but is not limited to: (1) defining the service related factors that affect the operational life of commuter aircraft and (2) reducing, analyzing, and providing processed data in statistical formats that will enable the FAA to reassess continued suitability of existing certification criteria. Equally important, these new data will also enable the FAA, aircraft manufacturers, and airlines to better understand and control those factors that influence the structural integrity of commuter aircraft. One final use will be by designated engineering representatives and original equipment manufacturers, who will be able to utilize the data to compute and recompute their fatigue and damage tolerance analysis of repairs and alterations.

A prior technical report published by the University of Dayton Research Institute (UDRI) contains the results from the processing and analysis of digital flight recorder data obtained from 903 flights. These flights represented approximately 585 flight hours recorded on 28 BE-1900D aircraft during typical operational usage by a single commuter airline. However, the number of flights was deemed insufficient to reliably characterize the usage of the BE-1900D aircraft.

The present document reports on a similar effort undertaken at Wichita State University. This work extends that of UDRI with a much larger number of flights. Flight recorder data from 11,299 flights, recorded on a fleet of six BE-1900D aircraft during typical operational usage by a single commuter airline, were processed. The results are presented here. The data used for the present study contained no information on the propulsion units but included additional parameters that were not available to UDRI. Findings of this report were compared with Title 14 Code of Federal Regulations Part 23 regulations, related advisory circulars, and usage of other civil transports, if applicable.

17. Key Words:	18. Distribution Statement
Flight profiles, Flight loads, Ground loads, Statistical loads data	This document is available to the public through the National Technical Information Service (NTIS), Springfield, Virginia 22161. This document is also available from the Federal Aviation Administration William J. Hughes Technical Center at actlibrary.tc.faa.gov.

19. Security Classif. (of this report)	20. Security Classif. (of this page)	21. No. of Pages	22. Price
Unclassified	Unclassified	117	

ACKNOWLEDGEMENTS

The work reported in this document was performed by the Flight Dynamics Laboratory of the College of Engineering, in association with the National Institute for Aviation Research at Wichita State University (WSU). This effort was funded by the Federal Aviation Administration (FAA) through its Airworthiness Assurance Center of Excellence.

The principal investigators at WSU were Dr. Kamran Rokhsaz and Linda K. Kliment of the Department of Aerospace Engineering. Richard B. Bramlette, at the time a graduate student at WSU, developed the data reduction algorithms and software and established the data reduction criteria, and Ravi Shankar Vatsavai, another WSU graduate student at the time, performed the data processing. The format used for the presentation of the statistical data was adopted from previous work conducted by the University of Dayton Research Institute. The program manager for the FAA was Thomas DeFiore of the FAA William J. Hughes Technical Center in Atlantic City, New Jersey.

TABLE OF CONTENTS

LIST OF FIGURES

LIST OF TABLES

LIST OF ABBREVIATIONS AND ACRONYMS

g	Gravity constant, 32.17 ft/sec^2
nmi	Nautical mile
AGL	Above ground level
CFR	Code of Federal Regulations
DFDR	Digital flight data recorders
FAA	Federal Aviation Administration
GPS	Global positioning system
KIAS	Knots-indicated air speed
MSL	Mean sea level
UDRI	University of Dayton Research Institute
WSU	Wichita State University

EXECUTIVE SUMMARY

The Federal Aviation Administration William J. Hughes Technical Center funded Wichita State University (WSU) to conduct a survey of the operational loads experienced by a fleet of commuter aircraft. The program involved the creation of a database from, and analysis of, actual operational flight and ground loads data collected from digital flight data recorders installed on a fleet of six BE-1900D aircraft operated by a single commuter airline. The analysis pertained to separation of the loads for different phases of flight and ground operations and a statistical presentation of the results in a final report. The operator collected the data on site from the BE-1900D aircraft and provided WSU with disks containing data on 15 parameters, 12 of which were reliably usable. WSU processed and analyzed the data, and the results are presented in this report.

Presented here are analyses and statistical summaries of data collected from 11,299 flight operations recorded on 6 BE-1900D aircraft during routine commuter service over a period of 3 years. Basic flight parameters (e.g., airspeed, altitude, flight duration, bank and pitch angles, and flap usage) are shown in a form that allows easy comparison with the manufacturer's design criteria. Vertical and horizontal ground loads are presented for ground operations. Maneuver and gust loads are presented for different flight phases and altitude bands. In addition, derived gust velocities, V-n diagrams, and various coincident flight events are shown and compared with published operational limits.

The statistical formats used here were developed by the University of Dayton Research Institute. The data presented in this form should allow an objective comparison of the existing certification and design criteria with actual usage data, thereby affording the aircraft manufacturer and operators a better understanding and better control of those factors that influence the structural integrity of commuter aircraft. These data could also be used by manufacturers, modifiers, and designated engineering representatives for repairs and alterations.

1. INTRODUCTION

The Federal Aviation Administration (FAA) funded the National Institute for Aviation Research at Wichita State University (WSU) to conduct a comprehensive operational loads analysis, the scope of which was to collect, process, and perform statistical evaluations of the flight and ground loads collected from a fleet of BE-1900D aircraft in commuter service. The objectives of this program were to acquire, evaluate, and utilize typical operational in-service data: 1) for comparison with the data used in the design and qualification testing of civil transport aircraft, and 2) to provide a basis to improve the structural criteria and methods of design, evaluation, and substantiation of future airplanes.

Operational data were collected from digital flight data recorders (DFDR) installed on a fleet of six BE-1900D commuter aircraft. WSU received the data via data cards from the operator for the purpose of extracting, editing, organizing, reducing and processing, and analyzing this final report. The resulting aircraft usage data and statistical flight and ground loads are presented here in formats that were developed by the University of Dayton Research Institute (UDRI). This report includes aircraft usage and statistical loads derived from recorded data obtained over the course of approximately 3 years. The data consisted of 11,299 flight files from a single operator. A summary of these flight files is shown in tables 1 and 2.

Table 1. Flight data files used for this report

Tail Number	Good Data	Bad Data
N85C1CA	82	0
N840CA	567	1770
N842CA	2251	1
N854CA	2893	0
N855CA	560	0
N857CA	3175	0
Totals for 6 Aircraft	9528	1771

Basic statistical information on a variety of design-related parameters is shown in formats that can be easily compared with the manufacturer's existing design criteria. Information on loads includes maneuver and gust accelerations for different altitude bands, derived gust velocities, and longitudinal, lateral, and vertical loads during ground operations. Aircraft usage data include various airspeeds and coincident altitudes, flight duration and distance, maximum bank and pitch angles, and flap usage during various phases of flight.

The statistical formats used here are those developed by UDRI. The data presented in this form should allow an objective comparison of the existing certification and design criteria with actual usage data, thereby affording aircraft manufacturer and operators a better understanding and better control of those factors that influence the structural integrity of commuter aircraft.

Table 2. Complete and incomplete flights

Bad Data	
Number of Files	1,770
Total Flights (Complete and Incomplete)	1,799
Complete Flights	1,644
Total Number of Hours*	1,321
Total Number of Nautical Miles*	300,704
Good Data	
Number of Files	9,529
Total Flights (Complete and Incomplete)	9,849
Complete Flights	9,356
Total Number of Hours*	6,958
Total Number of Nautical Miles*	1,582,690

*Note: For complete flights only.

2. AIRCRAFT DESCRIPTON

Some of the operational characteristics of the BE-1900D aircraft equipped with DFDR are shown in table 3. The three-view drawing of the aircraft is also shown in figure 1. The information in table 3 and figure 1 was reproduced from [1].

Table 3. BE-1900D aircraft characteristics

Parameter	Value
Maximum Taxi Weight	17,060 lb
Maximum Takeoff Weight	16,950 lb
Maximum Landing Weight	16,600 lb
Zero-Fuel Weight	15,000 lb
Operating Empty Weight*	10,350 lb*
Fuel Capacity	668 U.S. gallons
Two P&W PT6A-76D Turboprops	1,279 shp** each
Wing Span	57 ft 11.25 in
Wing Reference Area	310 ft^2
Wing MAC	5.32 ft
Length	57 ft 10 in
Height	15 ft 6 in
Tread	17 ft 2 in
Wheel Base	23 ft 9.5 in

* Operating Empty Weight is not a [1] value but was provided by the airline.
** shp = shaft horsepower.

3. AIRLINE DATA COLLECTION AND EDITING SYSTEM

3.1 FLIGHT DATA

The airline data collection and editing system consisted of two major components: (1) the data collection system installed on board the aircraft and (2) the ground data editing station. The airline performed the collection and pre-processing of the BE-1900D recorded data and then provided these data to WSU on disks. The data were extracted at WSU and recorded in the database in the form of text files. The parameters provided to WSU are listed in table 4.

3.2 RECORDED DATA

All the parameters listed in table 4, with the exception of the output of the gyros, were used. These parameters were not always recorded correctly and mostly showed a value of -90. Also, in most cases, the first few lines of data showed unreasonable fluctuations in some of the recorded parameters. Therefore, the first 20 lines (20 seconds) of each data file were ignored in subsequent calculations.

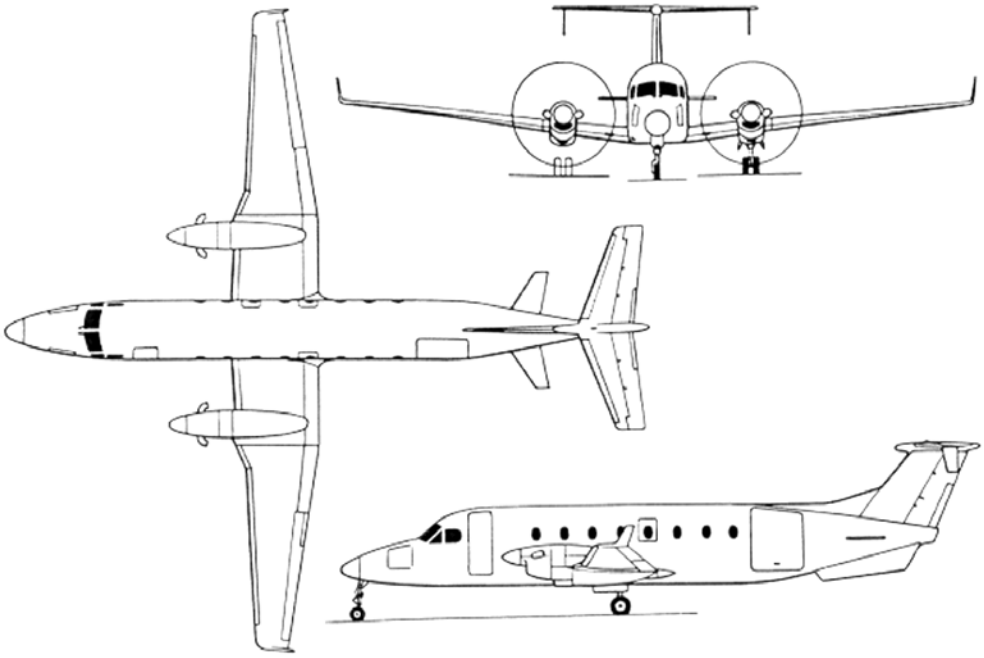

Figure 1. BE-1900D three-view drawing

Table 4. Recorded flight loads parameters

Parameter (Units)	Sample Rate	Resolution
Vertical Acceleration (g)	8 Hz	0.00247
Longitudinal Acceleration (g)	4 Hz	0.00054
Lateral Acceleration (g)	4 Hz	0.00054
Flap Position (discrete)	1 Hz	Up/Approach/Down
Heading (deg)	1 Hz	0.088 deg
Pitch Angle (deg)	1 Hz	1.5 deg
Roll Angle (deg)	1 Hz	1.5 deg
Indicated Airspeed (knots)	1 Hz	0.56 KIAS (approx.)
Altitude (ft)	1 Hz	31.62 ft
GPS - Lat. & Long. (degrees & minutes)	1 Hz	0.01 minute
Gyros (deg/sec)	1 Hz	Unknown
Weight on Wheel (discrete)	1 Hz	OnGround/InAir

KIAS = knots-indicated air speed

4. WSU DATA PROCESSING

4.1 FILTERING AND NORMALIZING

The resolution in the recorded altitude made it impossible to calculate a reliable rate of climb. The latter parameter was needed in separation of flight phases. Therefore, the recorded altitude was filtered using a 10-second running average.

All accelerometer output values were normalized relative to the 20-second average of their data while the aircraft was on the ground. This required using the average acceleration output of t = 21–40 seconds.

4.2 DERIVED AND EXTRACTED PARAMETERS

Some information, such as rate of climb, was not recorded and, therefore, had to be extracted or derived from the time history of other parameters. In those cases for which aircraft parameters had to be derived (e.g., aircraft lift-curve slope), for consistency, the values used were those of [1]. In addition, because the recorded data contained no information about the aircraft's inertial properties, a weight of 16,500 pounds was used throughout wherever this parameter was required. Issues pertaining to specific calculations and the derivations of the required parameters are described in the following subsections.

4.2.1 Identification of Liftoff and Touchdown

For the analysis in [1], the authors determined the approximate time of liftoff and touchdown from changes in pitch angle and accelerations. The exact points of liftoff and touchdown were then identified manually by inspection of the data in the vicinity of the approximate point.

In the present case, squat switch information was available but proved not to correlate with liftoff and touchdown. Manual inspection of several files showed that the exact liftoff would occur anywhere from 0–8 seconds after the squat switch indicated the event. Also, the liftoff was not always accompanied with a change in the pitch angle. Likewise, the touchdown point could not be correlated with the squat switch indication. Finally, because of the large volume of data, manual identification was not feasible.

It was reasoned that the liftoff point should be the only instance for which a positive change in the pitch angle would coincide with a positive change in the longitudinal acceleration because of the loss of ground friction. Likewise, the touchdown point should be the only instance for which a reduction in the pitch angle would coincide with a negative change in the longitudinal acceleration. Therefore, an algorithm was developed to implement this logic and search the occurrences of these conditions over a specified length of time surrounding the squat switch indications. However, the results were still not acceptable in that the code predicted higher touchdown speeds than liftoff speeds. The primary cause was identified as the low resolution of the pitch data compared to that of the longitudinal acceleration.

4.2.2 Flight Distance

Flight distance was calculated by: 1) integration of the true airspeed, 2) integration of the global positioning system (GPS) data, and 3) direct distance between the departure and arrival airports.

4.2.2.1 Integration of Airspeed

Flight distance from integration of the true airspeed was determined from:

$$D = \sum_{t_{liftoff}}^{t_{touchdown}} V_T(\Delta t) \tag{1}$$

Again, in the absence of additional information, the indicated airspeed was assumed to be the same as calibrated airspeed. Also, because the airspeeds were not large enough to require inclusion of compressibility effects, true airspeed was derived from the indicated airspeed using the ratio of air densities; that is:

$$V_T = V_C \sqrt{\frac{\rho_0}{\rho}} \approx V_i \sqrt{\frac{\rho_0}{\rho}} \tag{2}$$

In the absence of pressure and temperature recordings, local air density was derived from the pressure altitude, assuming standard atmosphere. Therefore, local density was derived from:

$$\rho = \rho_0 \left(1 - 6.876 \times 10^{-6} \times H_p\right)^{4.256} \tag{3}$$

where ρ_0 = 0.0023769 slug/ft^3 is air density at sea level and H_p is pressure altitude (ft), which is a recorded parameter.

4.2.2.2 Integration of GPS Coordinates

GPS locations were recorded in the form of degrees and minutes, with the latter given to two decimal places. This resolution of the angles corresponded to a 60-foot resolution in position. The method outlined in appendix B of [2] was used to convert the GPS data into distances. To minimize the effect of possible accumulation of error, the GPS-derived change in the position was calculated every 2 minutes. Summation of these displacements resulted in the GPS-integrated distances.

4.2.2.3 Direct Distance

A database of airport identifiers and their coordinates was obtained from [3]. Each airport's latitude and longitude were given in degrees, with eight significant figures. The GPS coordinates of the aircraft before takeoff and after landing were compared with these data to determine the most likely departure and arrival airports. This information was also used to find the direct distance between the two airports.

4.2.3 Flight Duration

The flight duration is defined as the time from aircraft liftoff to touchdown.

4.2.4 Design Load Factor Definition

Load factors were divided into gust and maneuver based on their durations in accordance with [4]. Load factors lasting 2 seconds or longer were considered to be due to maneuvers, whereas the rest were placed in the category of gust.

Originally, the gust maneuver load spectra were specified in AFS-120-73-2 [5]. However, this report was superseded by AC23-13A [6]. The load spectra in this report are expressed in terms of a load factor ratio of A_N/A_{NLLF}. AFS-120-73-2 defines this ratio as the incremental load factor at operating weight divided by the incremental design limit load factor at maximum gross weight. The design limit load factor for both gust and maneuver were those estimated in [1]. These limit load factors do not necessarily reflect the true design values.

For the gust spectra comparison, the incremental gust design limit load factor is specified in AC23-13A as follows:

$$A_{NLLF} = \frac{30KVm}{498W/S} \tag{4}$$

$$K = \begin{cases} \frac{1}{2}\left(\frac{W}{S}\right)^{1/4} & \text{for } W/S < 16 \text{ psf} \\ 1.33 - \frac{2.67}{\left(W/S\right)^{3/4}} & \text{for } W/S > 16 \text{ psf} \end{cases} \tag{5}$$

V = airplane design cruising speed, V_c (knots)
m = aircraft lift-curve slope, C_{L_α} (per radian)
W/S = wing loading at maximum gross weight (psf)

AC23-13A does not specify the method for determining the incremental maneuver design limit load factor. Therefore, this load factor was calculated in accordance with the approach specified in Title 14 Code of Federal Regulations (CFR) Part 23.337 using the takeoff gross weight of 16,500 lb.

For the positive incremental load factor:

$$A_{NLLF} = 2.1 + \left[24{,}000/\left(W + 10{,}000\right)\right] - 1 \tag{6}$$

For the negative incremental load factor:

$$A_{NLLF} = -0.4\left\{2.1 + \left[24{,}000/\left(W + 10{,}000\right)\right]\right\} - 1 \tag{7}$$

4.2.5 Derived Gust Velocity

Derived gust velocities were calculated from measured normal accelerations, only for vertical gusts. For these calculations, air density was estimated from equation 3. Equivalent airspeed was determined from:

$$V_e = V_T\sqrt{\frac{\rho}{\rho_0}} \tag{8}$$

Earlier, it was explained that because of a lack of additional information, calibrated airspeed was assumed to be the same as indicated airspeed. Therefore, equivalent airspeed was also assumed to have the same values as indicated airspeed.

With this information, derived gust velocity was computed from the values of gust incremental normal acceleration as:

$$U_{de} = \frac{\Delta n_z}{\overline{C}} \tag{9}$$

where the aircraft response factor, $\overline{C}$, was calculated from:

$$\overline{C} = \frac{\rho_0 V_e C_{L_\alpha} S}{2W} K_g \tag{10}$$

ρ_0 = 0.002377 slug/ft^3, standard sea level air density
V_e = equivalent airspeed (ft/s)
C_{L_α} = aircraft lift-curve slope (per radian)
S = wing reference area (ft^2)
W = 16,500 lb, gross weight
K_g = $\frac{0.88\mu}{5.3+\mu}$, gust alleviation factor
μ = $\frac{2W}{\rho g \bar{c} C_{L_\alpha} S}$, reduced mass
ρ = air density at altitude from equation 3
g = 32.17 ft/s^2, acceleration of gravity
$\bar{c}$ = wing mean geometric chord (ft)

Following the procedure used in [1], the aircraft lift-curve slope, C_{L_α}, was determined from wing lift-curve slope, C_{l_α}, given by:

$$C_{L_\alpha} = \frac{2\pi A_r}{2 + \left[4 + A_r^2 \beta^2 \left(1 + \frac{\tan^2 \Lambda}{\beta^2} \right) \right]} \tag{11}$$

A_r = b^2 / S, wing aspect ratio
b = wing span (ft)
β = $\sqrt{1-M^2}$, compressibility effect
C_{l_α} = wing lift-curve slope (per radian)
Λ = wing quarter-chord sweep angle
M = V_T / a, flight Mach number
a = $a_0 \sqrt{\left(1 - 6.876 \times 10^{-6} H_p\right)}$, local speed of sound (ft/s)
a_0 = 1116.4 ft/s, speed of sound at sea level

4.3 DATA MANAGEMENT

All incoming data were initially screened for obvious anomalies, such as missing or incomplete data fields and accelerometer readings that did not appear to be correct. These files were placed in folders named BAD DATA. The rest of the files were placed in another folder named GOOD DATA. Within each folder, a subfolder was established for each tail number. These folders contained subfolders named according to the date when the card was removed from the flight data recorder. Each of these subfolders contained data from different flights, numbered sequentially. In all, a total of 1771 flight files were placed in the BAD DATA folders, whereas the GOOD DATA folder contained 9528 flight files, as shown in table 1.

Most of the files identified as BAD DATA had incorrect accelerometer data but still contained useful information about aircraft usage and, therefore, were used for this purpose. Also, some of the files placed in the GOOD DATA category contained incomplete flights. In addition, one aircraft had an unreliable flap signal switch. Therefore, some of the flight phases could not be identified for it. Nonetheless, some flight phases could be extracted from these files and used for statistical analysis.

Because of the above issues, not all flight data files were used in assembling the statistical information for every phase of flight. Therefore, in all of the subsequent plots, the number of data files used for extracting the information is indicated in the figure.

4.4 DATA REDUCTION CRITERIA

4.4.1 Phases of Flight

Each flight was divided into 12 phases, although not all were used in the subsequent analysis. These phases consisted of:

- Ground operations:
  - Taxi out
  - Takeoff roll
  - Landing roll
  - Runway turnoff
  - Taxi in
- Airborne phases:
  - Takeoff rotation (not used)
  - Departure (initial climb with flaps deflected)
  - Climb (flaps retracted)
  - Cruise
  - Descent (flaps retracted)
  - Initial approach (flaps in the first detent)
  - Final approach (flaps in the second detent)

These phases are shown schematically in figure 2. For comparison, a typical flight time history is presented in figure 3.

Conditions for determining the starting times for each phase are listed in table 5. It should be noted that an airborne phase can occur several times per flight because it is determined by the rate of climb and the position of the flaps.

4.4.1.1 Ground Phases

Specific data reduction criteria were developed and used to identify the beginning and end of each ground phase of operation (taxi-out, takeoff roll, landing roll, runway turnoff, and taxi-in).

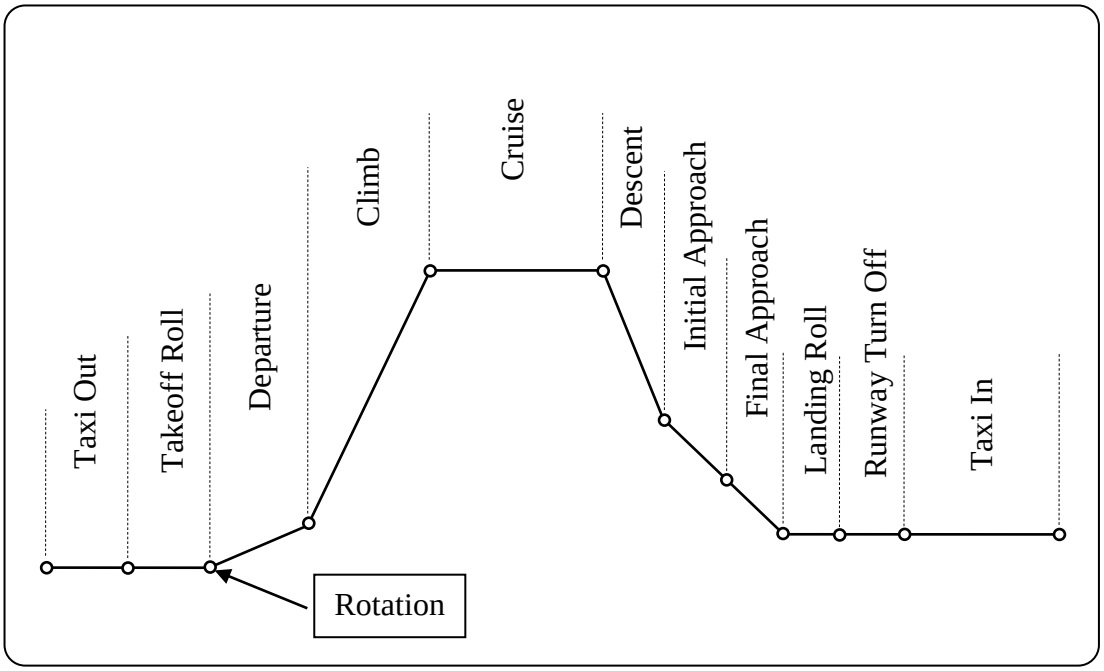

Figure 2. Schematic of various flight phases

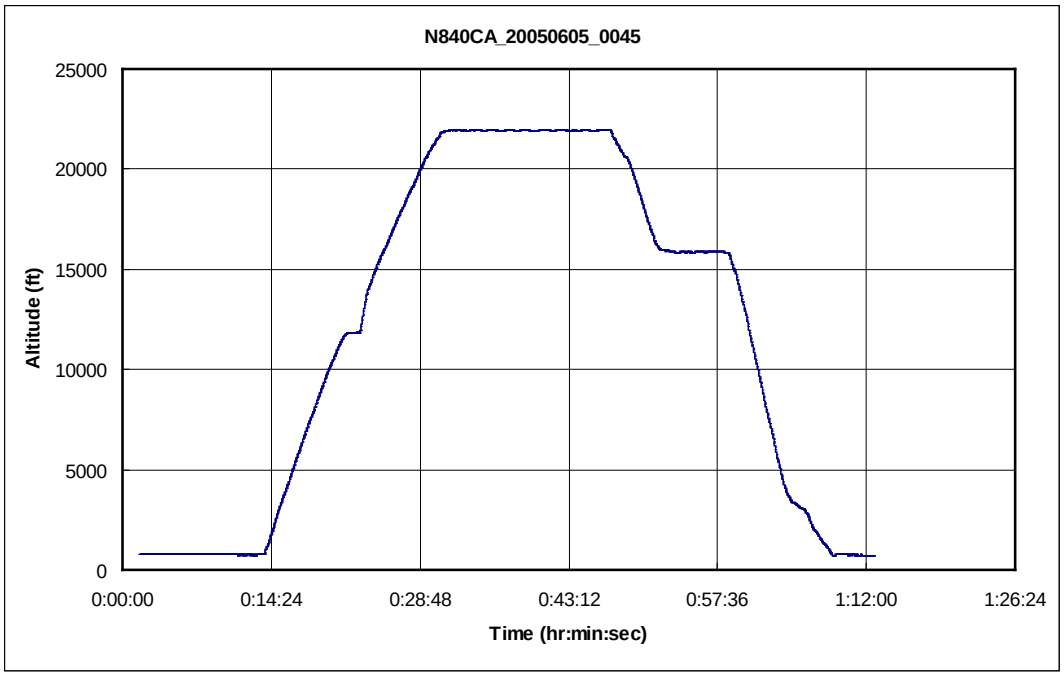

Figure 3. Typical flight time history

The taxi-out phase was assumed to begin when the aircraft heading changed by more than 20° in 5 seconds. All aircraft movements until the aircraft began its takeoff roll were defined as taxi-out.

Table 5. Criteria for separating flight phases

Flight Phase	START Time (t_1) Identification	STOP Time (t_2) Identification
Taxi-Out	Heading(I+5) - Heading(I) > 20 deg. (dHDG(I) < 270 deg.; On ground)	(t_1 of Roll) minus 5 sec.
Roll	ACCELX > 0.15g (On Ground, Airspeed is increasing)	dPITCH(I) > 3 deg.
Rotation	t_2 of Roll	PITCH(I) > 15 deg OR PITCH - PITCH_ref > 10 deg
Departure	t_2 of Rotation	Flaps are up
Climb	RC > 750 fpm for 20 sec. AND Flaps are up (Not on ground)	RC < 750 fpm for 20 sec. (Not on ground; flaps up)
Cruise	|RC| < 200 fpm for 20 sec. (Not on ground; flaps up)	|Δh| > 250 ft (from avg of ISTARTCRUISE+20 sec.) (Not on ground; flaps up)
Descent	RC < -750 fpm for 20 sec. (Not on ground; flaps are up)	Flaps are In Transit or set to Approach (Not on ground) OR RC > -750 fpm for 20 sec. (Not on ground)
Initial Approach	Flaps are appr. AND RC < 0 fpm for 10 sec. (Not on ground and negative RC)	Flaps are down (Not on ground)
Final Approach	t_2 of Initial Appr.	(OnGround) minus 3 sec.
Landing Roll	t_2 of Final Appr.	ΔHDG (from t_1) > 13.5
Runway Turnoff	t_2 of Landing Roll	dHDG < 2 deg for 5 sec.
Taxi-In	t_2 of Runway Turnoff	GPS shows no change for 30 sec. (GPS is nonzero) or End of File

The beginning of the takeoff roll was found by searching for longitudinal acceleration exceeding 0.15 g while on ground. Takeoff roll was assumed to end when the aircraft pitch angle changed more than 3° from its average while on the ground.

The landing roll phase was defined as beginning 3 seconds before the squat switch signaled that the landing touchdown had occurred and ending when the aircraft heading angle deviated more than 13.5° from that of the runway.

The start of the turnoff was set to be the end of the landing roll. Turnoff was assumed to be complete if the aircraft heading did not change more than 2° over 5 seconds.

Taxi-in was set to start at the point where the aircraft completed its turnoff from the active runway after its landing roll to the point at which the aircraft was either parked at the gate or the recorder had shut down. In cases for which the files contained more than one flight, the end of the first taxi-in and the start of the second taxi-out were separated using the GPS coordinates. If the aircraft GPS coordinates did not change for 30 seconds, the taxi-in phase was assumed to be complete.

4.4.1.2 Airborne Phases

The airborne portion of each flight profile was separated into phases called rotation, departure, climb, cruise, descent, initial approach, and final approach. The criteria for the start and end of each of the phases are shown in table 5. Phases that lasted less than 1 minute were eliminated from the analysis. Also, it should be noted that an airborne phase could occur several times per flight (e.g., cruise at multiple altitudes). When this occurred, each leg was treated separately.

4.4.2 Computer Programs

In all, nine FORTRAN codes were developed to separate the flight phases and analyze the flight data. These were:

1. Depart.FOR–To identify and analyze the loads for taxi out, takeoff roll, rotation, and departure
2. Climb.FOR–To identify and analyze the climb loads
3. ClimbGust.FOR–To identify and analyze the climb-derived gust velocities
4. Cruise.FOR–To identify and analyze cruise loads
5. CruiseGust.FOR–To identify and analyze cruise-derived gust velocities
6. Descent.FOR–To identify and analyze the descent loads
7. DescentGust.FOR–To identify and analyze the descent-derived gust velocities
8. Approach.FOR–To identify and analyze the loads for initial approach, final approach, landing roll, runway turnoff, and taxi in
9. Overall.FOR–To examine aircraft and systems usage data

In addition, a number of codes were developed in C# that would facilitate the process of running all of the flight files through these codes. The latter codes developed master files containing the results of the processing of the data for each flight phase. The information in master files was used in turn to create the statistical results presented in this report.

4.4.3 Sign Convention

Acceleration data were recorded in three directions: normal (z), longitudinal (x), and lateral (y). As shown in figure 4, the positive z direction is up, and the positive x direction is forward.

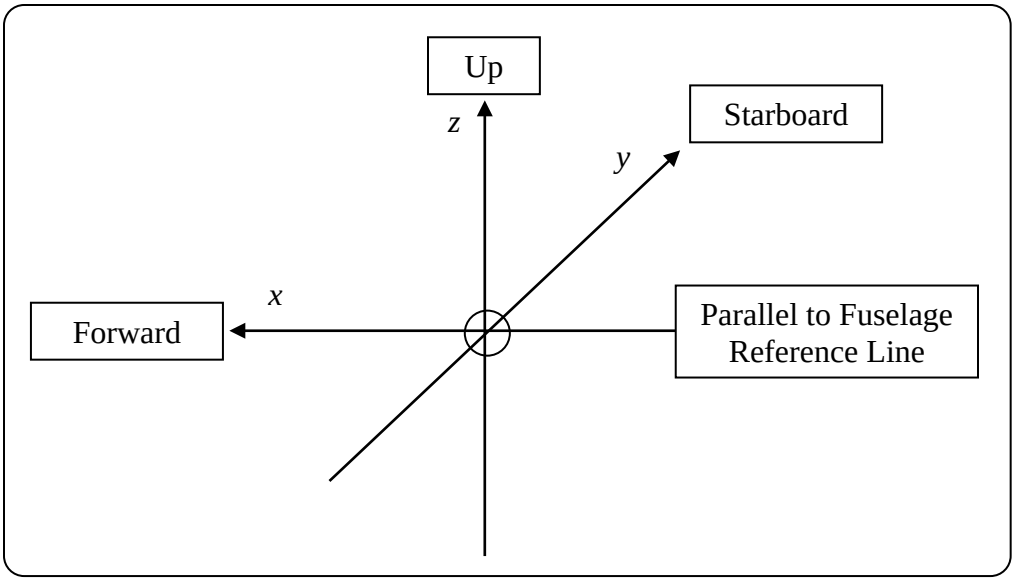

Figure 4. Sign convention for airplane accelerations

4.4.4 Peak-Valley Selection

The peak-between-means method of [7] was used to select the peaks and valleys in the acceleration and derived gust velocity data. This method is consistent with past practices and pertains to all accelerations whether due to gusts or maneuvers. In this method, only one peak or valley is counted between two successive crossings of the mean. A threshold zone (dead band) is used in the data reduction to ignore irrelevant load variations around the mean. This is shown schematically in figure 5. The same dead band values were used for gusts and maneuvers. The dead bands associated with the loads and the derived gust velocity are shown in table 6.

4.4.5 Separation of Maneuver and Gust Load Factors

The incremental acceleration measured at the center of gravity of the aircraft may be the result of either maneuvers or gusts. To derive gust and maneuver statistics, the maneuver-induced accelerations and gust response accelerations had to be separated from the total acceleration history. Reference [4] reports the results of a UDRI study to evaluate methods of separating maneuver and gust load factors from measured acceleration time histories. As a result of this study, it was recommended and accepted by the FAA that a cycle duration rule be used to separate gusts and maneuvers. A cycle duration of 2 seconds was recommended for use with B-737 and MD-82/83 aircraft. A review of the BE-1900D response characteristics has shown that this cycle duration can also be used with the BE-1900D data. To avoid the inclusion of peaks and valleys associated with very small load variations that are insignificant to the aircraft structure, a threshold zone of $\Delta n_z = \pm 0.05$ g was established. Similar dead bands were also established for longitudinal and lateral load factors, as shown in table 6. An algorithm was then developed to extract the acceleration peaks and valleys.

For each flight, the maximum and minimum total accelerations were determined from just after liftoff to just before touchdown. For the in-flight phases, the cumulative occurrences of

incremental load factors were determined as cumulative counts per nautical mile (nmi) and cumulative counts per 1000 hours using the peak-between-means counting method of [7], as explained in the previous section.

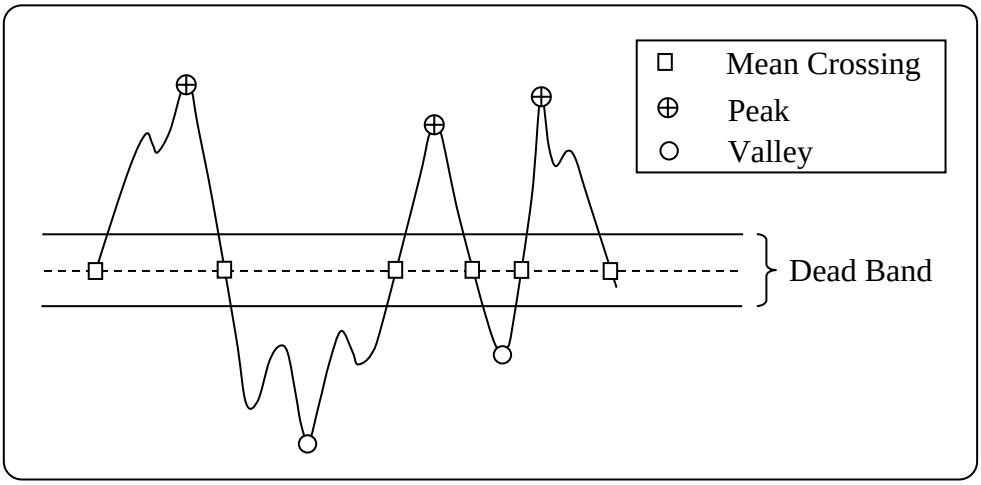

Figure 5. Peak-between-means classification of loads

Table 6. Peak-valley dead band limits

Parameter (Units)	Dead Band Width
Incremental Vertical Acceleration (g)	±0.050
Longitudinal Acceleration (g)	±0.005
Lateral Acceleration (g)	±0.005
Derived Vertical Gust velocity (ft/s)	±2.00

4.4.6 Flap Detents

Four possible states for flap deflection were recorded: 1) up, 2) in transit, 3) approach, and 4) down. The second indication (in transit) was not used for any flight phase identification and was not associated with any of the other detents. On one aircraft, the flap indication was “in transit” most of the time.

When flaps were extended, the effective deflection was considered to be that of the applicable detent, as indicated in table 7. The flap deflection ranges and associated placard speeds reflect the flap design limitations [8].

Table 7. BE-1900D flap detents

Flap Detent	Flap Setting	Operational Placard Speed (IKAS)
0	Retracted	248
1	Half	188
2	Full	154

4.4.7 Altitude Bands

For the departure and approach phases of flight, the altitudes were referenced to that of the departure airport and arrival airport, respectively. Therefore, in these cases, the altitude bands used were in above-ground level (AGL) and are shown in table 8. Absolute pressure altitude was used for all other phases of flight, with the altitude bands shown in table 9.

Table 8. Altitude bands above airports

Bands	Altitude Above Ground Level (ft)
1	0–250
2	251–500
3	501–750
4	751–1000
5	1001–1500
6	1501–2000
7	2001–3000
8	3001–4000
9	4001–5000
10	>5000

4.4.8 Acceleration Bias Correction

A bias for each of the accelerometers was established for each flight based on its readings before the aircraft started moving. This bias was based on the 20-second average of readings, starting from the point at which codes began to use the recorded data (i.e., for elapsed times inclusive of 21–40 seconds after the start of the file). These biases were used as corrections for all measured load factor values for the flight.

Table 9. Absolute pressure altitudes

Bands	Absolute Pressure Altitude (ft)
1	<500
2	501–1,500
3	1,501–4,500
4	4,501–9,500
5	9,501–14,500
6	14,501–19,500
7	19,501–24,500
	>24,500

5. DATA PRESENTATION

This section presents statistical summaries of aircraft usage data, ground loads data, flight loads data, and systems operational data collected from BE-1900D aircraft during typical operational usage by a single commuter airline. Statistical data are presented for parameters such as gust and maneuver acceleration; airspeed; altitude; flight duration and distance; derived gust velocity; V-n diagrams; and vertical, lateral, and longitudinal accelerations during ground operations. These data were reduced and processed into statistical formats that are typically used in presenting these types of data. These data can then be used by the FAA, aircraft manufacturers, and airlines to assess existing certification criteria contained in the FAA's CFR or by the airlines and aircraft manufacturer to better understand and control those factors, which influence the structural integrity of commuter aircraft.

During data editing, it was found that the recorded data for certain flights/aircraft exhibited random errors and were unreliable. However, if the remainder of the data appeared correct, they were used for statistical analysis of the associated flight phase. Furthermore, some flights contained multiple legs of the same phase, such as cruise or descent. Therefore, the data presented in these figures are not always based on an identical number of flights or flight hours. Consequently, it was deemed more appropriate to show the number of phases and associated flight hours used for arriving at the data presented in subsequent figures. Presented in table 10 is the list of the statistical data formats and the identification of the corresponding figure for which the processed data plot or table can be found in appendix A. The figures have been grouped into categories identified as aircraft usage, ground loads, flight loads, and operational data for the flap system. Each figure is discussed in the following paragraphs.

Table 10. Statistical formats

GROUND-AIR-GROUND CYCLE DATA	Figure/Table
FLIGHT DISTANCE AND DURATION DATA	
Correlation of maximum altitude and flight distance, percent of flights	Table A-1
Percent of integrated distance in altitude bands (climb, cruise, descent)	Table A-2
Correlation of GPS-integrated and airspeed-integrated flight distance	Figure A-1
Cumulative probability of flight distance	Figure A-2
Number of flights vs. flight duration	Figure A-3
Cumulative probability of flight duration	Figure A-4
ALTITUDE AND SPEED DATA—ALL PHASES	
Correlation of maximum altitude and coincident flight distance, all flight phases	Figure A-5
Correlation of maximum altitude and coincident flight duration, all flight phases	Figure A-6
Coincident altitude at maximum indicated airspeed, all flight phases	Figure A-7
Coincident indicated airspeed at maximum altitude, all flight phases	Figure A-8
ALTITUDE AND SPEED DATA—DEPARTURE	
Maximum airspeed and coincident altitude during departure	Figure A-9
Maximum altitude and coincident airspeed during departure	Figure A-10
Cumulative probability of maximum and minimum pitch angle during departure	Figure A-11
Cumulative probability of maximum and minimum bank angle during departure	Figure A-12
Cumulative probability of average rate of climb during departure	Figure A-13
ALTITUDE AND SPEED DATA—CLIMB	
Maximum airspeed and coincident altitude during climb	Figure A-14
Maximum altitude and coincident airspeed during climb	Figure A-15
Cumulative probability of average rate of climb during climb	Figure A-16
Cumulative probability of the pitch angle during climb	Figure A-17
Cumulative probability of the bank angle during climb	Figure A-18
ALTITUDE AND SPEED DATA—CRUISE	
Maximum airspeed and coincident altitude during cruise	Figure A-19
Maximum altitude and coincident airspeed during cruise	Figure A-20
Cumulative probability of altitude during cruise	Figure A-21
Cumulative probability of bank angle during cruise	Figure A-22
ALTITUDE AND SPEED DATA—DESCENT	
Maximum airspeed and coincident altitude during descent	Figure A-23
Maximum altitude and coincident airspeed during descent	Figure A-24
Cumulative probability of pitch angle during descent	Figure A-25
Cumulative probability of bank angle during descent	Figure A-26
Cumulative probability of average descent rate during descent	Figure A-27

Table 10. Statistical formats (continued)

ALTITUDE AND SPEED DATA—INITIAL APPROACH	
Maximum indicated airspeed and coincident altitude during initial approach	Figure A-28
Maximum altitude and coincident indicated airspeed during initial approach	Figure A-29
Cumulative probability of pitch angle during initial approach	Figure A-30
Cumulative probability of bank angle during initial approach	Figure A-31
Cumulative probability of average descent rate during initial approach	Figure A-32
ALTITUDE AND SPEED DATA—FINAL APPROACH	
Maximum indicated airspeed and coincident altitude during final approach	Figure A-33
Maximum altitude and coincident indicated altitude during final approach	Figure A-34
Cumulative probability of pitch angle during final approach	Figure A-35
Cumulative probability of bank angle during final approach	Figure A-36
Cumulative probability of average descent rate during final approach	Figure A-37
Maximum lateral load factor versus coincident incremental vertical load factor during final approach (within 10 seconds from touchdown)	Figure A-38
LIFTOFF AND TOUCHDOWN	
Probability distribution of airspeed at liftoff and touchdown	Figure A-39
Cumulative probability of airspeed at liftoff and touchdown	Figure A-40
Probability distribution of pitch angle at liftoff and touchdown	Figure A-41
Cumulative probability of pitch angle at liftoff and touchdown	Figure A-42
GAG LOADS DATA	
Ground-air-ground cycle occurrences of maximum and minimum incremental vertical load factor (good data only)	Table A-3
V-n diagram for all phases (good data only)	Figure A-43
Takeoff and landing occurrences per airport	Figure A-44
GROUND LOADS DATA	
LATERAL LOAD FACTOR, n_y	
Normal probability of maximum and minimum lateral load factor while taxiing out	Figure A-45
Cumulative probability of maximum and minimum lateral load factor while taxiing out	Figure A-46
Cumulative occurrences of lateral load factor per 1000 flights while taxiing	Figure A-47
Cumulative occurrences of lateral load factor per 1000 flights while on takeoff roll and landing roll	Figure A-48
Normal probability of maximum and minimum lateral load factor at liftoff	Figure A-49
Cumulative probability of maximum and minimum lateral load factor at liftoff	Figure A-50
Normal probability of maximum and minimum lateral load factor at touchdown	Figure A-51
Cumulative probability of maximum and minimum lateral load factor at touchdown	Figure A-52

Table 10. Statistical formats (continued)

GROUND LOADS DATA	
LATERAL LOAD FACTOR, n_y	
Cumulative occurrences of lateral load factor per 1000 flights at liftoff and touchdown	Figure A-53
Probability distributions of turning angle during runway turnoff	Figure A-54
Normal probability of maximum and minimum lateral load factor during runway turnoff	Figure A-55
Cumulative probability of maximum and minimum lateral load factor during runway turnoff	Figure A-56
Cumulative occurrences of lateral load factor per 1000 flights during runway turnoff	Figure A-57
Normal probability of maximum and minimum lateral load factor while taxiing in	Figure A-58
Cumulative probability of maximum and minimum lateral load factor while taxiing in	Figure A-59
LONGITUDINAL LOAD FACTOR, n_x	
Cumulative occurrences of longitudinal load factor per 1000 flights during taxi operations	Figure A-60
Cumulative occurrences of longitudinal load factor per 1000 flights during takeoff roll and landing roll	Figure A-61
VERTICAL LOAD FACTOR, n_z	
Cumulative occurrences of incremental vertical load factor per 1000 flights during taxi operations	Figure A-62
Cumulative occurrences of incremental vertical load factor per 1000 flights during takeoff roll and landing roll	Figure A-63
Cumulative occurrences of incremental vertical load factor per 1000 flights at liftoff and touchdown	Figure A-64
Normal probability distribution of incremental vertical load factor at takeoff rotation	Figure A-65
Cumulative probability of incremental vertical load factor at takeoff rotation	Figure A-66
Normal probability distribution of incremental vertical load factor at touchdown	Figure A-67
Cumulative probability of incremental vertical load factor at touchdown	Figure A-68
FLIGHT LOADS DATA	
DEPARTURE (FLAPS IN APPROACH POSITION)	
Longitudinal Loads	
Cumulative occurrences of longitudinal load factor per 1000 hours for departure phase	Figure A-69
Cumulative occurrences of longitudinal load factor per nmi for departure phase	Figure A-70
Lateral Loads	Figure/Table
Cumulative occurrences of lateral load factor per 1000 hours for departure phase	Figure A-71
Cumulative occurrences of lateral load factor per nmi for departure phase	Figure A-72

Table 10. Statistical formats (continued)

Vertical Loads	
Cumulative occurrences of incremental gust vertical load factor per 1000 hours for departure phase	Figure A-73
Cumulative occurrences of incremental gust vertical load factor per nmi for departure phase	Figure A-74
Cumulative occurrences of incremental maneuver vertical load factor per 1000 hours for departure phase	Figure A-75
Cumulative occurrences of incremental maneuver vertical load factor per nmi for departure phase	Figure A-76
CLIMB (FLAPS RETRACTED)	
Longitudinal Loads	
Cumulative occurrences of longitudinal load factor per 1000 hours for climb phase	Figure A-77
Cumulative occurrences of longitudinal load factor per nmi for climb phase	Figure A-78
Lateral Loads	
Cumulative occurrences of lateral load factor per 1000 hours for climb phase	Figure A-79
Cumulative occurrences of lateral load factor per nmi for climb phase	Figure A-80
Vertical Loads	
Cumulative occurrences of incremental gust vertical load factor per 1000 hours for climb phase	Figure A-81
Cumulative occurrences of incremental gust vertical load factor per nmi for climb phase	Figure A-82
Cumulative occurrences of incremental maneuver vertical load factor per 1000 hours for climb phase	Figure A-83
Cumulative occurrences of incremental maneuver vertical load factor per nmi for climb phase	Figure A-84
Derived Gust Velocities	
Cumulative occurrences of derived gust velocity per nmi for climb phase	Figure A-85
CRUISE (FLAPS RETRACTED)	Figure/Table
Longitudinal Loads	
Cumulative occurrences of longitudinal load factor per 1000 hours for cruise phase	Figure A-86
Cumulative occurrences of longitudinal load factor per nmi for cruise phase	Figure A-87
Lateral Loads	
Cumulative occurrences of lateral load factor per 1000 hours for cruise phase	Figure A-88
Cumulative occurrences of lateral load factor per nmi for cruise phase	Figure A-89

Table 10. Statistical formats (continued)

Vertical Loads	
Cumulative occurrences of incremental gust vertical load factor per 1000 hours for cruise phase	Figure A-90
Cumulative occurrences of incremental gust vertical load factor per nmi for cruise phase	Figure A-91
Cumulative occurrences of incremental maneuver vertical load factor per 1000 hours for cruise phase	Figure A-92
Cumulative occurrences of incremental maneuver vertical load factor per nmi for cruise phase	Figure A-93
Derived Gust Velocities	
Cumulative occurrences of derived gust velocity per nmi for cruise phase	Figure A-94
DESCENT (FLAPS RETRACTED)	
Longitudinal Loads	
Cumulative occurrences of longitudinal load factor per 1000 hours for descent phase	Figure A-95
Cumulative occurrences of longitudinal load factor per nmi for descent phase	Figure A-96
Lateral Loads	
Cumulative occurrences of lateral load factor per 1000 hours for descent phase	Figure A-97
Cumulative occurrences of lateral load factor per nmi for descent phase	Figure A-98
Vertical Loads	Figure/Table
Cumulative occurrences of incremental gust vertical load factor per 1000 hours for descent phase	Figure A-99
Cumulative occurrences of incremental gust vertical load factor per nmi for descent phase	Figure A-100
Cumulative occurrences of incremental maneuver vertical load factor per 1000 hours for descent phase	Figure A-101
Cumulative occurrences of incremental maneuver vertical load factor per nmi for descent phase	Figure A-102
Derived Gust Velocities	
Cumulative occurrences of derived gust velocity per nmi for descent phase	Figure A-103
INITIAL APPROACH (FLAPS IN APPROACH POSITION)	
Longitudinal Loads	
Cumulative occurrences of longitudinal load factor per 1000 hours for initial approach phase	Figure A-104
Cumulative occurrences of longitudinal load factor per nmi for initial approach phase	Figure A-105

Table 10. Statistical formats (continued)

Lateral Loads	
Cumulative occurrences of lateral load factor per 1000 hours for initial approach phase	Figure A-106
Cumulative occurrences of lateral load factor per nmi for initial approach phase	Figure A-107
Vertical Loads	
Cumulative occurrences of incremental gust vertical load factor per 1000 hours for initial approach phase	Figure A-108
Cumulative occurrences of incremental gust vertical load factor per nmi for initial approach phase	Figure A-109
Cumulative occurrences of incremental maneuver vertical load factor per 1000 hours for initial approach phase	Figure A-110
Cumulative occurrences of incremental maneuver vertical load factor per nmi for initial approach phase	Figure A-111
FINAL APPROACH (FLAPS IN DOWN POSITION)	Figure/Table
Longitudinal Loads	
Cumulative occurrences of longitudinal load factor per 1000 hours for final approach phase	Figure A-112
Cumulative occurrences of longitudinal load factor per nautical mile for final approach phase	Figure A-113
Lateral Loads	
Cumulative occurrences of lateral load factor per 1000 hours for final approach phase	Figure A-114
Cumulative occurrences of lateral load factor per nmi for final approach phase	Figure A-115
Vertical Loads	
Cumulative occurrences of incremental gust vertical load factor per 1000 hours for final approach phase	Figure A-116
Cumulative occurrences of incremental gust vertical load factor per nmi for final approach phase	Figure A-117
Cumulative occurrences of incremental maneuver vertical load factor per 1000 hours for final approach phase	Figure A-118
Cumulative occurrences of incremental maneuver vertical load factor per nmi for final approach phase	Figure A-119
COMPARISONS WITH OTHER AIRCRAFT	
Comparison of cumulative occurrences of incremental vertical gust load factor per nmi, BE-1900D vs. AC23-13A for cruise	Figure A-120
Comparison of cumulative occurrences of incremental vertical maneuver load factor per nmi, BE-1900D vs. AC23-13A for cruise	Figure A-121
Comparison of cumulative occurrences of incremental vertical gust load factor per 1000 hours, BE-1900D vs. B-737-400 and B-747-400 for cruise	Figure A-122

Table 10. Statistical formats (continued)

COMPARISONS WITH OTHER AIRCRAFT	
Comparison of cumulative occurrences of incremental vertical gust load factor per nmi, BE-1900D vs. B-737-400 and B-747-400 for cruise	Figure A-123
SYSTEMS OPERATIONAL DATA	
FLAP SYSTEM USAGE	
Probability of maximum indicated airspeed at flap deployment	Figure A-124
Cumulative probability of maximum indicated airspeed at flap deployment	Figure A-125
Percentage of flights with flaps deployed for N855CA	Figure A-126
Percentage of flights with flaps deployed excluding N855CA	Figure A-127

5.1 AIRCRAFT USAGE DATA (GROUND-AIR-GROUND CYCLE)

The aircraft usage data include flight profile statistics, such as altitudes, speeds, and flight distance information. This information is useful for deriving typical flight profiles; defining loading spectra for structural fatigue, durability, and damage tolerance analyses; and developing future design criteria. This information is presented in the following order:

1. Flight distance and duration data
2. Altitude and speed data for all phases
3. Altitude and speed data for departure
4. Altitude and speed data for climb
5. Altitude and speed data for cruise
6. Altitude and speed data for descent
7. Altitude and speed data for initial approach
8. Altitude and speed data for final approach
9. Liftoff and touchdown
10. Overall flight loads

5.1.1 Flight Distance and Duration Data

Correlation of maximum altitude and flight distance is given in table A-1 in appendix A. Flight distance in this figure represents that obtained from the integration of the true airspeed. These data show that all altitude bands, except for the lowest and the highest, were almost equally represented in the data. However, the majority of the flights (96%) were over distances of less than 300 nmi.

Table A-2 presents the percentage of integrated distance in various altitude bands as a percentage of flight distance. The departure and approach phases could not be included in these calculations because of the manner in which altitude bands were defined. Conversely, the climb and descent distances are slightly larger than the level flight distance because of the inclination of the flight path. Also, head- or tail-wind contributions remained unknown but were considered to be small.

A correlation of GPS-integrated and airspeed-integrated flight distance is shown in figure A-1, whereas the cumulative probability of flight distance, evaluated from different methods, is given in figure A-2. These data clearly show that in some cases, the difference between the GPS-integrated and airspeed-integrated distances grew larger with increasing flight distance. However, for distances below 250 nmi, the differences were not too large.

The bar chart in figure A-3 contains a breakdown of the number of flights flown versus the time duration of each flight from takeoff to landing. The mean flight length was determined to be 45.16 minutes with a standard deviation of 17.78 minutes. Figure A-4 presents the same flight duration data in a cumulative probability format. These results pertain to all complete flights, including those with erroneous accelerometer information.

5.1.2 Altitude and Airspeed Data for All Phases

Correlations of maximum altitude with coincident flight distance and coincident flight duration for all flight phases are given in figures A-5 and A-6. The maximum operating altitude is also marked on these figures. It is obvious from these figures that the maximum operating altitude was not significantly exceeded. Also, the predominance of flight levels above 18,000 ft separated by 1000 ft is clear in these figures.

Coincident altitude at maximum indicated airspeed and indicated airspeed at maximum altitude per flight for all flight phases are shown in figures A-7 and A-8. These figures also show the maximum operating airspeed limits. It is obvious from figure A-7 that, in many cases, the aircraft was flown slightly faster than the limit airspeeds. However, in no case did the indicated airspeed exceed 260 knots-indicated air speed (KIAS). Furthermore, the vast majority of these cases occurred at or below 15,000 ft and were associated with rapid descents, as will be shown later.

5.1.3 Altitude and Airspeed Data for Departure

The departure phase was defined to be the initial climb immediately following liftoff, with the flaps in the approach position.

A total of 8740 departure phases were used in the analysis. All departure phases with zero time and zero distance were removed for statistical analysis. Departure phases longer than 10 minutes were determined to be unreliable and eliminated from the analysis. The breakdown of the remaining departure phases with altitude, duration, and distance is shown in table 11. It is obvious from these numbers that more than 97% of the departure times occurred at altitudes below 1000 ft AGL.

Correlations between indicated airspeed and altitude are presented in figures A-9 and A-10. Figures A-11–A-13 show the cumulative probabilities of pitch angle, bank angle, and average rate of climb, respectively, for this phase.

Table 11. Statistical data for departure phases

	Duration (sec)	Duration (hr)	Distance (nmi)
Departure Totals	170,830	47.45	6,595.99
<250 ft	78,256	21.74	2,894.97
250–500 ft	64,888	18.02	2,571.26
500–750 ft	21,144	5.87	859
750–1000 ft	2,558	0.71	104.3
1000–1500 ft	1,658	0.46	67.71
1500–2000 ft	1,020	0.28	41.74
2000–3000 ft	901	0.25	38.57
3000–4000 ft	246	0.07	10.77
4000–5000 ft	120	0.03	5.64
>5000 ft	39	0.01	2.03

5.1.4 Altitude and Airspeed Data for Climb

This phase was defined as that of climbing flight with the flaps retracted. A total of 16,181 climb phases were detected because many flight files contained more than one climb phase. From these, 1645 flight phases were deemed unreliable for a variety of reasons, including those with a flight duration of less than 1 minute. Accordingly, 14,536 climb phases were used for the subsequent analyses. Table 12 shows the breakdown of all cruise phases with altitude, duration, and distance.

Correlations between airspeed and altitude are presented in figures A-14 and A-15. It is clear from these figures that at no point was the maximum indicated airspeed or altitude exceeded. Figures A-16–A-18 show the cumulative probabilities of average rate of climb, pitch angle, and bank angle, respectively.

Table 12. Statistical data for climb phases

	Duration (sec)	Duration (hr)	Distance (nmi)
Climb Totals	4,412,417	1,225.67	225,903.36
<500 ft	7,658	2.13	316.21
500–1,500 ft	156,402	43.44	6,758.45
1,500–4,500 ft	891,415	247.61	41,282.52
4,500–9,500 ft	1,394,748	387.43	69,778.56
9,500–14,500 ft	1,040,751	289.10	56,126.26
14,500–19,500 ft	665,984	185.00	37,094.37
19,500–24,500 ft	254,927	70.81	14,515.79
>24,500 ft	532	0.15	31.2

5.1.5 Altitude and Airspeed Data for Cruise

Most flights included multiple cruise legs, defined as level flight with the flaps retracted. A total of 23,617 such phases longer than one minute were detected. From this, 44 phases were eliminated on the basis of being unreliable. Therefore, 23,573 cruise phases were used for statistical analysis, shown in table 13 correlated with altitude, duration, and distance.

Figures A-19 and A-20 show the correlation of the maximum airspeed with altitude and maximum altitude with airspeed, respectively. In these figures, limitations on operating airspeed and altitude are also marked for reference. Cumulative probabilities of average cruise altitude and maximum and minimum bank angle are also shown in figures A-21 and A-22.

5.1.6 Altitude and Airspeed Data for Descent

This phase was defined as descending flight with the flaps stowed. When all descent phases that were shorter than 1 minute were eliminated, 21,003 segments were identified. These are shown in table 14 in duration and distance for various mean sea level (MSL) altitude bands.

Maximum airspeed and coincident altitude are shown in figure A-23, whereas maximum altitude and coincident airspeed are presented in figure A-24. The published maximum operating airspeed is also shown in these figures. The results shown in figure A-23 correlate well with those of figure A-7.

Table 13. Statistical data for cruise phases

	Duration (sec)	Duration (hr)	Distance (nmi)
Cruise Totals	10,834,613	3010.00	743,001.80
<500 ft	0	0	0
500–1,500 ft	1,942	0.5	107.81
1,500–4,500 ft	833,474	231.5	47,414.35
4,500–9,500 ft	2,808,351	780	180,043.90
9,500–14,500 ft	2,252,652	626	155,751.2
14,500–19,500 ft	2,846,561	791	204,201.0
19,500–24,500 ft	2,046,825	569	152,123.9
>24,500 ft	44,808	12	3,359.71

Figures A-25–A-27 show the cumulative probabilities of maximum and minimum pitch angle, bank angle, and average descent rate during this phase, respectively.

Table 14. Statistical data for descent phases

	Duration (sec)	Duration (hr)	Distance (nmi)
Descent Totals	3,955,202	1,098.67	272,543.19
<500 ft	678	0.19	26.67
500–1,500 ft	14,493	4.03	708.12
1,500–4,500 ft	647,025	179.73	37,522.91
4,500–9,500 ft	1,406,617	390.73	93,845.64
9,500–14,500 ft	1,068,170	296.71	78,263.36
14,500–19,500 ft	632,469	175.69	47,890.16
19,500–24,500 ft	185,525	51.53	14,269.32
>24,500 ft	225	0.06	17.01

5.1.7 Altitude and Airspeed Data for Initial Approach

As a reminder, these were the descent cases with the flaps in the “Approach” detent. A total of 7195 initial approach phases were found after dismissing those that were longer than 20 minutes as unreasonably too long. These are shown in duration and distance for different AGL altitude bands in table 15.

Figures A-28 and A-29 show the maximum airspeed, the coincident altitude, the maximum altitude, and the coincident airspeed, respectively. In very few cases, the maximum operating airspeed appears larger than the operating limit for this flap detent. However, the number of incidents was so small that they were not statistically significant. Also, the white vertical bands

across the data in these figures were thought to be due to the plotting package. However, closer examination showed an absence of data in this range.

Table 15. Statistical data for initial approach phases

	Duration (sec)	Duration (hr)	Distance (nmi)
Initial Approach Totals	681,365	189.27	28,441.69
<250 ft	2,571	0.71	99.18
250–500 ft	44,975	12.49	1,738.75
500–750 ft	113,979	31.66	4,489.29
750–1,000 ft	118,083	32.80	4,763.43
1,000–1,500 ft	200,460	55.68	8,400.72
1,500–2,000 ft	119,800	33.28	5,246.31
2,000–3,000 ft	66,982	18.61	3,017.82
3,000–4,000 ft	10,950	3.04	513.20
4,000–5,000 ft	2,372	0.66	109.85
>5,000 ft	1,193	0.33	63.14

Cumulative probabilities of pitch and bank angles and average descent rate are shown in figures A-30–A-32. Comparing the data in figures A-32 and A-27, the average descent rate for the initial approach appears to be much smaller than that of the descent phase with the flaps stowed. However, this is because of the lower airspeeds during initial approach compared with descent. In fact, both cases resulted in an average 3° glide slope.

5.1.8 Altitude and Airspeed Data for Final Approach

Final approach phases were descending flights with the flaps in the “Down” detent. A total of 7732 final approach phases were identified. In table 16, these are shown in duration and distance for different AGL altitude bands.

The maximum airspeed, coincident altitude, maximum altitude, and coincident airspeed are shown in figures A-33 and A-34, respectively. These figures also show the maximum placard airspeed for operation with full flaps. Again, close examination of airspeeds showed an unexplained absence of values of approximately 125 KIAS. Also, these figures show that in a noticeable number of cases, the aircraft were flown on final approach at speeds higher than the limit set for operation with full flaps.

Cumulative probabilities of pitch and bank angles and average descent rate are shown in figures A-35–A-37. A comparison of the data in figure A-37 to that in figures A-27 and A-32 shows that the average descent rate for the final approach was much smaller than the others. However, this was due to the lower airspeeds during final approach.

Maximum lateral load factor and its coincident incremental vertical load factor within 10 seconds of touchdown are shown in figure A-38. For the most part, maximum lateral accelerations remained well below +/- 0.3 g.

Table 16. Statistical data for final approach phases

	Duration (sec)	Duration (hr)	Distance (nmi)
Final Approach Totals	390,977	108.60	13,920.79
<250 ft	204,032	56.68	6,815.65
250–500 ft	117,590	32.66	4,343.02
500–750 ft	32,405	9.00	1,232.74
750–1,000 ft	12,085	3.36	474.54
1,000–1,500 ft	13,961	3.88	574.57
1,500–2,000 ft	6,623	1.84	286.61
2,000–3,000 ft	3,751	1.04	170.17
3,000–4,000 ft	388	0.11	17.17
4,000–5,000 ft	120	0.03	5.42
>5,000 ft	22	0.01	0.90

5.1.9 Liftoff and Touchdown

It became clear in the early stages of the analysis that the squat switch did not accurately indicate the points of liftoff or touchdown. Manual processing of some data showed that the actual liftoff or touchdown could differ from that indicated by the squat switch by as much as 3–4 seconds, in which time the airspeed was changing rapidly.

To automate the recognition of the liftoff and touchdown airspeeds, it was reasoned the liftoff point would be the only point in flight when an increase in pitch angle would be accompanied by an increase in airspeed because of the loss of ground contact. Conversely, the point of touchdown would be the only point in flight at which decreasing pitch angle would be accompanied by decreasing airspeed, again because of ground contact. Therefore, in either case, the product of the change in pitch angle and airspeed would be positive.

A code was developed to identify these points within +/- 5 seconds of the time indicated by the squat switch. For those cases in which the algorithm could not successfully identify the liftoff or touchdown point, it was assumed they occurred at the squat switch indication.

On more detailed examination of the results, the following observations could be made:

- Tail number N840CA consistently showed lower liftoff and touchdown speeds than the rest of the fleet (approximately 10 KIAS).
- The data for the liftoff speed showed larger scatter than that of the touchdown speed, as indicated in figure 6.

- Data removed from N857CA between January 12, 2006 and July 9, 2006 (inclusive) showed unreasonably high touchdown speeds, as shown in figure 6.
- Some liftoff and touchdown speeds were clearly unreasonable, being either well below the stall speed or in excess of 160 KIAS.

A summary of all these anomalies and their associated number of cases are shown in table 17. After removing the anomalous data, 9332 cases remained. These were the cases used for figures A-39 and A-40. These data showed average liftoff and touchdown airspeeds of 99.8 and 95.8 KIAS, respectively, with standard deviations of 15.2 and 8.4 KIAS, respectively. The larger spread in the liftoff airspeed values is consistent with the data shown in figure 7.

Figures A-41 and A-42 show the distribution and cumulative probabilities of the pitch angle at liftoff and touchdown. The trends given in these figures are consistent with those expected for these phases.

Table 17. Analysis of liftoff and touchdown airspeeds

Cases and Anomalies	Number	Remainder
Total cases	11,299	—
Incomplete cases	661	10,638
N857CA from January 12, 2006 to July 9, 2006	701	9,937
Negative pitch angle at liftoff	203	9,734
Pitch angle at liftoff greater than 20°	4	9,730
Pitch angle at touchdown less than -10°	None	9,730
Pitch angle at touchdown greater than 13.5°	None	9,730
Liftoff airspeed less than 60 KIAS	339	9,391
Liftoff airspeed greater than 160 KIAS	32	9,359
Touchdown airspeed less than 60 KIAS	13	9,346
Touchdown airspeed greater than 160 KIAS	14	9,332

5.1.10 GAG Loads Data

Ground-air-ground cycle occurrences of maximum and minimum incremental vertical load factor are shown in table A-3. Because the “bad data” contained erroneous accelerometer output values, it was not used for generating this figure. Likewise, the V-n diagram shown in figure A-43 contains only the good data.

Figure A-44 shows the frequency of landings and takeoffs from various airports. This information was deduced from the GPS data and shows that the majority of the flights originated from, or terminated at, Cleveland-Hopkins International Airport.

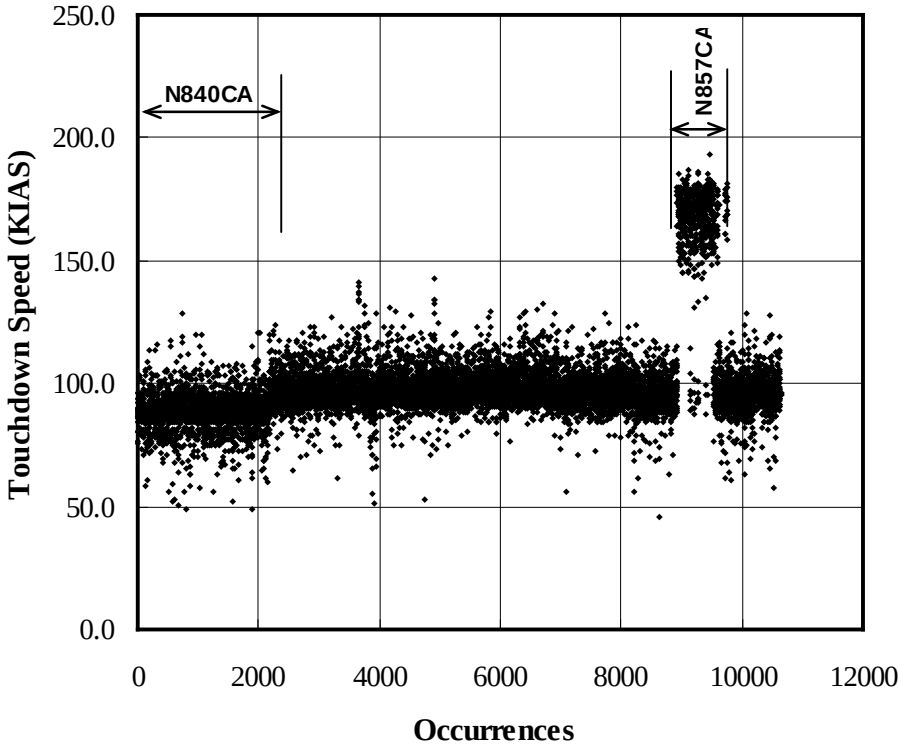

Figure 6. Indicated touchdown airspeed

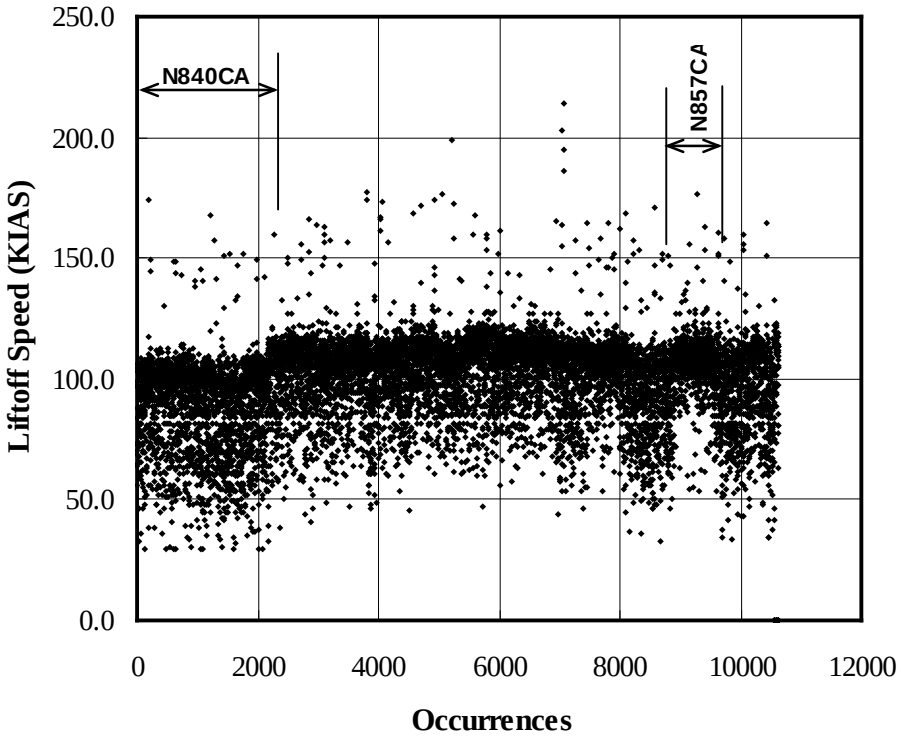

Figure 7. Indicated liftoff airspeed

5.2 GROUND LOADS DATA

This section contains information on loads during ground operations. Ground operations are defined here as taxi-out, takeoff roll, landing roll, runway turnoff, and taxi-in. Information is included on touchdown and liftoff, where appropriate.

In those cases for which the file contained more than one flight, GPS coordinates were used to separate the two. When encountering multiple flights, if the last digit in the GPS coordinates did not change for 30 seconds or more, the flight was assumed terminated and that point in the data was marked as the start of the second flight. There were no cases in which more than two flights were present in one file.

These data are divided into three broad sections, one for each of the load components.

5.2.1 Lateral Load Factor

A total of 9043 taxi-out cases and 7712 taxi-in cases were detected, as shown in table 18. The minimum recorded airspeed was approximately 36 KIAS, regardless of the actual speed of the aircraft. Therefore, reliable distances could not be determined for ground operations.

Table 18. Statistical data for ground phases

Phase	Number	Duration (hr)
Taxi out	9043	810
Takeoff roll	8992	50
Landing roll	7330	60
Turnoff	7290	48
Taxi in	7712	195

Normal probability distribution for the lateral load factor, while taxiing out, is presented in figure A-45, with cumulative probability shown in figure A-46. It is obvious from these figures that right and left lateral load factors occurred with nearly equal probability. Cumulative occurrences of lateral load factor per 1000 flights, while taxiing, are shown in figure A-47. This information compares with that given in figure A-48 for the takeoff and landing rolls. It is noted that the latter phases contained fewer occurrences of the same load factor. This is expected because the taxi phases include all turns made by the aircraft.

Normal and cumulative probabilities of the maximum and minimum lateral load factor at liftoff are shown in figures A-49 and A-50. The corresponding plots for touchdown are shown in figures A-51 and A-52. Also, cumulative occurrences of maximum and minimum lateral load factor at liftoff and touchdown per 1000 flights are shown in figure A-53. As a reminder, the maximum lateral load factor was defined as that which occurred within +/-5 seconds of the liftoff or touchdown, indicated by the squat switch.

Runway turnoff was recognized by a change in the heading of more than 13.5° after landing. In some cases, the aircraft was stopped without making a turn, so fewer runway turnoff cases were found than landing cases (7290 versus 7330).

Runway turnoff information is presented in figures A-54–A-57. Figure A-54 shows the probability distribution for runway turnoff angle. Normal and cumulative probabilities of maximum and minimum lateral load factor during turnoff are shown in figures A-55 and A-56. Cumulative occurrences of lateral load during runway turnoff are shown in figure A-57. Understandably, these show much higher lateral loads than other cases involving ground operations.

Figures A-58 and A-59 show the normal and cumulative probabilities of maximum and minimum lateral load factor while taxiing in. A comparison with figures A-45 and A-46 shows the taxi-in lateral loads to be comparable with those of taxiing out.

5.2.2 Longitudinal Load Factor, n_x

Longitudinal load factors during ground operations are grouped into those of taxi phases and takeoff and landing rolls. The cumulative occurrence of longitudinal load factor during taxi operations is shown in figure A-60. It is obvious that negative decelerations occurred with a higher frequency while taxiing in because of more frequent braking action, whereas positive accelerations were more dominant while taxiing out.

Figure A-61 shows the cumulative occurrence of longitudinal load factor during the takeoff and landing rolls. Understandably, positive accelerations dominate during the takeoff run, whereas negative values are dominant during the landing roll.

5.2.3 Vertical Load Factor, n_z

Cumulative occurrences of incremental vertical load factor for taxi operations are shown in figure A-62. These data indicate that higher load factors occurred at a slightly higher frequency while taxiing out. However, for incremental vertical load factors within +/-0.25 g, there were no differences between the two cases.

For takeoff and landing rolls, cumulative occurrences of incremental vertical load factor are shown in figure A-63. These cases were almost identical for negative values. However, positive values occurred with a slightly higher frequency during the landing roll. Analogously, cumulative occurrences of incremental vertical load factor at liftoff and touchdown are shown in figure A-64.

Normal and cumulative probabilities of maximum and minimum incremental vertical load factors at takeoff rotation are shown in figures A-65 and A-66. The corresponding values for touchdown are presented in figures A-67 and A-68. For this presentation, maximum values were determined within +/- 5 seconds of the squat switch indication. A comparison of figures A-65 and A-67 shows that landings occurred with a slightly larger vertical load factor than takeoffs. However, the spread in the data appeared to be the same in both cases.

5.3 FLIGHT LOADS DATA

In the subsequent discussions, the material is grouped according to the flight phase. Within the discussion of each phase, results are presented for lateral loads, longitudinal loads, and vertical loads. Incremental vertical loads are separated into gust and maneuver loads based on the 2-second rule. Also, each of the following cases involved a different number of total events due to a variety of factors. Therefore, the number of flight phases used for the analysis in each case is also indicated clearly in the subsequent discussions. Furthermore, each figure shows the number of events for its analysis, along with total distance and duration where applicable. In each case, the data are presented per 1000 hours of flight, as well as per nmi.

5.3.1 Departure

As a reminder, this phase was defined as that of initial climb with the flaps in the first detent. A total of 8740 departure phases were identified. Also, the loads data for this phase are presented by altitude bands above the departing airport.

Cumulative occurrences of longitudinal loads during departure are shown in figures A-69 and A-70. Understandably, positive accelerations dominated in this case because the aircraft was pitched up rather steeply in this flight phase. Similarly, the cumulative lateral load factors are shown in figures A-71 and A-72.

Cumulative occurrences of incremental vertical load factors, divided into gust loads and maneuver loads, are shown in figures A-73–A-76. An examination of the maneuver loads showed a curious trend that calls for further examination. For negative load factors, the frequency of occurrence was the lowest for the lowest altitude band and the highest for the third altitude band. However, this trend reversed for the positive altitude bands. A detailed examination of the data revealed no anomalies that could lead to this behavior. Furthermore, this trend reversal was observed also in the results shown in [1].

5.3.2 Climb

This phase was defined as that with climb rates greater than 200 ft per minute with the flaps retracted. A total of 14,536 climb phases were identified and used for this analysis. The altitude bands shown in the subsequent figures are relative to MSL.

Cumulative occurrences of longitudinal load factors are shown in figures A-77 and A-78. Again, positive load factors dominate because the aircraft is generally pitched up in this phase. Figures A-79 and A-80 show the cumulative occurrences of lateral load factors, whereas the cumulative incremental vertical load factors are shown in figures A-81–A-84. Finally, cumulative occurrences of derived gust velocities are shown in figure A-85.

These figures clearly show the effect of altitude on the lateral and vertical loads, with the largest number of occurrences associated with lower altitudes. As a reminder, a fixed weight of 16,500 pounds was assumed for determining the derived gust velocities.

5.3.3 Cruise

Cruise was defined as flight phases longer than 1 minute, with the flaps retracted, and at rates of climb or descent of less than 200 ft per minute. Based on these criteria, 23,573 cruise phases were identified in the data. Again, the altitude bands shown in the subsequent figures are relative to MSL.

Cumulative occurrences of longitudinal and lateral load factors per 1000 hours and per nmi are shown in figures A-86–A-89. The incremental vertical load factors, separated into gust and maneuver, are shown in figures A-90–A-93. The variations with altitude were consistent with those of other flight phases and were as expected. Also, figures A-92 and A-93 show that positive incremental vertical load factors due to maneuvers occurred with a higher frequency than those with negative values. This was expected for a commercial aircraft for which intentional maneuvers with negative incremental load factors are generally avoided. Cumulative occurrences of derived gust velocities are shown in figure A-94.

5.3.4 Descent

As a reminder, this phase was that of descending flights with flaps retracted. As explained earlier, 21,003 descent phases were identified and used in this analysis. Similar to climb and cruise phases, the data in these cases were also separated into MSL altitude bands.

Figures A-95 and A-96 show the cumulative occurrences of longitudinal load factor. The dominance of negative load factors is obvious in these figures. This was expected because the aircraft was generally flown at lower pitch attitudes than in the previous cases and it was generally slowed in preparation for approach. Expected trends in lateral load factor can be seen in figures A-97 and A-98. Both sets of figures show a great deal of scatter in the longitudinal and lateral data at low altitudes. This could be attributed to the scarcity of data at these altitudes. After all, not many cases found the aircraft engaged in descending flight below 1500 ft with the flaps retracted. However, for altitudes above 1500 ft, the data showed definite and consistent trends.

To some extent, the same can also be said for the incremental vertical load factors shown in figures A-99–A-102. However, in these cases, the scatter at low altitudes is not as obvious because the same load would occur at frequencies that were two orders of magnitude larger than those in longitudinal and lateral cases.

Again, cumulative occurrences of derived gust velocities are shown in figure A-103. These figures show derived gust velocities closer to those of cruise cases than to climb. This could be attributed to the similarities in airspeed between descent and cruise phases, whereas climb cases occurred at lower airspeeds.

5.3.5 Initial Approach

Initial approach was defined as descending flight with the flaps in the first detent. A total of 7195 initial approach phases were identified. Much like in the departure case, the data in these cases were divided into AGL altitude bands relative to the field elevation of the landing airport.

Cumulative occurrences of longitudinal load factors are shown in figures A-104 and A-105. The predominance of negative load factors in these figures is quite obvious. Cumulative occurrences of lateral load factors are shown in figures A-106 and A-107 and seem to indicate that negative load factors occurred at a slightly higher frequency than positive values. Figures A-108–A-111 show the cumulative occurrences of incremental vertical load factors, which are consistent with the previous cases.

5.3.6 Final Approach

Final approach was similar to initial approach, except with fully deployed flaps. Cumulative occurrences of longitudinal load factor are shown in figures A-112 and A-113. It is obvious from these figures that accelerations were biased toward negative values because the aircraft decelerated and were pitched down during this phase. It should be noted that no final approach phases were found at altitudes above 5000 ft. Furthermore, the case for the altitude band of 4000–5000 ft is based on only two incidences and, therefore, not statistically significant.

Figures A-114 and A-115 show the cumulative occurrences of lateral load factor. These data show the expected behavior of this parameter with altitude. The same dependence on altitude can also be seen in cumulative occurrences of incremental vertical load factors for gust and maneuver, which are presented in figures A-116–A-119. It is noteworthy that the maneuver data showed trends similar to those of the departure phase in figures A-75 and A-76. Furthermore, according to these data, the number of occurrences of negative maneuver load factors was fewer than the positive values during final approach, especially in the lowest altitude band where the difference was approximately one order of magnitude. The case for the altitude band of 4000–5000 ft is based on only two incidences and, therefore, is not statistically significant.

5.3.7 Comparison With Other Aircraft

Comparisons of the gust and maneuver loads during cruise with those prescribed by AC23-13A are shown in figures A-120 and A-121. In the case of gust loads, the data from AC23-13A are those for single- and twin-engine pressurized cases. Also, because the exact operational weights were not known, the data are presented here for three weights ranging from near-empty to near-gross weight.

It is obvious that the results extracted from flight data for gust loads remained well within the prescribed bounds. However, using the same data for maneuver loads placed the operational loads outside of the prescribed boundaries for incremental load factors greater than +/- 0.7. This could be attributed to two factors. The first reason could be the method used to separate gust and maneuver loads for the present report. There is evidence [9] that the 2-second rule may not result in correct separation of the two, depending on the aircraft weight. The second reason could be attributed to the method used to determine the limit load factor from equations 6 and 7. The results obtained from these equations may not be the same as those used in the design process.

Cumulative incremental vertical gust load factors were also compared with the results for two larger transport aircraft. For the purpose of comparison, the data from all cruise altitude bands were combined into a single curve. Figures A-122 and A-123 show the cumulative occurrences of incremental vertical gust load factor for Beech 1900D in contrast with those of

Boeing 737-400 [10] and Boeing 747-400 [2] airplanes. It is apparent from these figures that the frequencies and magnitudes are very different for the larger transport aircraft compared with one operating in a commuter role. This could be the result of the difference in the wing loadings and average operational cruise altitudes of these aircraft.

5.4 SYSTEMS OPERATIONAL DATA

Flaps were the only system whose operational data were recorded. Therefore, this section contains operational usage data recorded on the BE-1900D flap.

5.4.1 Flap System Data

Flap usage statistics are of value in the design of flap structure, backup structure, and other flap components. There are three flap positions for this aircraft: retracted, half, and full. The three detent positions were recorded as "Up," "Approach," and "Down." While the flaps were in motion, "InTransit" was indicated in the recorded data. Results showing the maximum airspeed while the flaps were deployed and the time the flaps were in use are presented in this section.

5.4.2 Airspeed at Flap Deployment

A number of flights did not show any flap deflection. The data from a total 10,070 flights with flap deflection were used for the subsequent statistical analysis. Normal and cumulative probabilities of maximum airspeed with the flaps deployed are shown in figures A-124 and A-125. These data pertained primarily to departure and approach phases. Also, the results are shown for each flap setting separately. It is obvious from these results that the maximum likely airspeeds were much lower than the flap placard limits of 188 KIAS and 154 KIAS for approach and down positions, respectively.

5.4.3 Time in Flap Detent Setting

The percentage of time operating with different flap settings was determined for all flights. This included the time spent for the flaps to transition between two adjacent settings. The results showed an unreasonably large percentage of time with "InTransit" recorded for the flap position. Closer scrutiny of the data revealed what appeared to be a faulty switch on N855CA, resulting in "InTransit" recordings when all other flight parameters indicated that the flaps were stowed. The results for this aircraft alone are shown in figure A-126.

After eliminating N855CA from the data, 10,488 flights remained for the analysis. Figure A-127 shows the percentage of time that the aircraft was operated in various flap settings. It is obvious that the "Approach" setting was used with almost twice the frequency of the "Down" setting. Furthermore, flaps spent a very small percentage of time transitioning from one setting to another.

6. CONCLUSIONS

Considering that the data were not collected in a controlled laboratory setting, the overall quality was quite good, with more than 10,000 flights available to obtain reasonable statistical stability in the data.

The statistical data formats allowed a very in-depth examination of various parameters. The results presented should be useful to the FAA, aircraft manufacturer, and airlines toward their better understanding of how these aircraft are operated.

For the most part, the processed data presented in this report appear to match the expected outcomes with only a few small exceptions. For instance, the altitude, airspeed, and flight distance data revealed flight profiles that were consistent with a commuter-type aircraft. The probabilities of right and left turns were the same, indicating that the aircraft experienced both with equal frequency. Flap usage was consistent with that expected on a commuter aircraft. However, comparisons of the BE-1900D statistical data—with their operational limits, published advisories, and published data from other aircraft—revealed some interesting anomalies that may require further study:

- For a small number of flights, the operational limit speed for flap deployment during descent and approach exceeded published placards. This was especially true on final approach when the flaps were fully deployed.
- The gust load factor spectra specified in AC23-13A for single-engine and twin-engine pressurized aircraft are considerably more severe than what was encountered by this fleet of BE-1900D aircraft.
- For single-engine and twin-engine pressurized usage, the maneuver spectra derived from the operational data did not agree well with the values presented in AC23-13A and 14 CFR 23.
- Comparisons of vertical load factor spectra for BE-1900D aircraft with larger transport aircraft showed large differences between the two categories. For both gusts and maneuvers, these differences could be attributed to the wing-loading and operational altitudes.
- The use of criteria for larger aircraft in assessing structural integrity in commuter category aircraft may not result in reliable conclusions.
- At lower altitudes, considerably higher load factors of vertical and lateral acceleration were measured as opposed to the same parameters at higher altitudes.
- Future digital flight data recorder installations should record additional related parameters, such as gross weight, fuel weight, wheel speed, and Mach number. This would make it possible to provide more in-depth, accurate information.
- Squat switch recordings, which identify when an airplane has weight on wheels, were inconsistent. This translated into potential inaccuracies in the determination of the start of departure and landing phases, and possibly the misplacement of load factor occurrences associated with these phases.

7. REFERENCES

1. Tipps, D.O., Skinn, D.A., Rustenburg, J.W., and Zeiler, T.A., “Statistical Loads Data for BE-1900D Aircraft in Commuter Operations,” FAA report DOT/FAA/AR-00/11, April 2000.

2. Jones, T., Rustenburg, J.W., Skinn, D.A., Tipps, D.O., and DeFiore, T., “Statistical Data for the Boeing-747-400 Aircraft in Commercial Operations,” FAA report DOT/FAA/AR-04/44, January 2005.

3. Williams, K.W. and Ball, J.D., "Usability and Effectivness of Advanced General Aviation Cockpit Displays for Visual Flight Procedures," December 2004, available at: http://www.cockpitgps.com/data/AirportsGDM.txt, last modified April 2006.

4. Rustenburg, J.W., Skinn, D.A., and Tipps, D.O., "An Evaluation of Methods to Separate Maneuver and Gust Load Factors From Measured Acceleration Time Histories," FAA report DOT/FAA/AR-99/14, April 1999.

5. "Fatigue Evaluation of Wing and Associated Structures on Small Aircraft," Department of Transportation Report No. AFS-120-73-2, May 1973.

6. "Fatigue, Fail-Safe, and Damage Tolerance Evaluation of Metallic Structure for Normal, Utility, Acrobatic, and Commuter Category Airplanes," Department of Transportation Report No. AC23-13A, September 2005.

7. de Jonge, B., "Reduction of Incremental Load Factor Acceleration Data to Gust Statistics," FAA report DOT/FAA/CT-94/57, August 1994.

8. FAA Type Certificate Data Sheet Number A-34CE, Revision 68.

9. Rustenburg, J.W., Tipps, D.O., and DeFiore, T., "Study of an Improved Maneuver-Gust Separation Criterion," preliminary contract report, University of Dayton Research Institute, December 2007.

10. Rustenburg, J.W., Skinn, D.A., and Tipps, D.O., "Statistical Loads Data for Boeing 737-400 Aircraft in Commercial Operations," FAA report DOT/FAA/AR-98/28, August 1998.

APPENDIX A–STATISTICAL FORMATS AND AIRCRAFT USAGE DATA

Table A-1. Correlation of maximum altitude and flight distance, percent of flights

BE-1900D 11,000 Flights, 8279 hrs, 1,883,394 nm		Maximum Altitude (1000 ft)						
		0-5	5-10	10-15	15-20	20-25	25-30	Total
Flight Distance (nm)	0–50	2.94	2.96	0.01	0.00	0.00	0.00	5.91
	50–100	0.60	9.83	1.45	0.01	0.00	0.00	11.89
	100–150	0.06	9.56	10.38	1.89	0.04	0.00	21.93
	150–200	0.00	2.39	8.33	9.02	3.50	0.04	23.28
	200–250	0.00	0.44	1.64	8.80	12.78	0.17	23.83
	250–300	0.00	0.05	0.76	3.26	4.76	0.34	9.17
	300–350	0.00	0.01	0.10	0.72	2.13	0.05	3.01
	350–400	0.00	0.00	0.07	0.13	0.55	0.01	0.76
	400–450	0.00	0.00	0.00	0.02	0.10	0.01	0.13
	450–500	0.00	0.00	0.00	0.01	0.05	0.00	0.06
	500–550	0.00	0.01	0.00	0.00	0.02	0.00	0.03
	Total	3.60	25.25	22.74	23.86	23.93	0.62	100.00

Table A-2. Percent of integrated distance in altitude bands (climb, cruise, and descent)

BE-1900D 9356 Flights, 5335 hrs, 1,241,448 nm		Distance of MSL Portion of Flight (nm)										
		0 to 50	50 to 100	100 to 150	150 to 200	200 to 250	250 to 300	300 to 350	350 to 400	400 to 450	450 to 500	500 to 550
Altitude Band (ft)	< 500	0.10	0.02	0.05	0.02	0.02	0.02	0.01	0.01	0	0	0
	500–1500	2.63	0.90	0.79	0.43	0.41	0.31	0.14	0.16	0.23	0.20	0.14
	1500–4500	34.24	17.90	12.58	7.25	5.89	5.05	4.79	3.22	2.89	3.97	1.94
	4500–9500	45.18	57.93	32.56	19.63	15.40	15.00	14.99	13.09	10.49	9.04	52.53
	9500–14,500	11.67	19.31	32.43	22.20	22.26	15.86	16.03	15.63	14.90	12.49	0.63
	14,500–19,500	4.46	3.13	18.12	30.44	32.95	32.03	25.23	14.42	31.73	14.80	0.67
	19,500–24,500	1.72	0.81	3.44	19.92	22.55	30.87	37.61	44.10	39.77	59.51	44.09
	> 24,500	0	0	0.04	0.12	0.52	0.86	1.20	9.38	0	0	0
Total Percent		100	100	100	100	100	100	100	100	100	100	100
Distance (nm)		25803	186,457	293,877	365,681	253,565	85,008	20,554	5932	1701	1841	1031

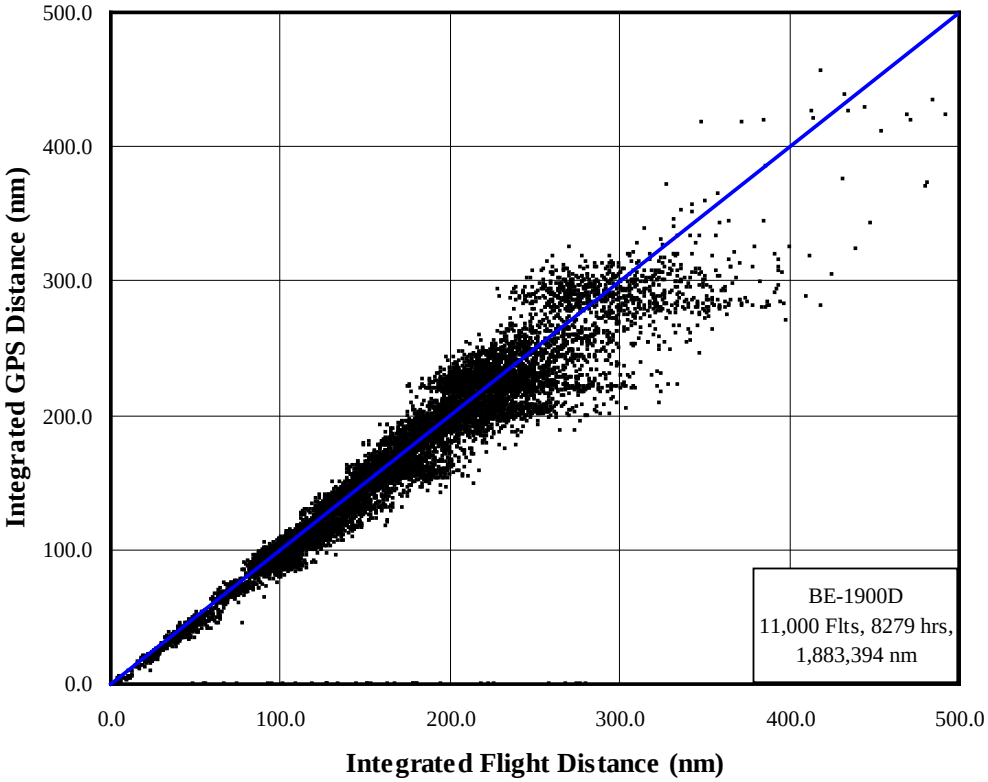

Figure A-1. Correlation of GPS-integrated and airspeed-integrated flight distance

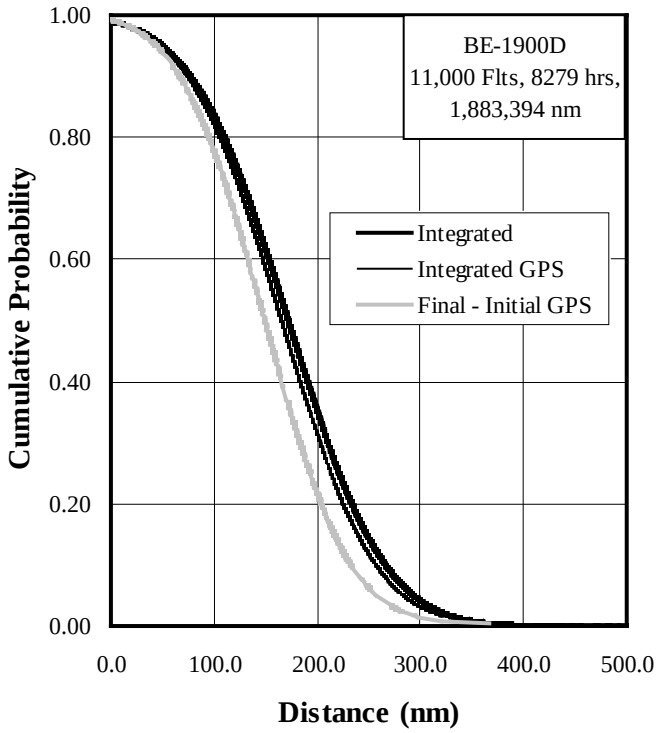

Figure A-2. Cumulative probability of flight distance

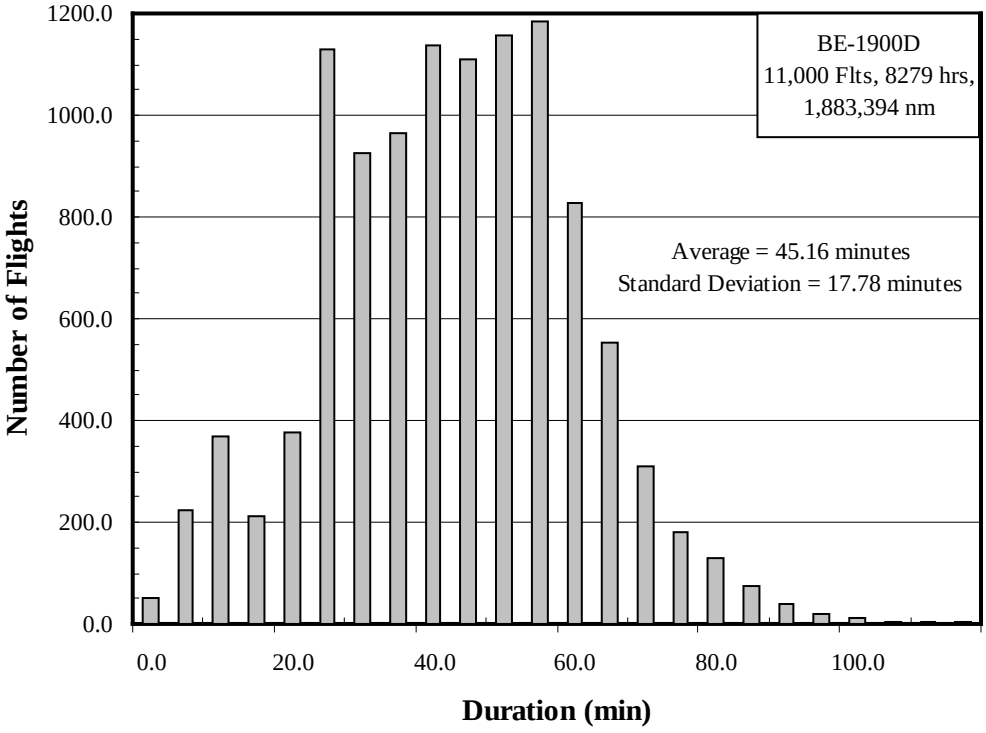

Figure A-3. Number of flights vs. flight duration

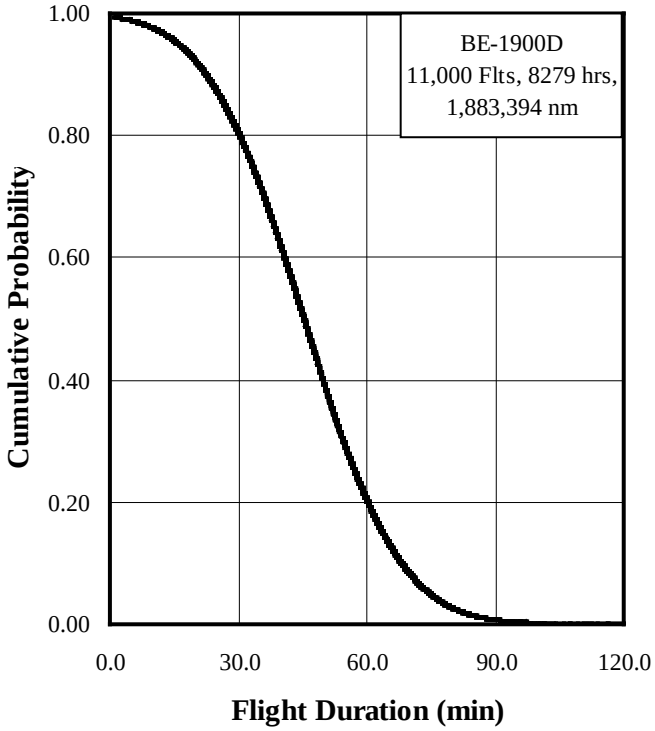

Figure A-4. Cumulative probability of flight duration

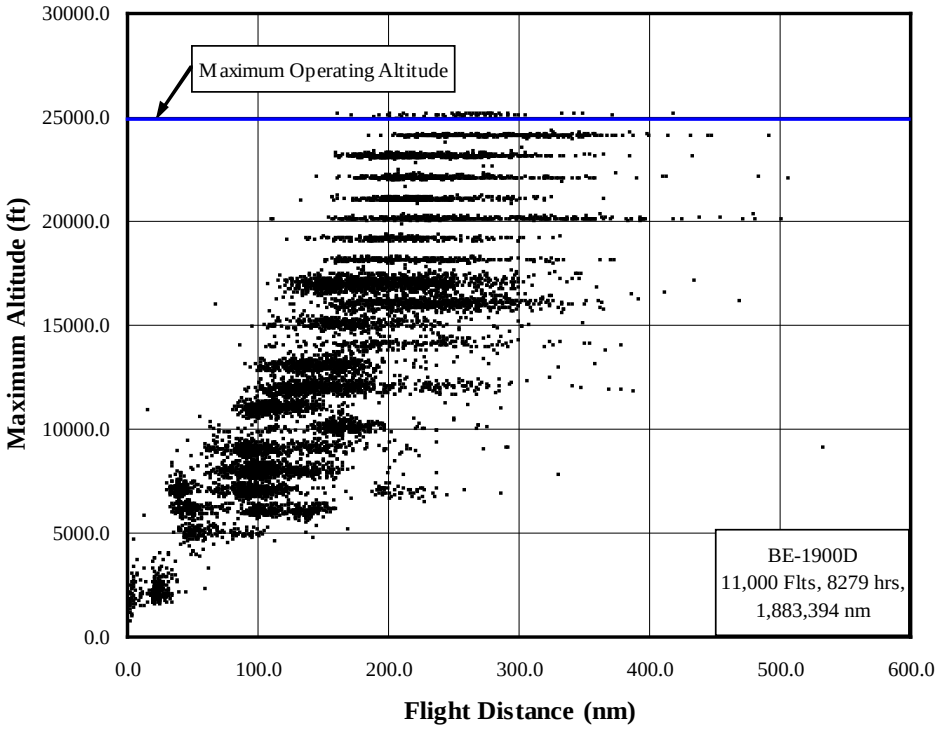

Figure A-5. Correlation of maximum altitude and coincident flight distance, all flight phases

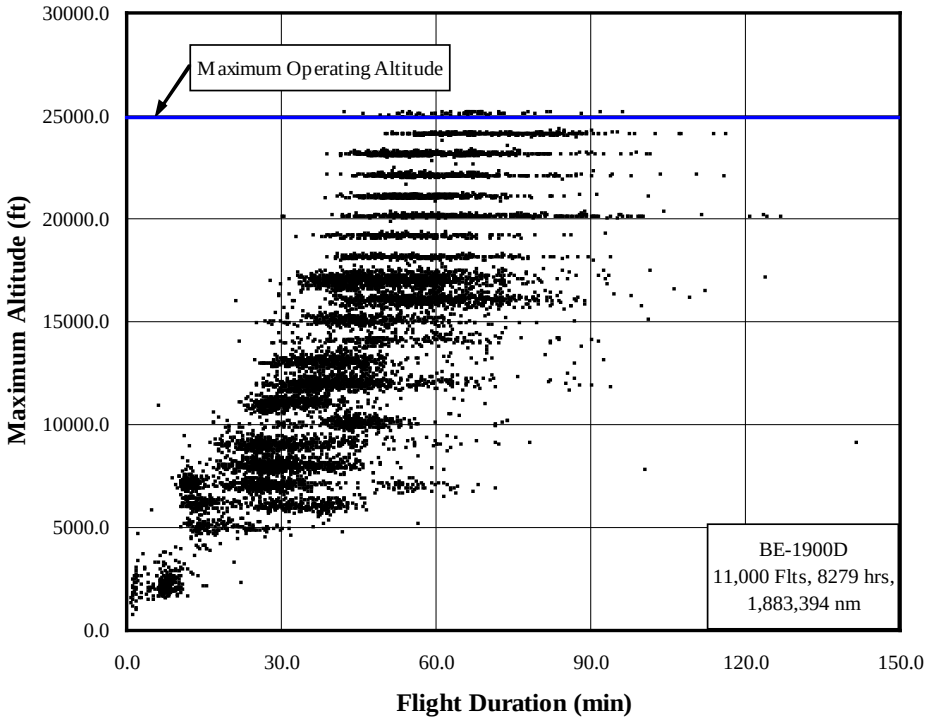

Figure A-6. Correlation of maximum altitude and coincident flight duration, all flight phases

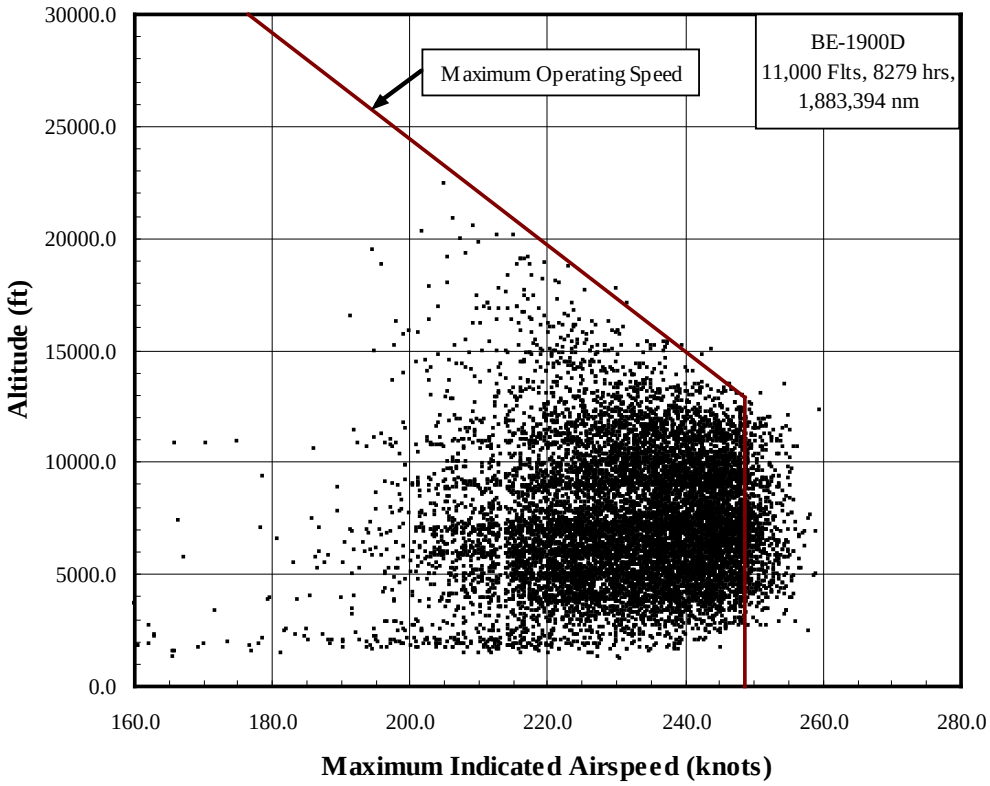

Figure A-7. Coincident altitude at maximum indicated airspeed, all flight phases

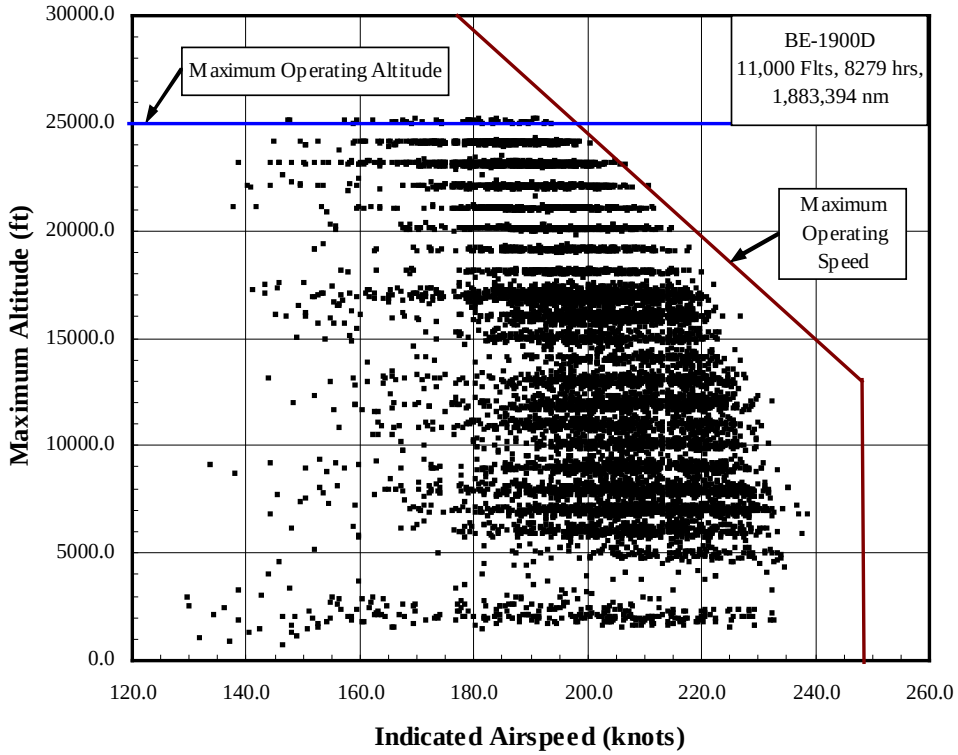

Figure A-8. Coincident indicated airspeed at maximum altitude, all flight phases

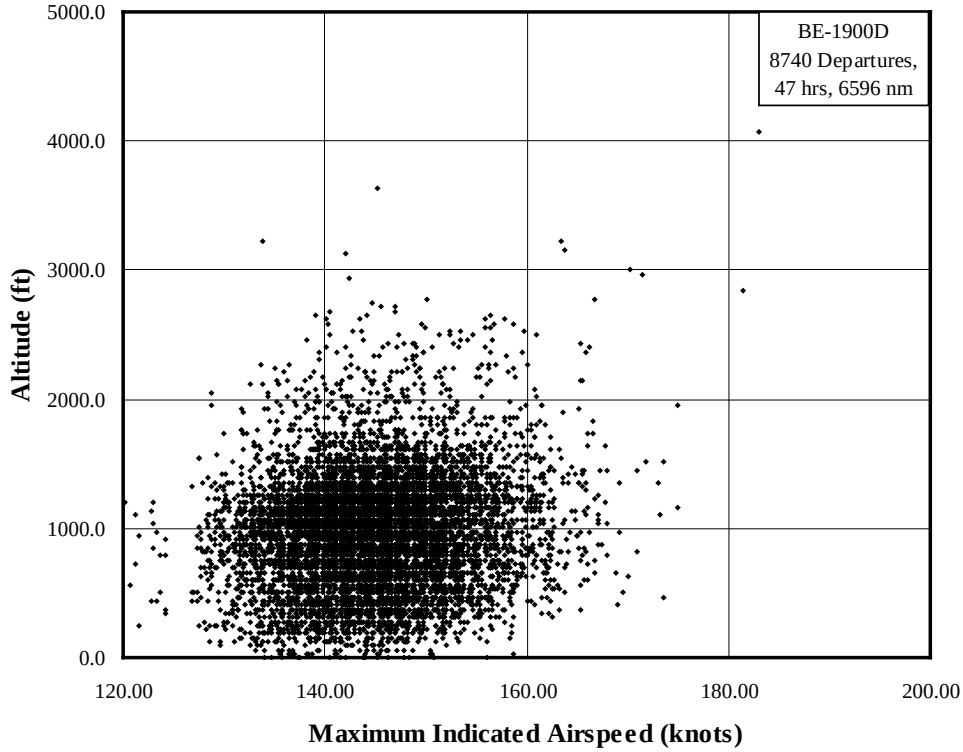

Figure A-9. Maximum airspeed and coincident altitude during departure

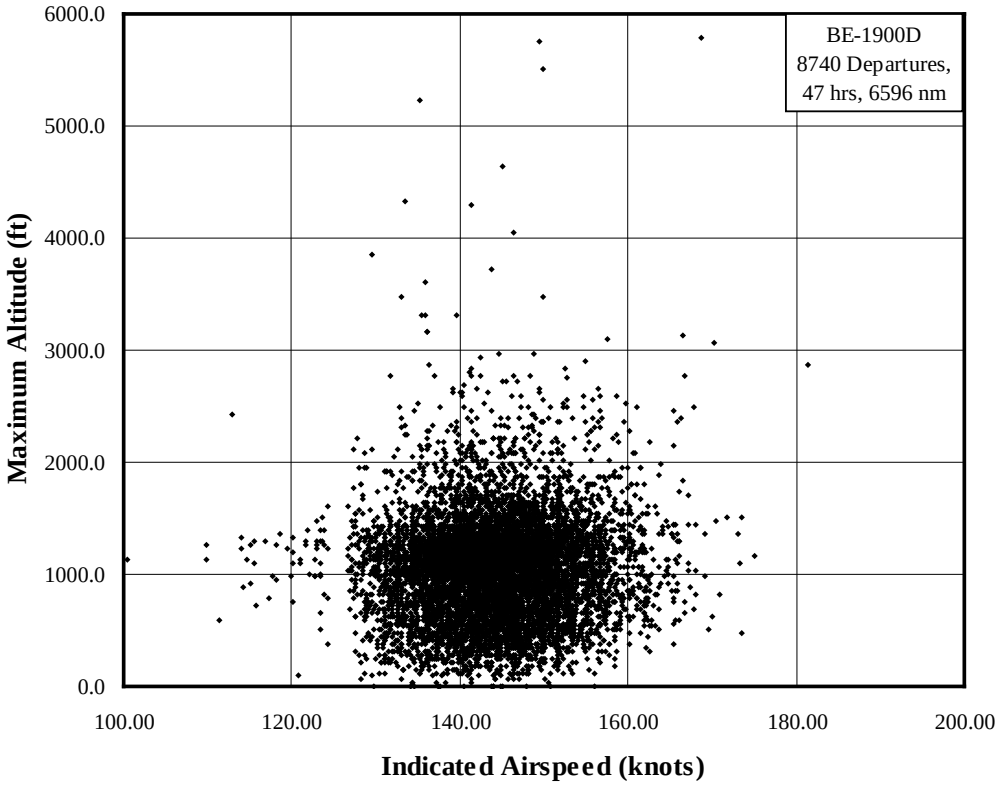

Figure A-10. Maximum altitude and coincident airspeed during departure

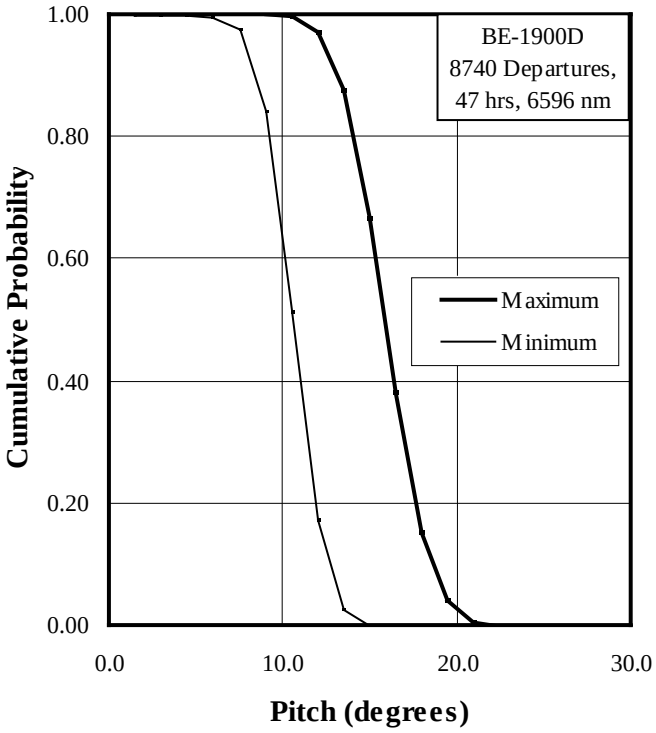

Figure A-11. Cumulative probability of maximum and minimum pitch angle during departure

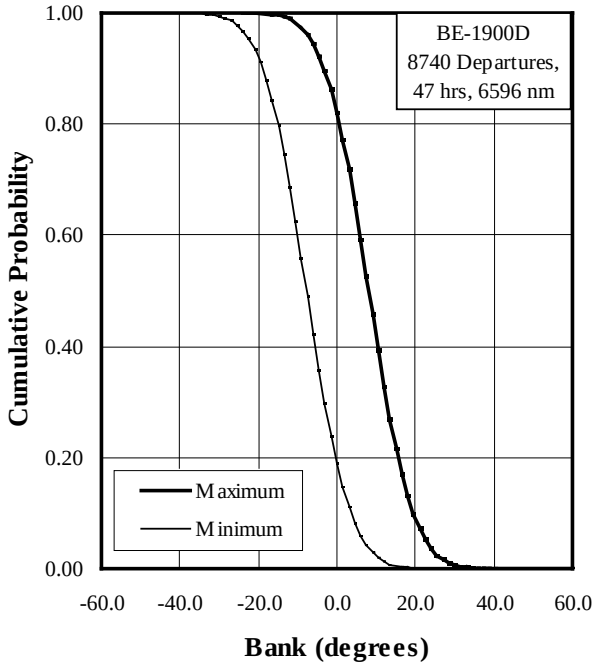

Figure A-12. Cumulative probability of maximum and minimum bank angle during departure

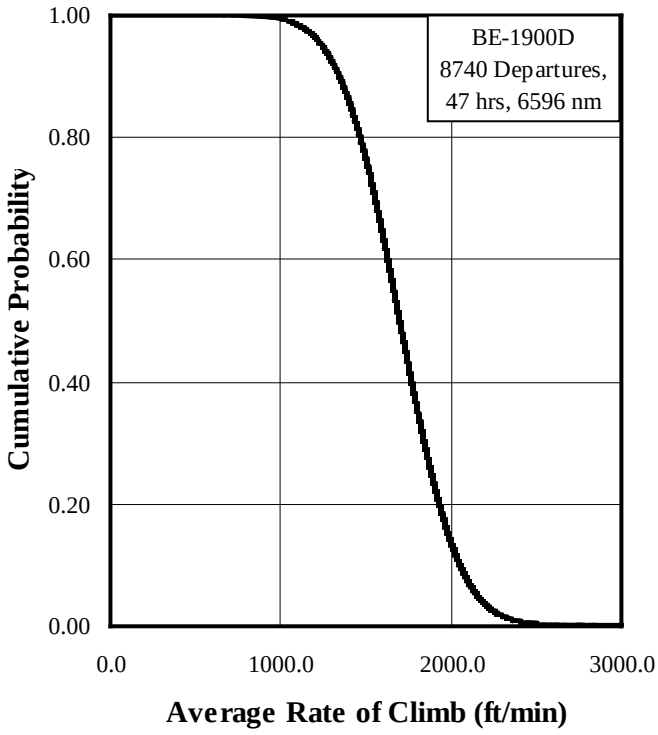

Figure A-13. Cumulative probability of average rate of climb during departure

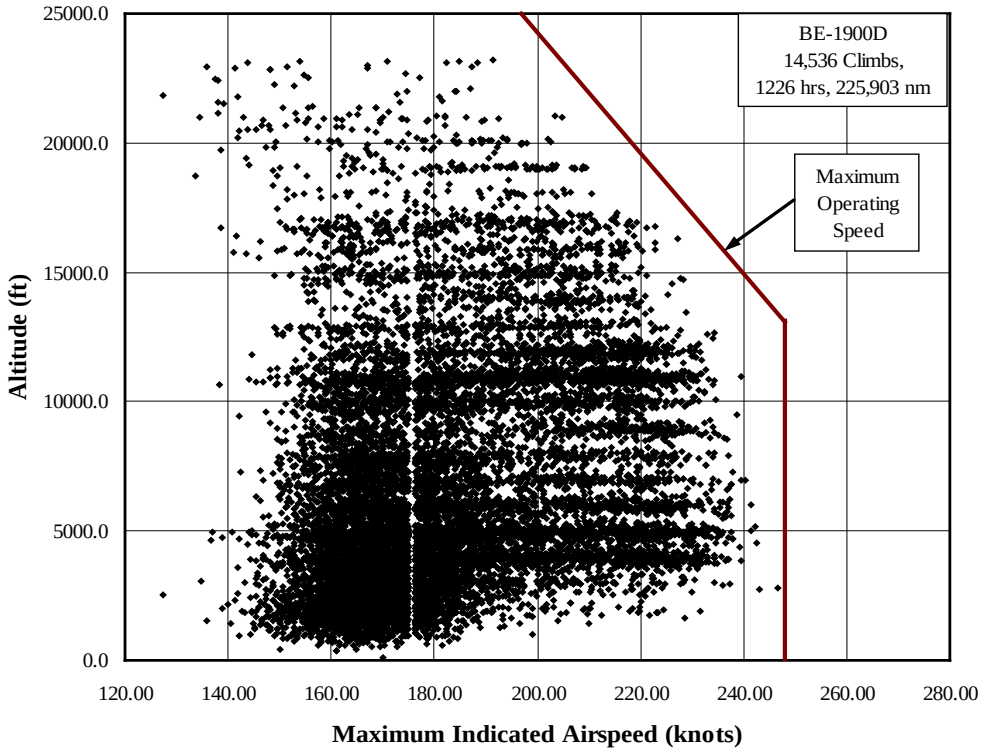

Figure A-14. Maximum airspeed and coincident altitude during climb

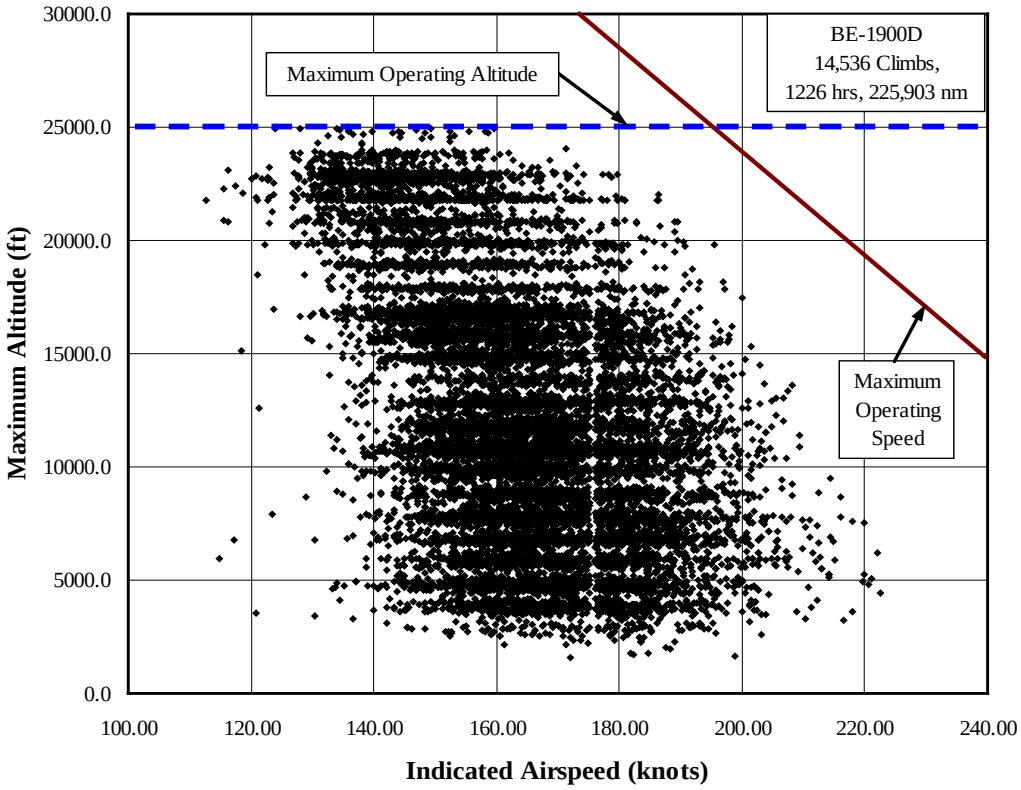

Figure A-15. Maximum altitude and coincident airspeed during climb

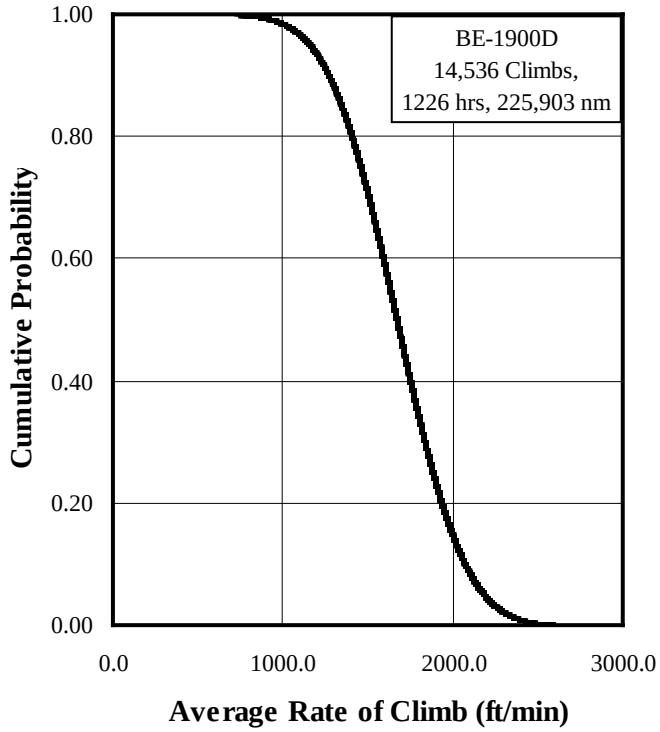

Figure A-16. Cumulative probability of average rate of climb during climb

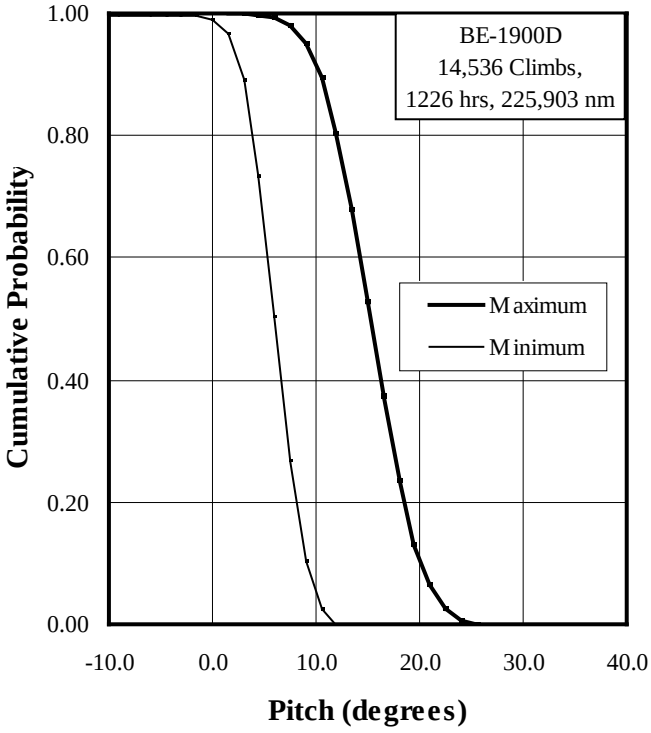

Figure A-17. Cumulative probability of the pitch angle during climb

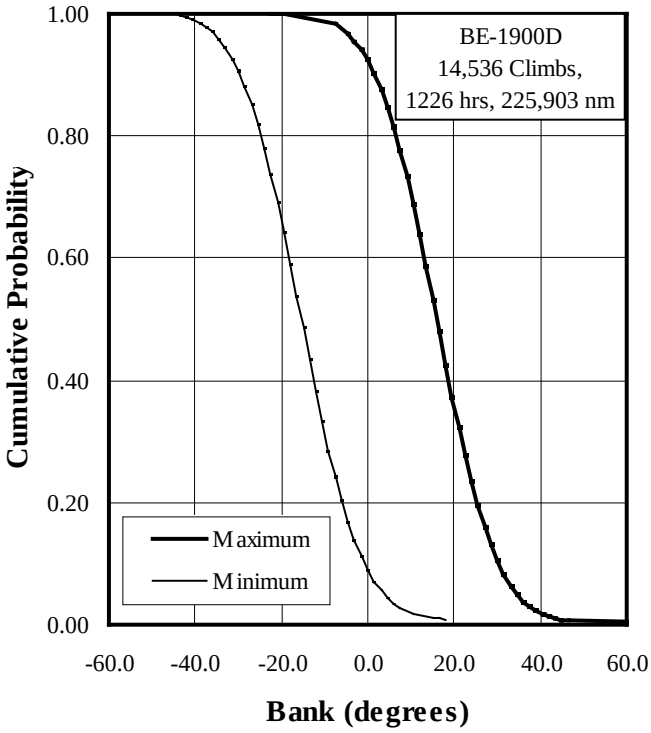

Figure A-18. Cumulative probability of the bank angle during climb

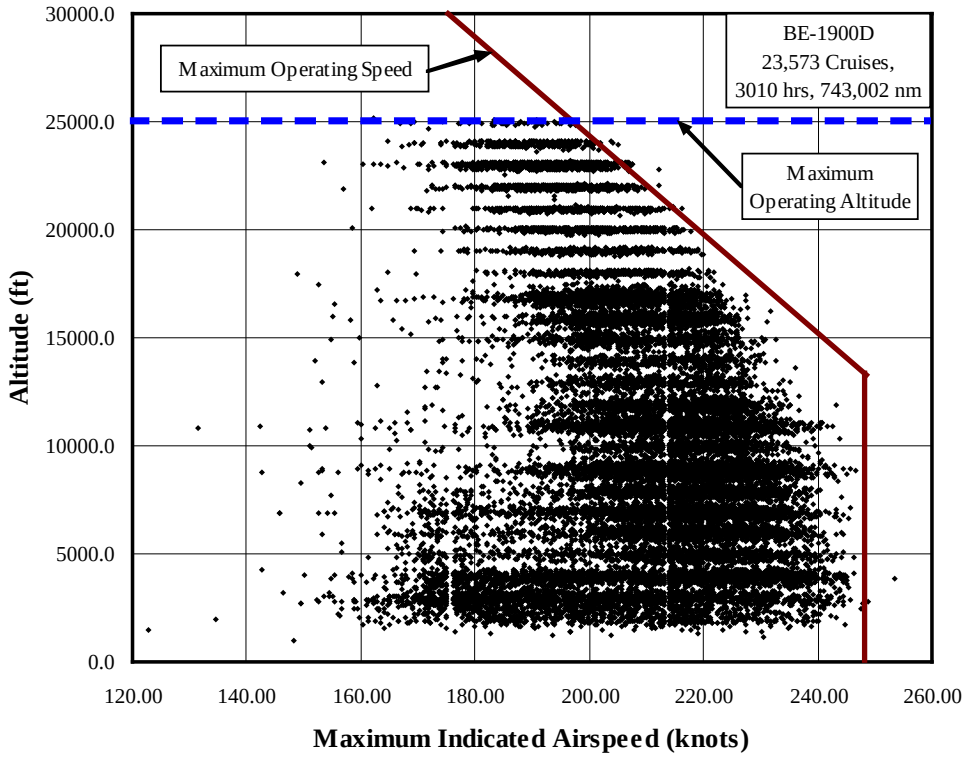

Figure A-19. Maximum airspeed and coincident altitude during cruise

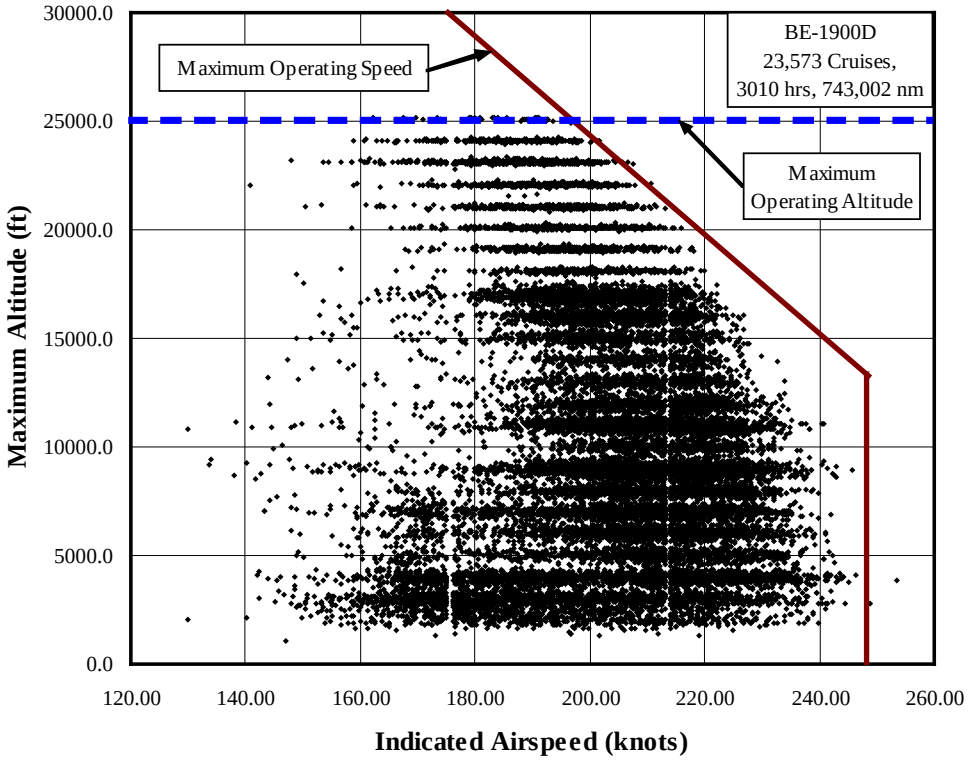

Figure A-20. Maximum altitude and coincident airspeed during cruise

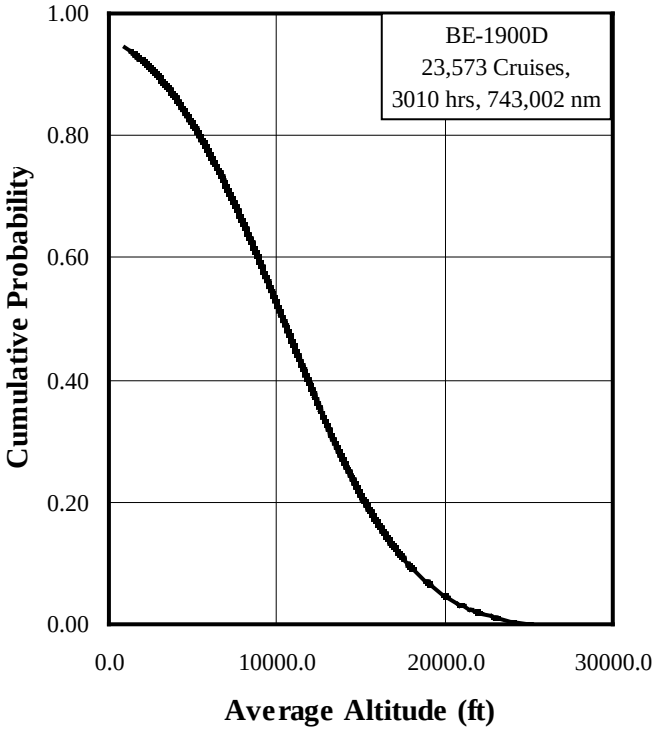

Figure A-21. Cumulative probability of altitude during cruise

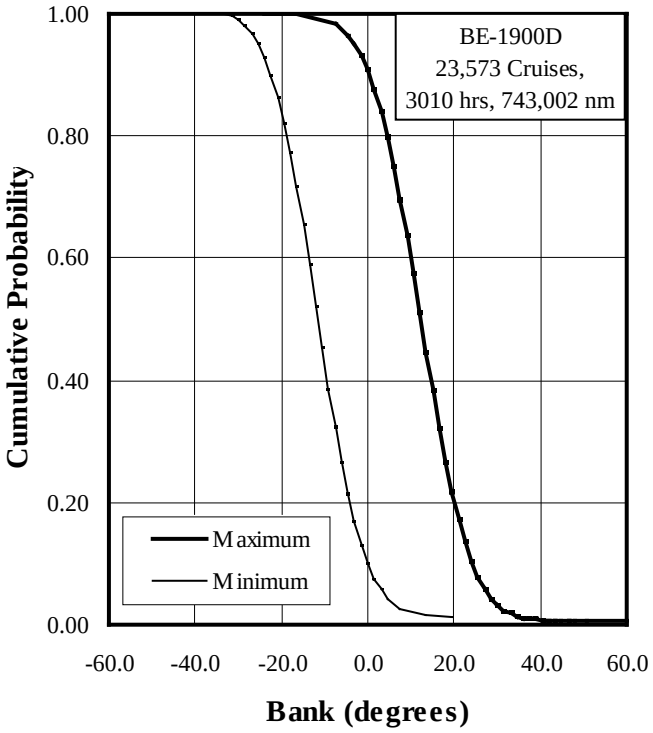

Figure A-22. Cumulative probability of bank angle during cruise

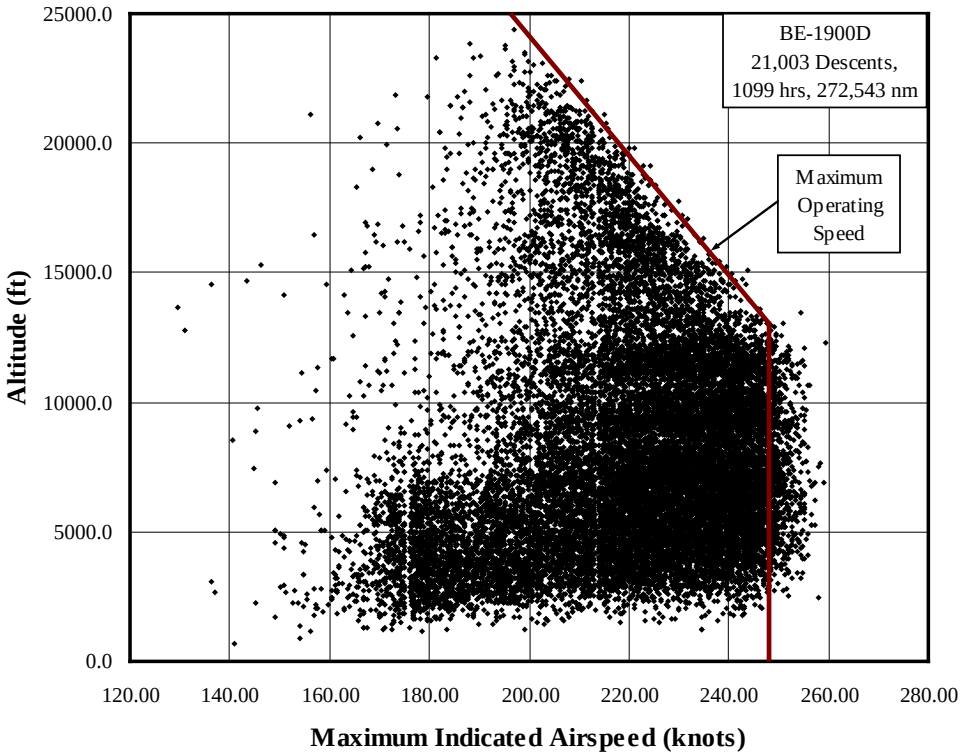

Figure A-23. Maximum airspeed and coincident altitude during descent

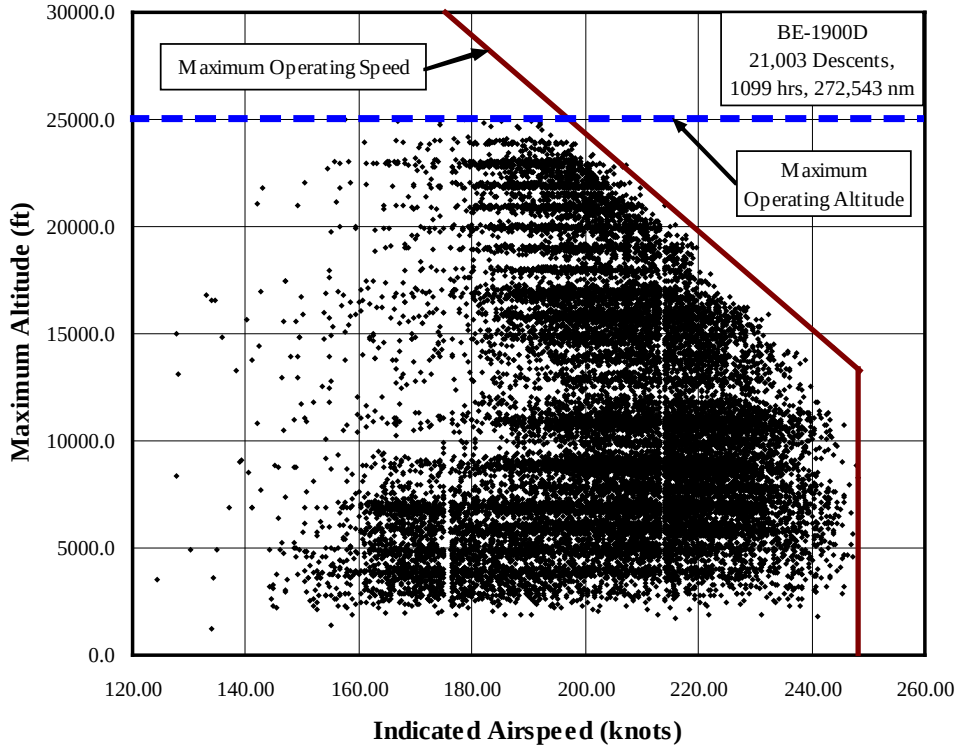

Figure A-24. Maximum altitude and coincident airspeed during descent

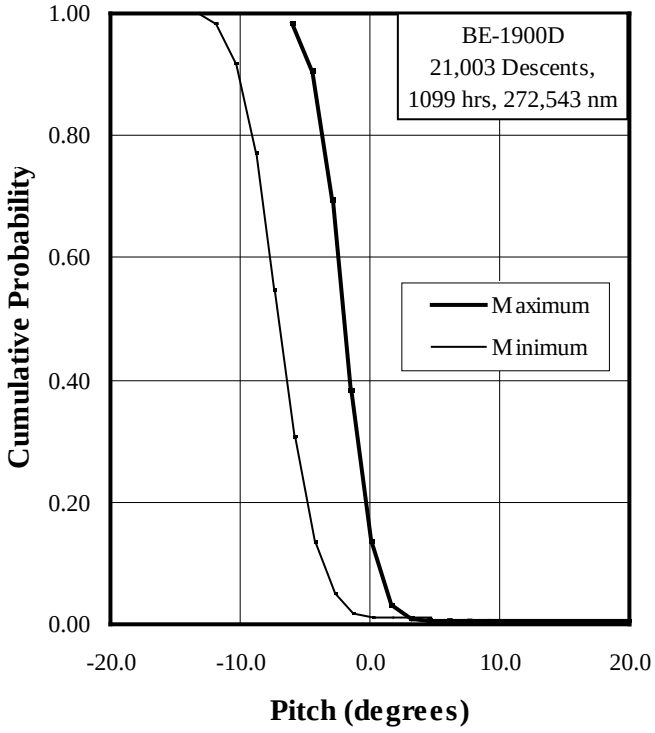

Figure A-25. Cumulative probability of pitch angle during descent

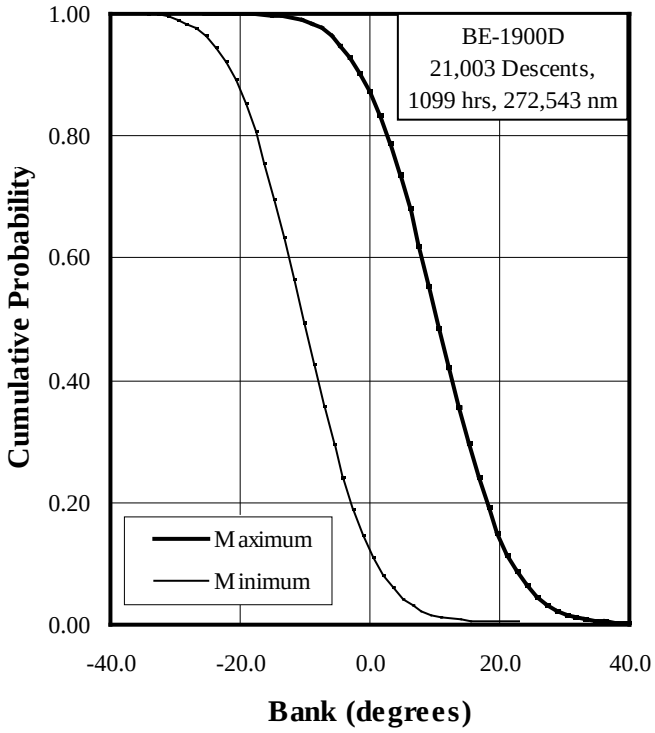

Figure A-26. Cumulative probability of bank angle during descent

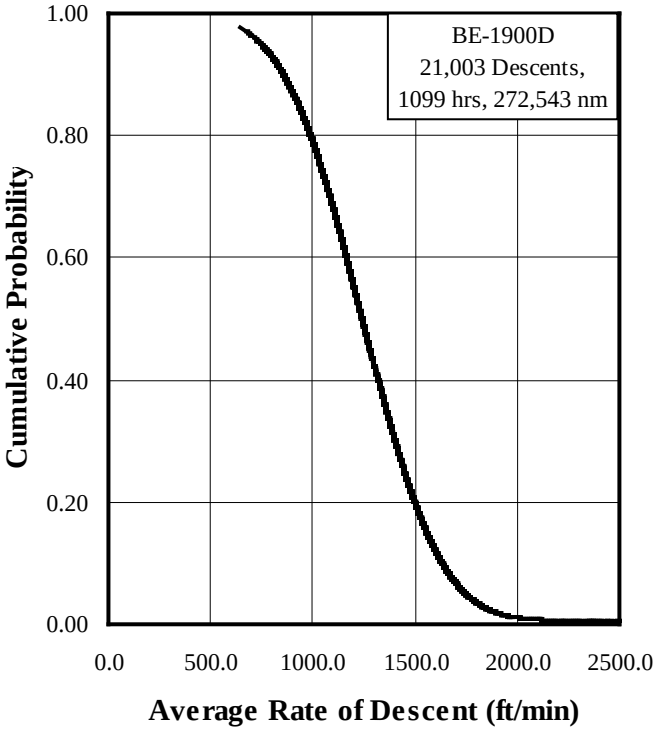

Figure A-27. Cumulative probability of average descent rate during descent

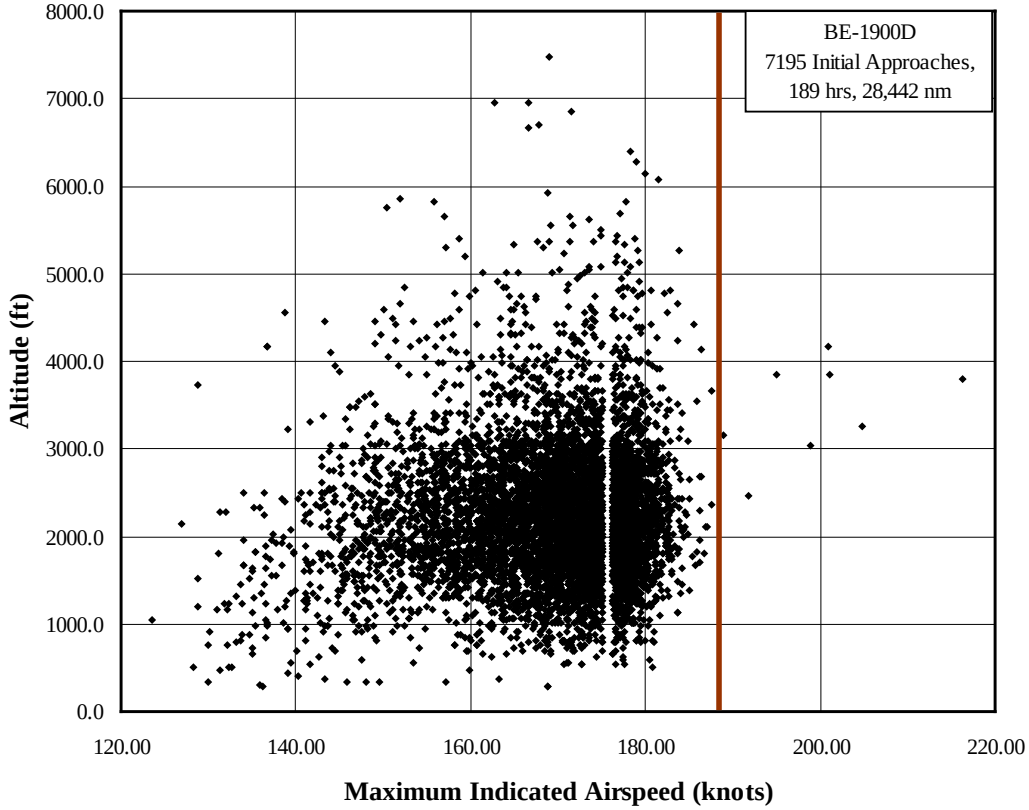

Figure A-28. Maximum indicated airspeed and coincident altitude during initial approach

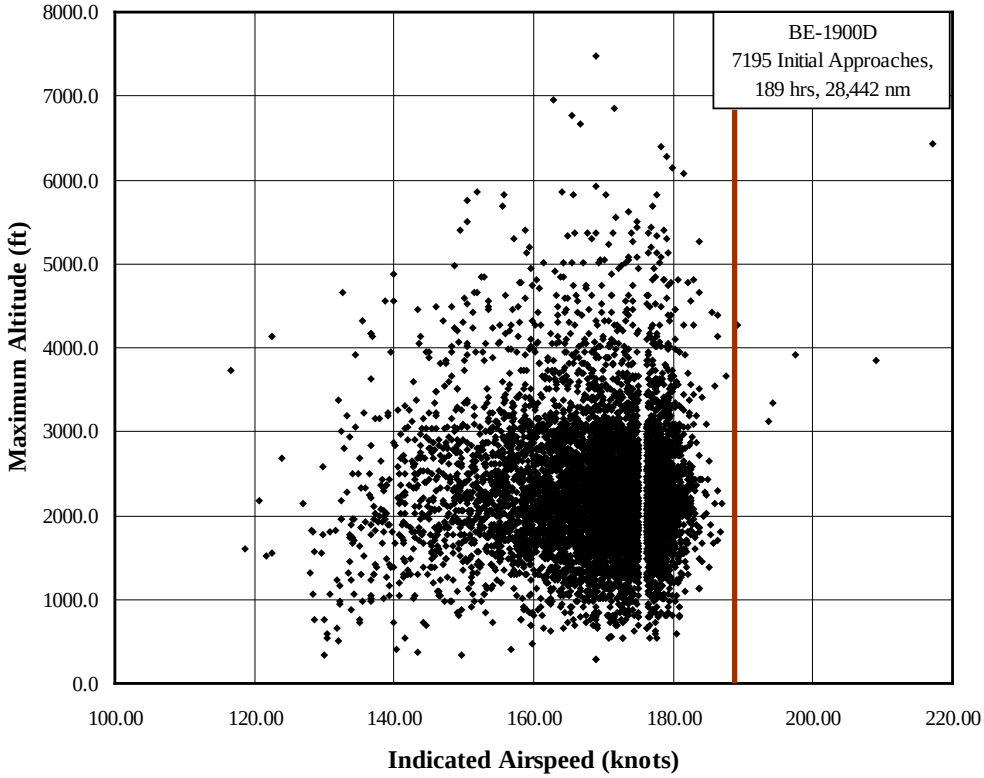

Figure A-29. Maximum altitude and coincident indicated airspeed during initial approach

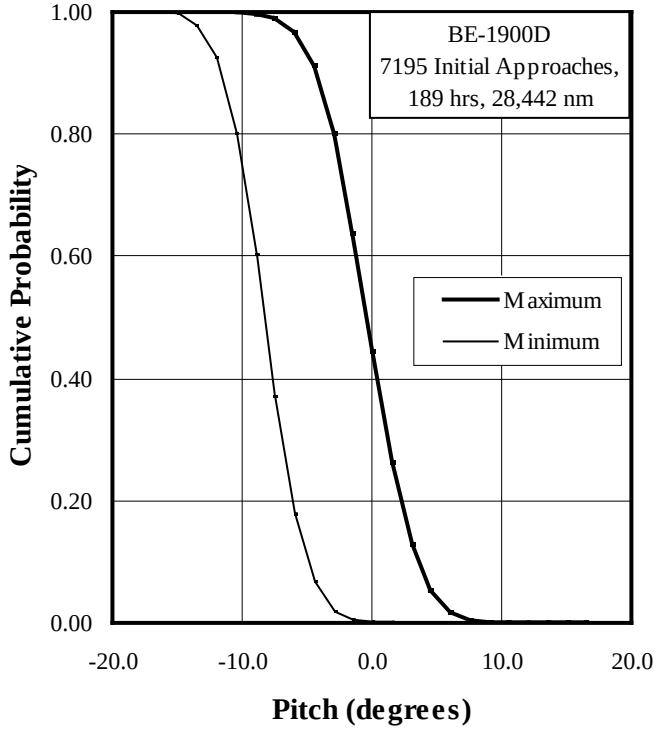

Figure A-30. Cumulative probability of pitch angle during initial approach

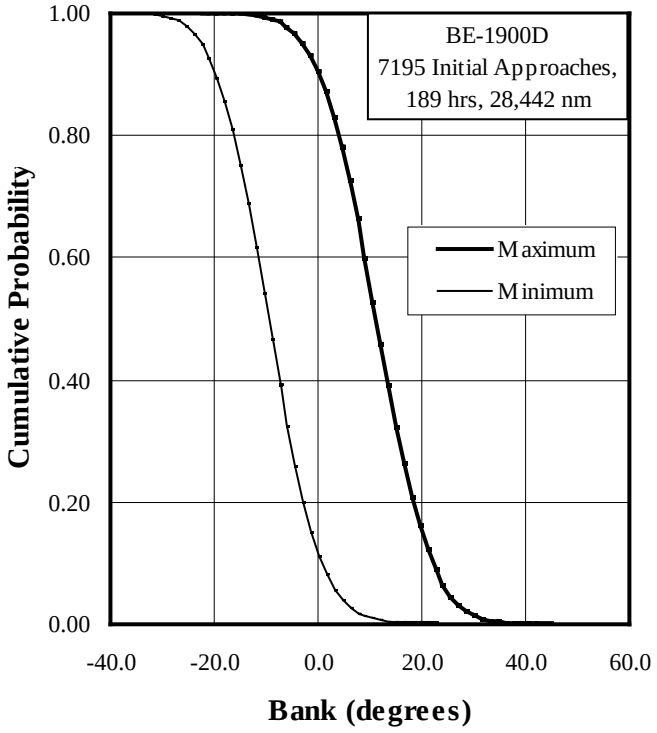

Figure A-31. Cumulative probability of bank angle during initial approach

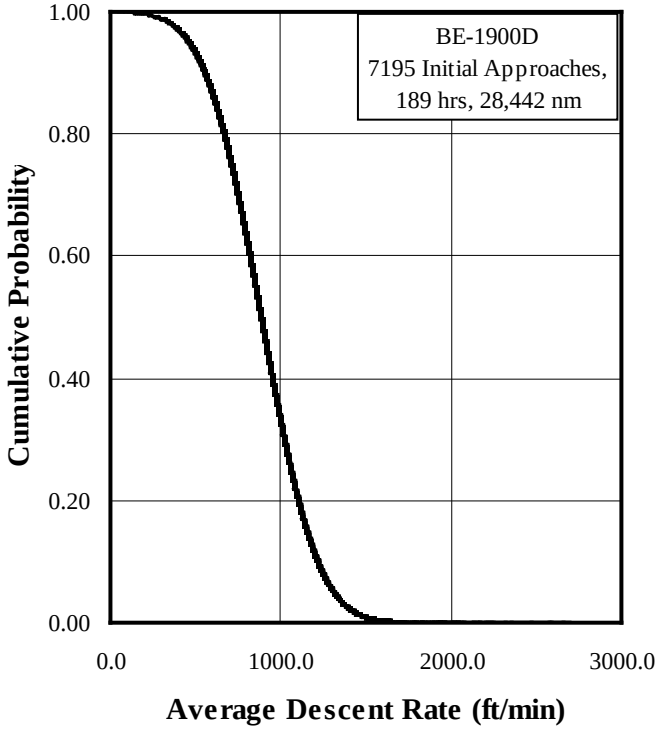

Figure A-32. Cumulative probability of average descent rate during initial approach

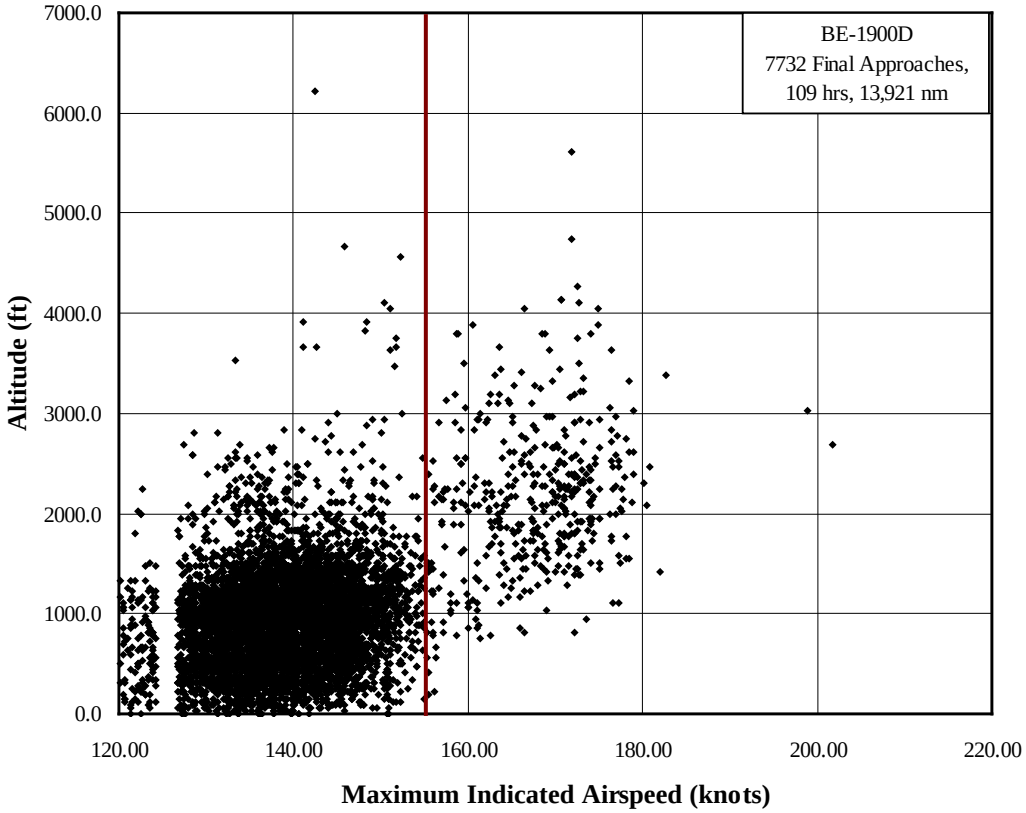

Figure A-33. Maximum indicated airspeed and coincident altitude during final approach

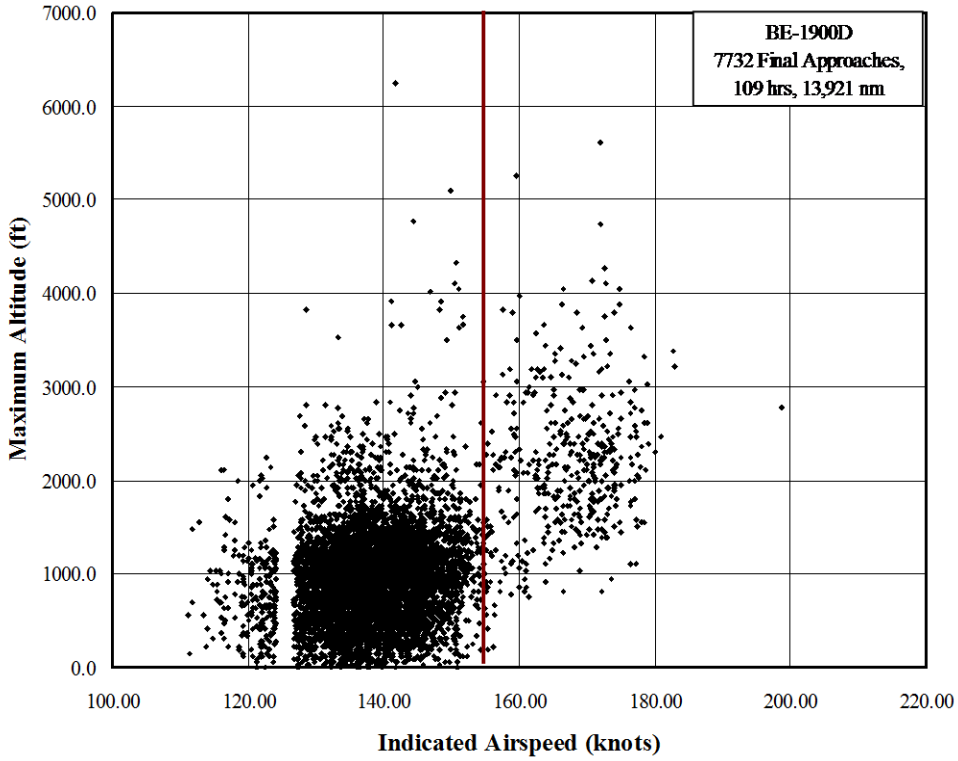

Figure A-34. Maximum altitude and coincident indicated altitude during final approach

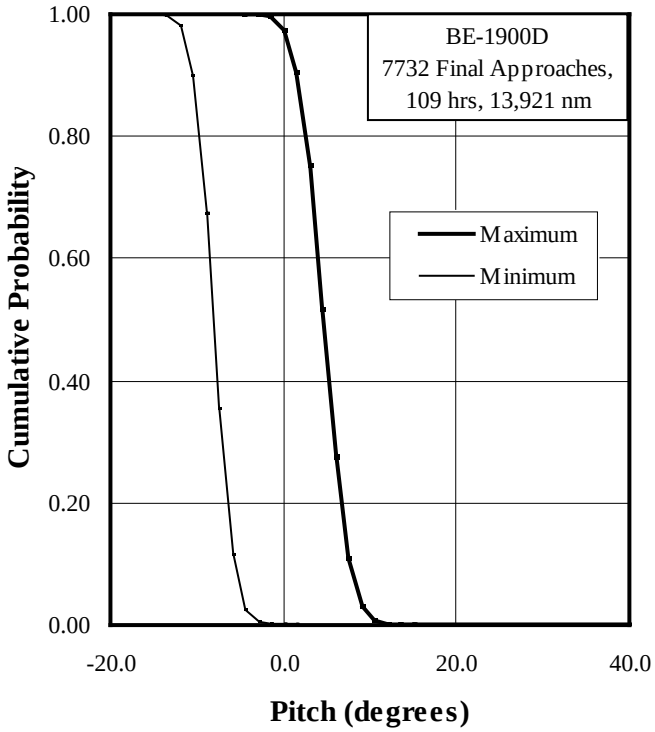

Figure A-35. Cumulative probability of pitch angle during final approach

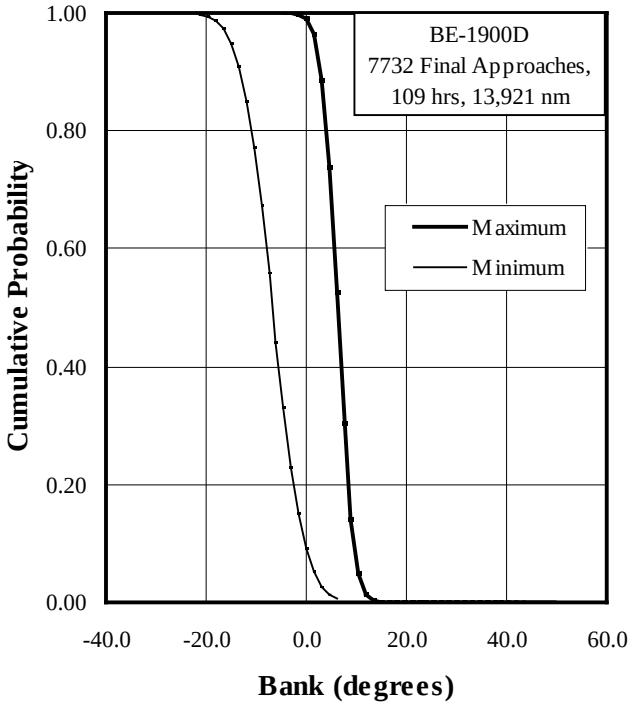

Figure A-36. Cumulative probability of bank angle during final approach

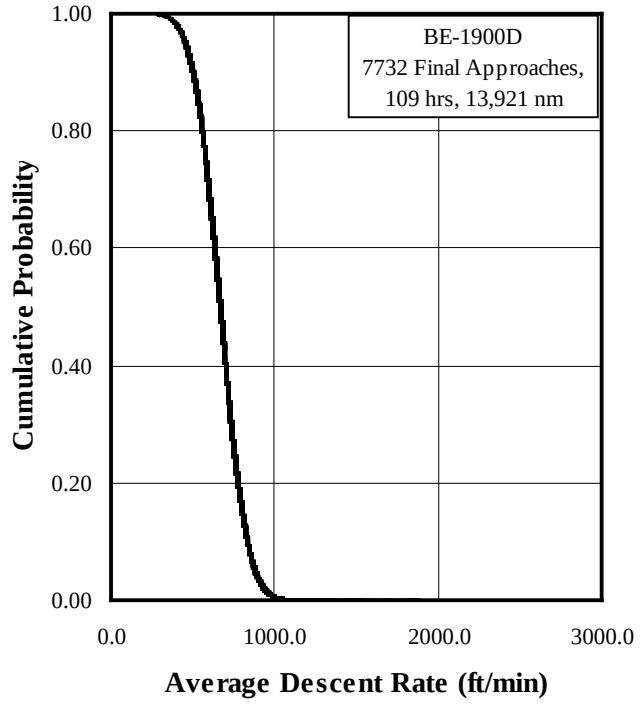

Figure A-37. Cumulative probability of average descent rate during final approach

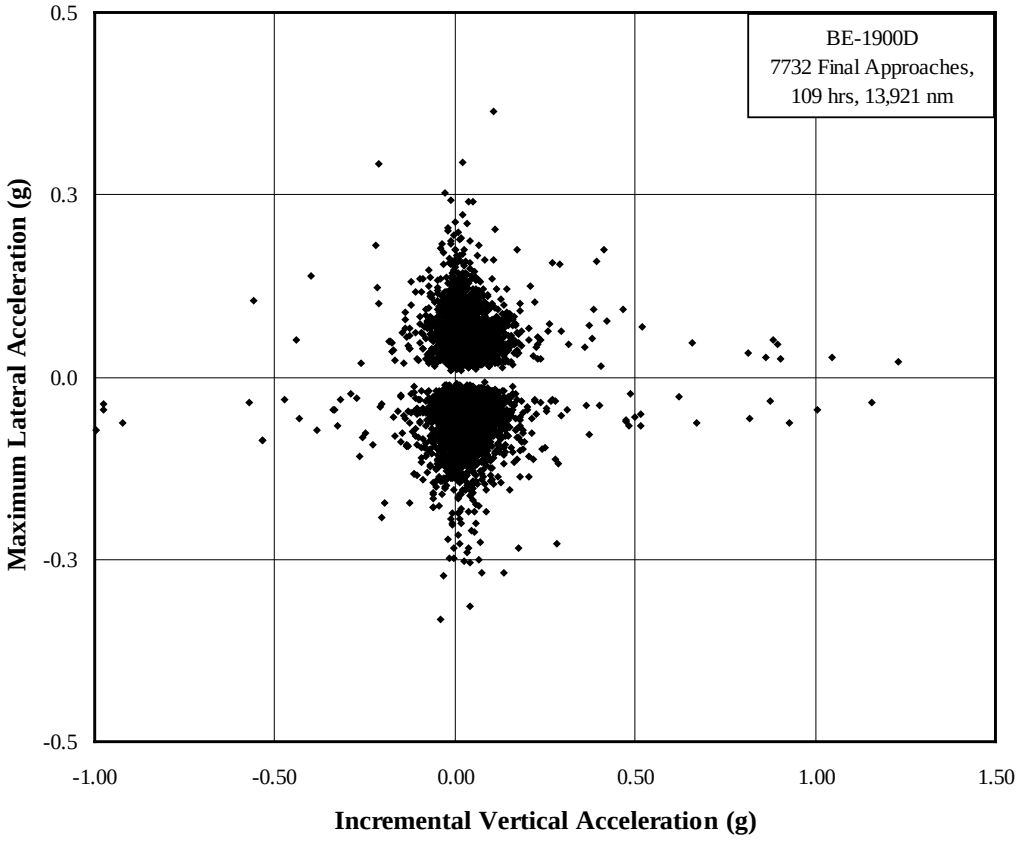

Figure A-38. Maximum lateral load factor vs. coincident incremental vertical load factor during final approach (within 10 seconds of touchdown)

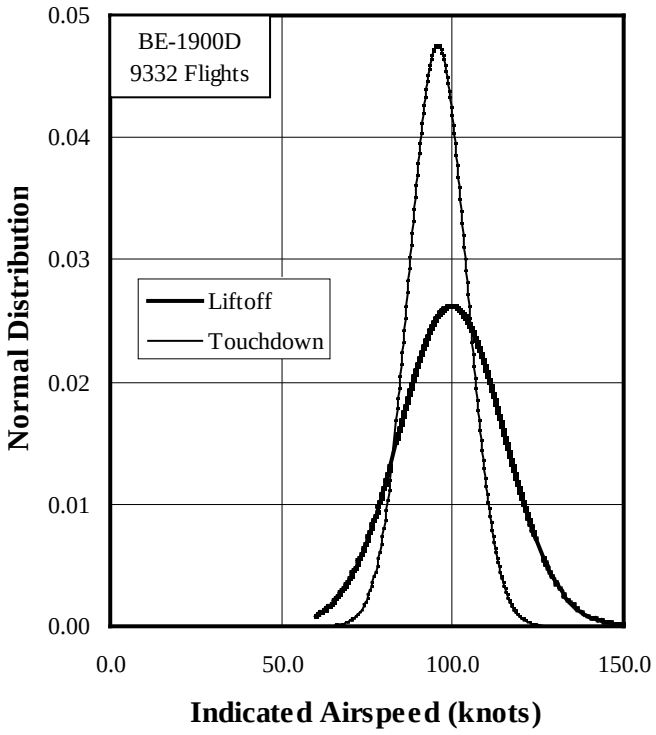

Figure A-39. Probability distribution of airspeed at liftoff and touchdown

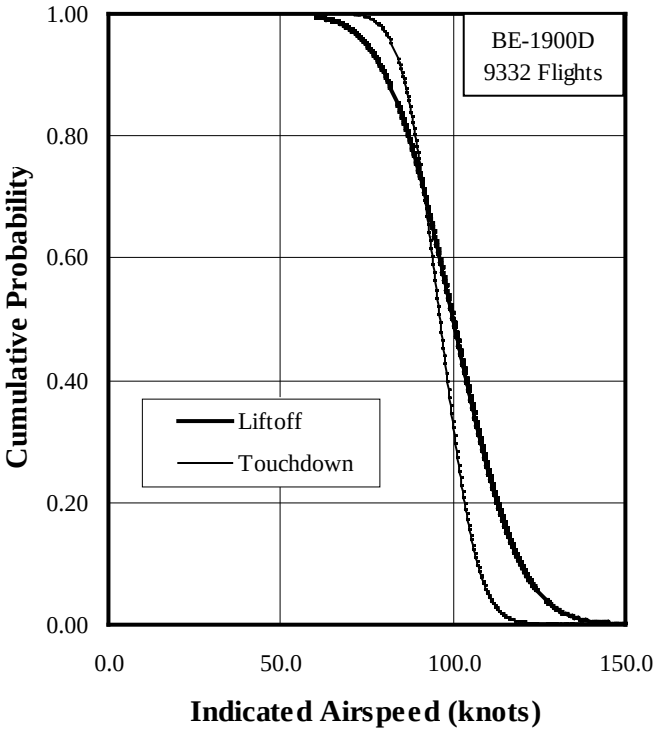

Figure A-40. Cumulative probability of airspeed at liftoff and touchdown

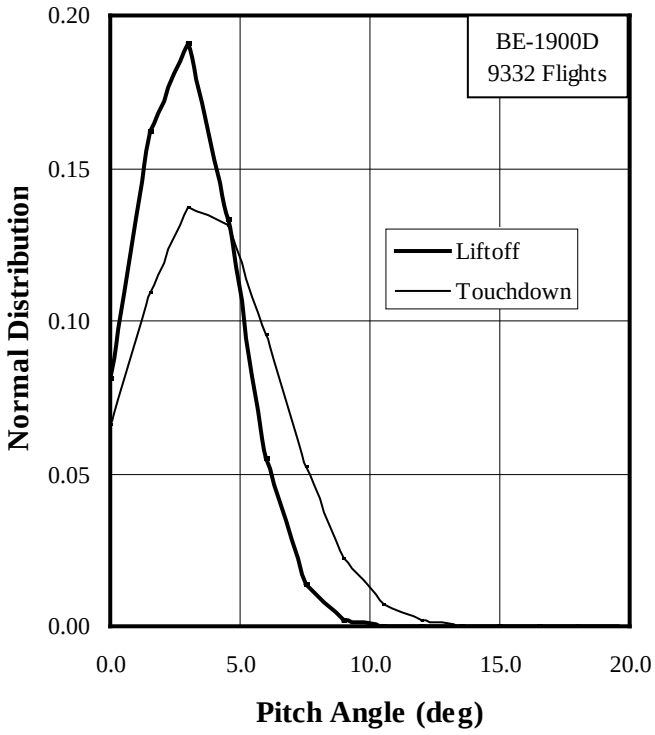

Figure A-41. Probability distribution of pitch angle at liftoff and touchdown

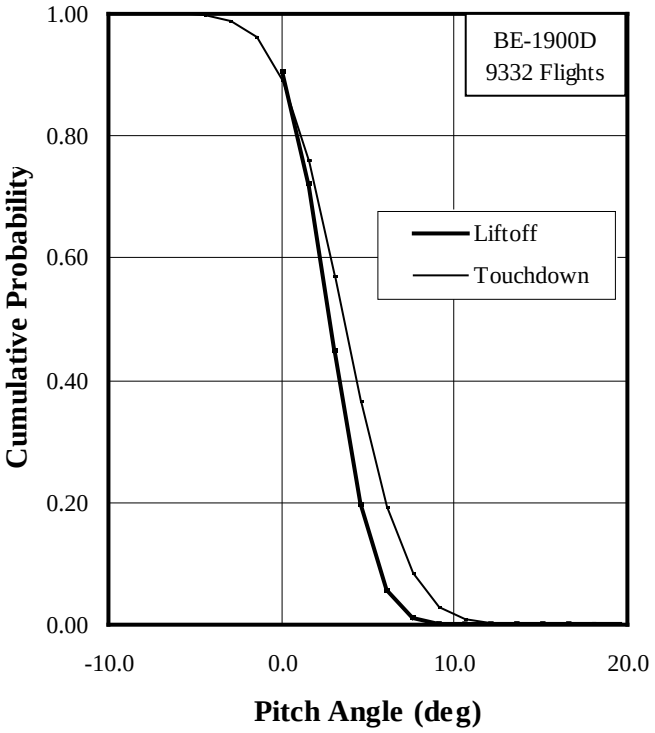

Figure A-42. Cumulative probability of pitch angle at liftoff and touchdown

Table A-3. Ground-air-ground cycle occurrences of maximum and minimum incremental vertical load factor (good data only)

BE-1900D 9356 Flts, 6958 hrs, 1,582,690 nmi		Maximum Incremental Vertical Load Factor (g)						
		-1.0 – -0.5	-0.5 – 0	0 – 0.5	0.5 – 1.0	1.0 – 1.5	1.5 – 2.0	Total
Minimum Incremental Vertical Load Factor (g)	-1.75 – -1.5	0.01	0.00	0.02	0.01	0.00	0.00	0.04
	-1.5 – -1.25	0.03	0.00	0.04	0.03	0.01	0.00	0.11
	-1.25 – -1.0	0.01	0.01	0.12	0.11	0.02	0.00	0.27
	-1.0 – -0.75	0.00	0.05	0.31	1.18	0.15	0.00	1.69
	-0.75 – -0.5	0.00	0.07	5.22	7.36	0.26	0.03	12.94
	-0.5 – -0.25	0.00	0.02	49.48	9.28	0.53	0.21	59.52
	-0.25 – 0	0.00	0.00	23.23	1.32	0.45	0.29	25.29
	0 – 0.25	0.00	0.00	0.00	0.10	0.01	0.01	0.12
	0.25 – 0.5	0.00	0.00	0.00	0.02	0.00	0.00	0.02
	Total	0.05	0.15	78.42	19.41	1.43	0.54	100.00

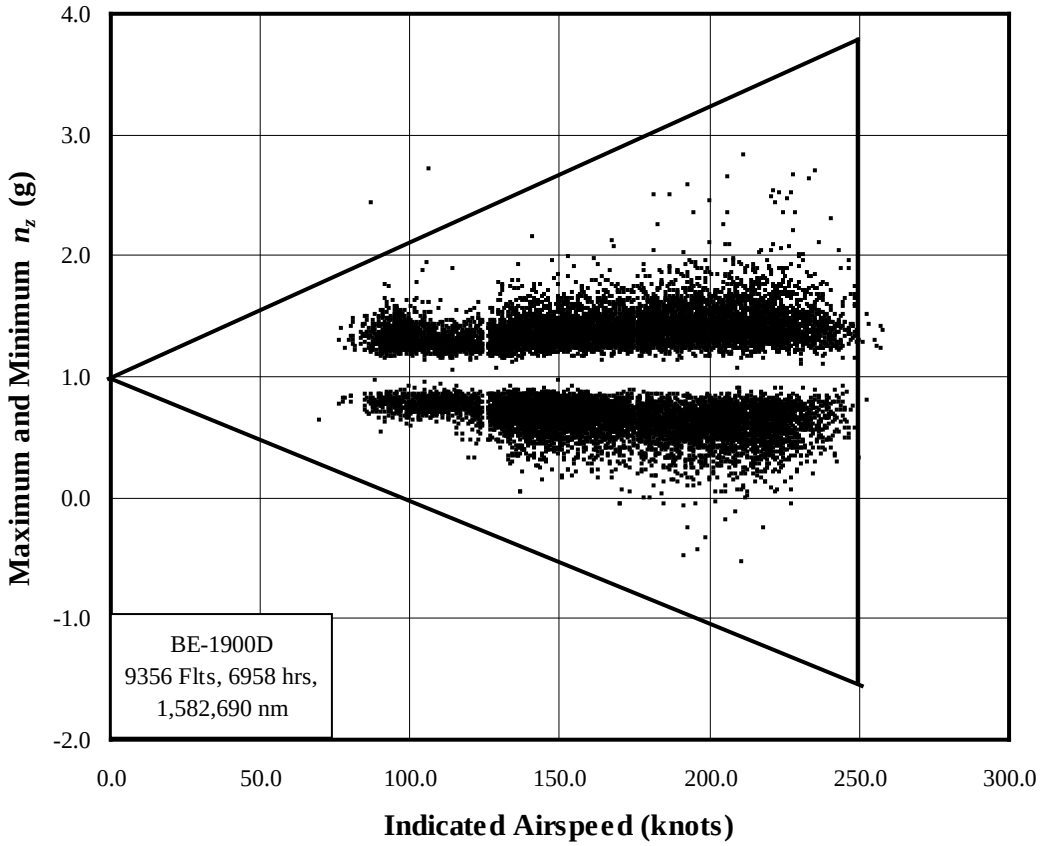

Figure A-43. V-n diagram for all phases (good data only)

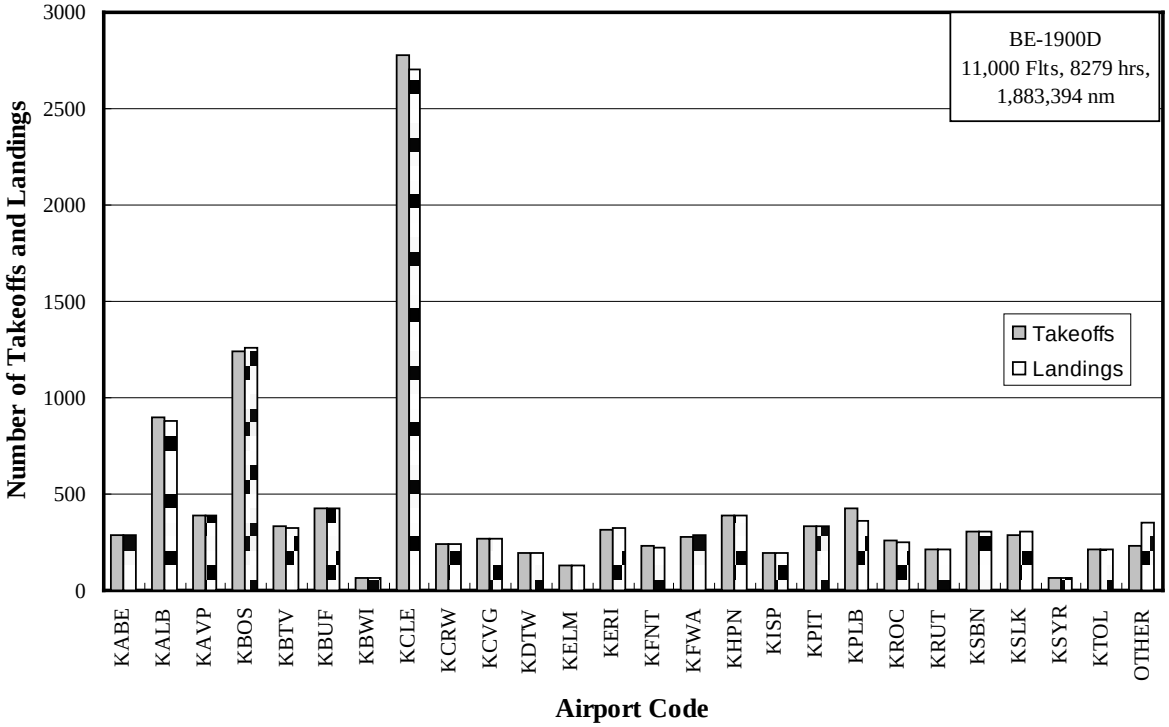

Figure A-44. Takeoff and landing occurrences per airport

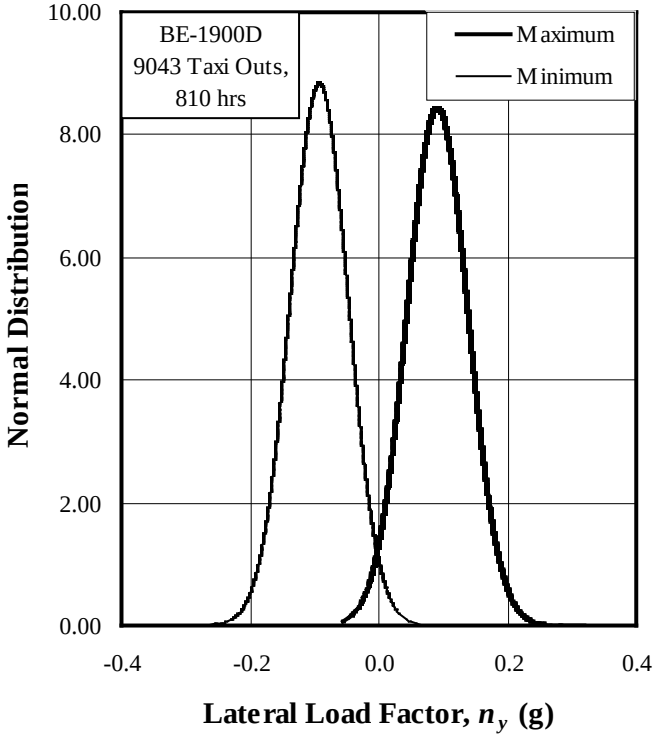

Figure A-45. Normal probability of maximum and minimum lateral load factor while taxiing out

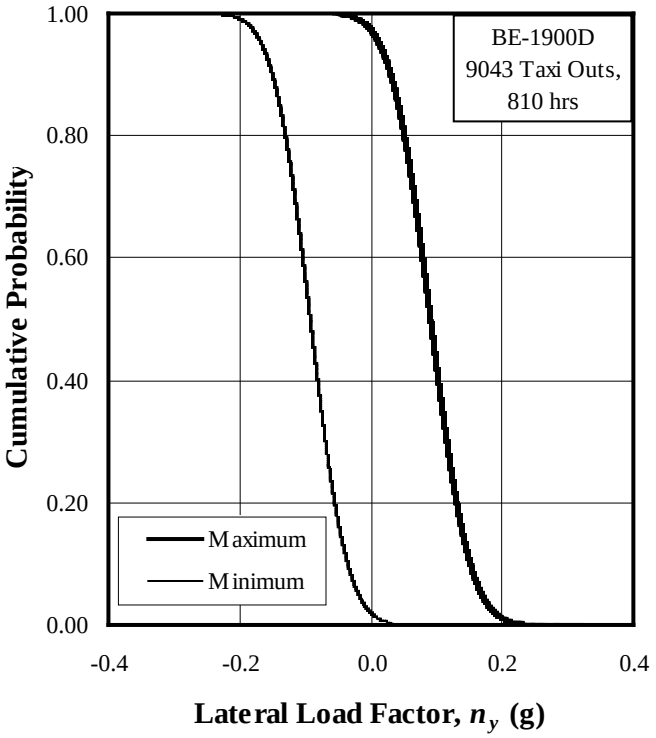

Figure A-46. Cumulative probability of maximum and minimum lateral load factor while taxiing out

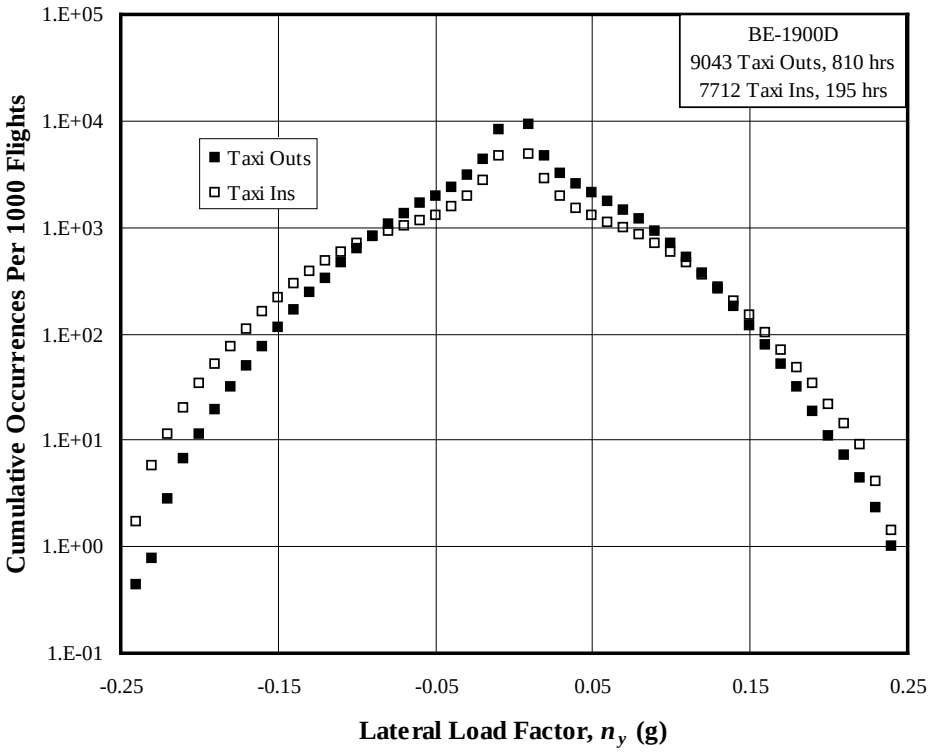

Figure A-47. Cumulative occurrences of lateral load factor per 1000 flights while taxiing

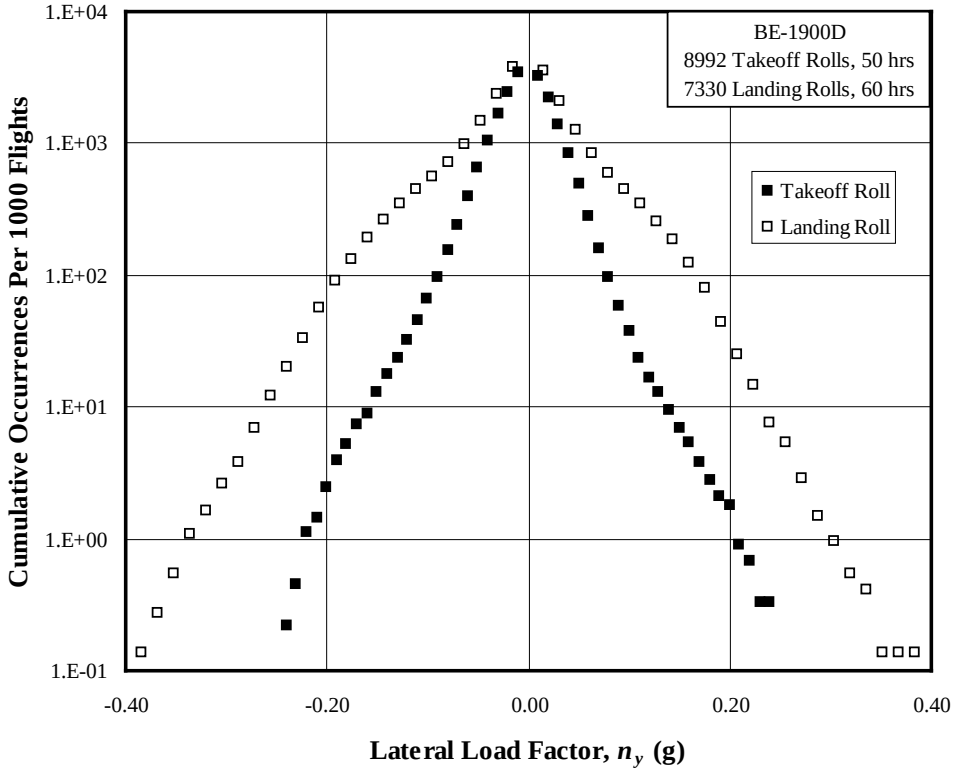

Figure A-48. Cumulative occurrences of lateral load factor per 1000 flights while on takeoff roll and landing roll

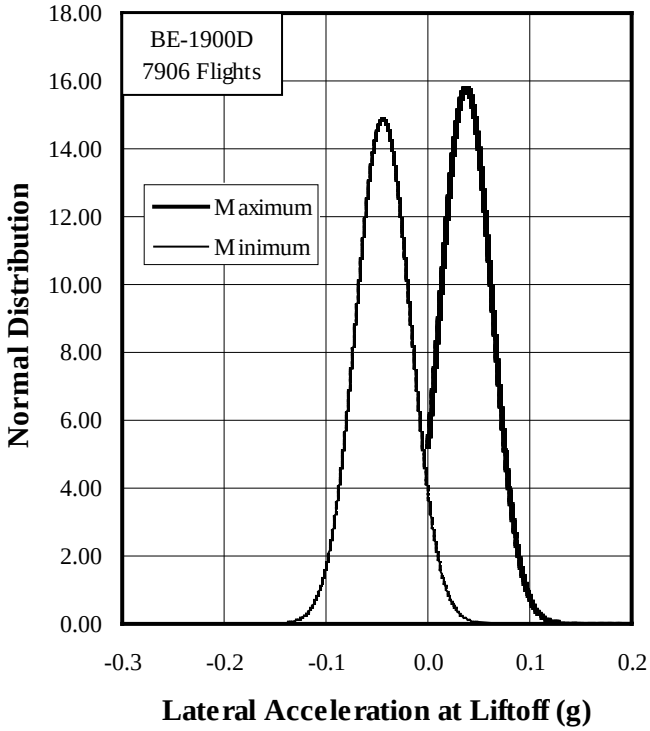

Figure A-49. Normal probability of maximum and minimum lateral load factor at liftoff

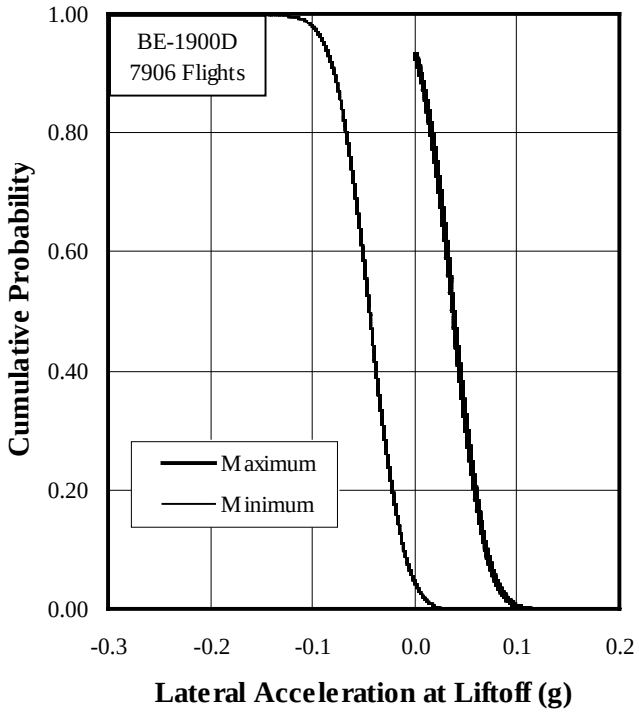

Figure A-50. Cumulative probability of maximum and minimum lateral load factor at liftoff

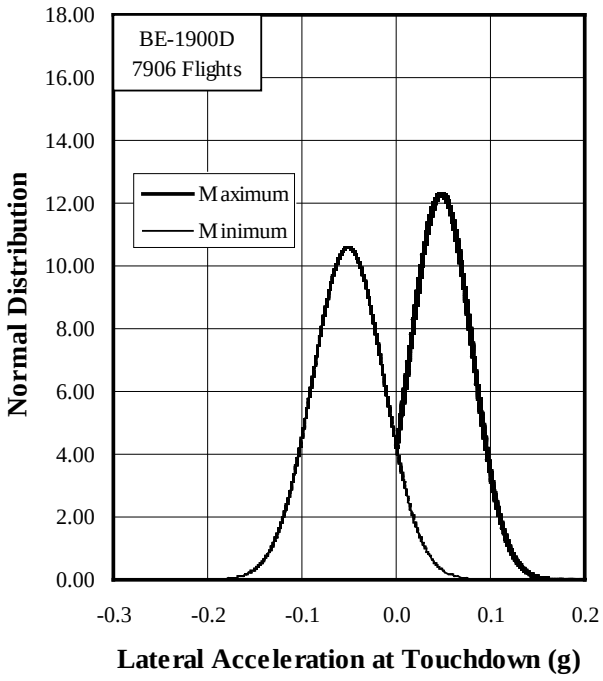

Figure A-51. Normal probability of maximum and minimum lateral load factor at touchdown

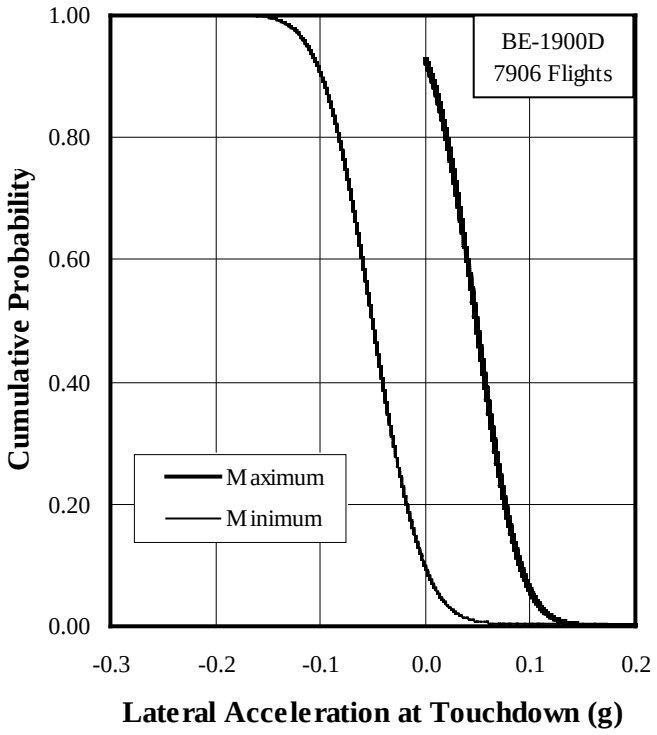

Figure A-52. Cumulative probability of maximum and minimum lateral load factor at touchdown

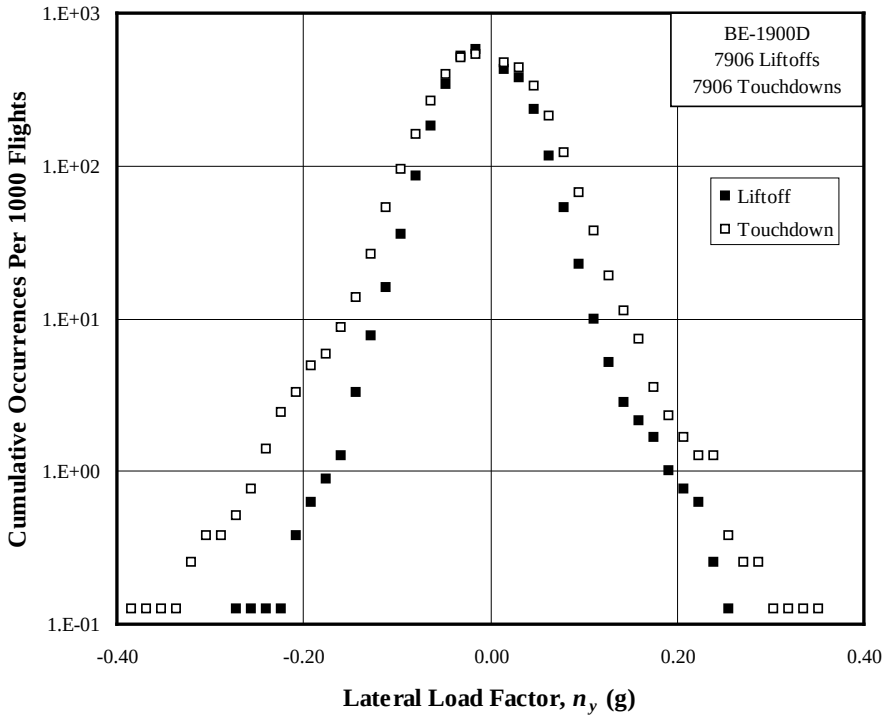

Figure A-53. Cumulative occurrences of lateral load factor per 1000 flights at liftoff and touchdown

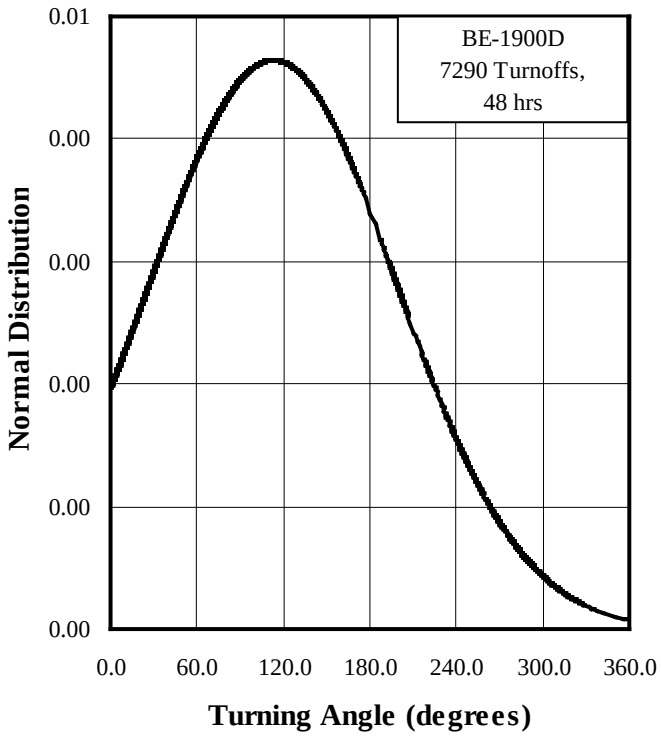

Figure A-54. Probability distributions of turning angle during runway turnoff

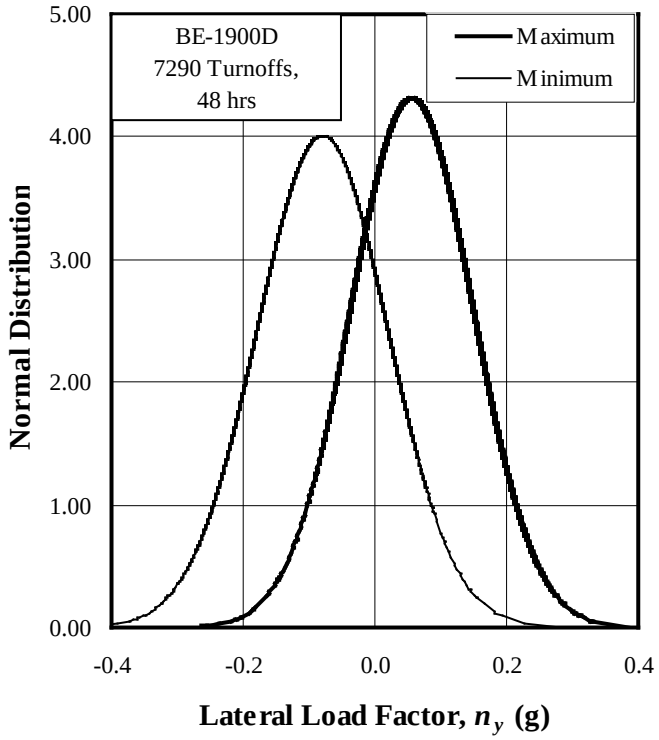

Figure A-55. Normal probability of maximum and minimum lateral load factor during runway turnoff

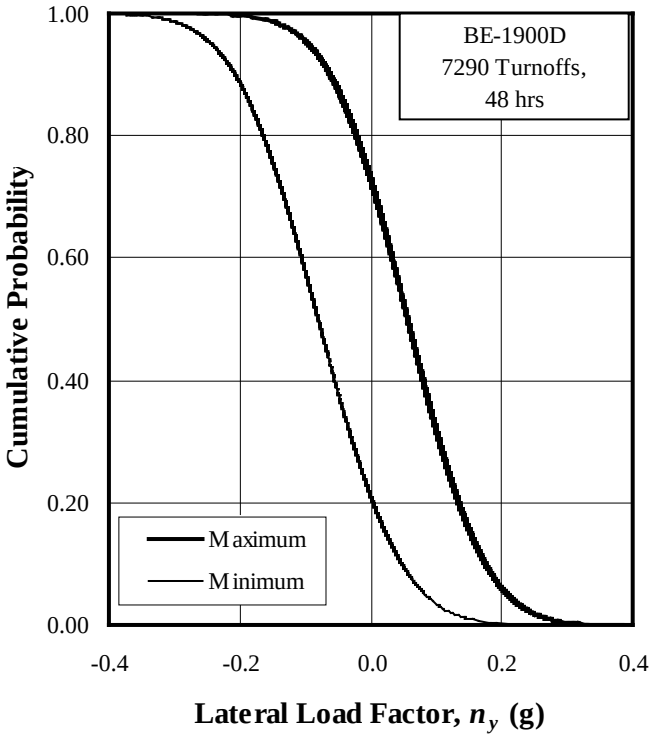

Figure A-56. Cumulative probability of maximum and minimum lateral load factor during runway turnoff

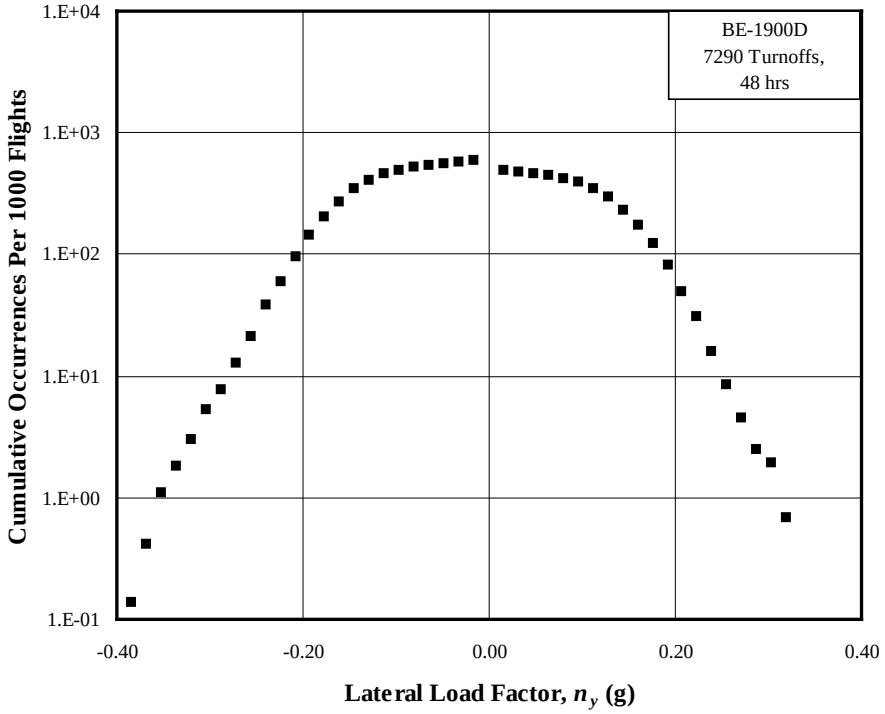

Figure A-57. Cumulative occurrences of lateral load factor per 1000 flights during runway turnoff

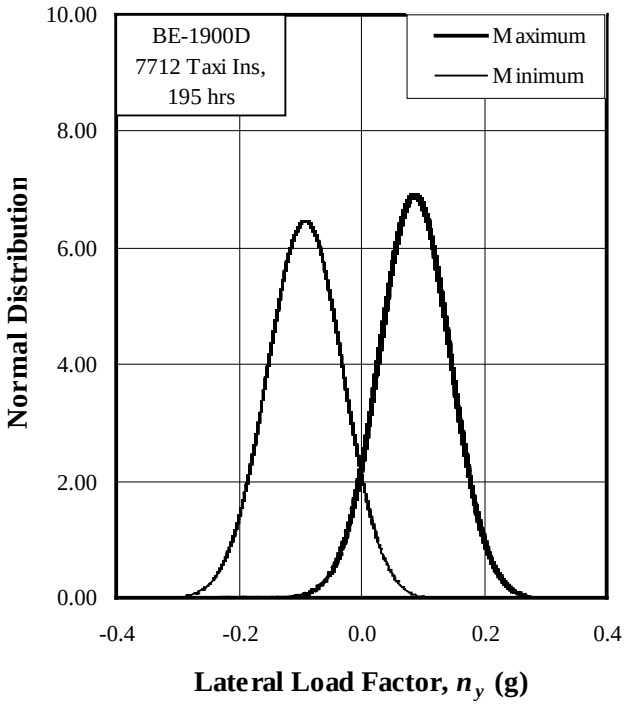

Figure A-58. Normal probability of maximum and minimum lateral load factor while taxiing in

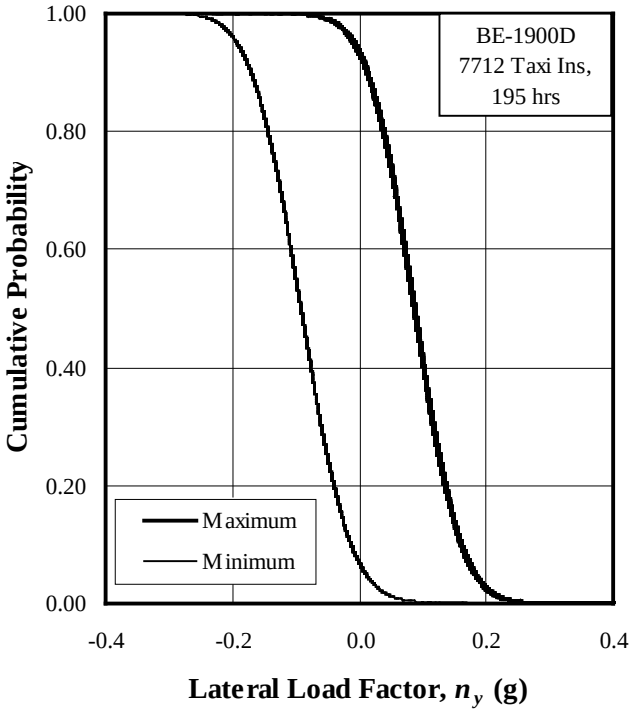

Figure A-59. Cumulative probability of maximum and minimum lateral load factor while taxiing in

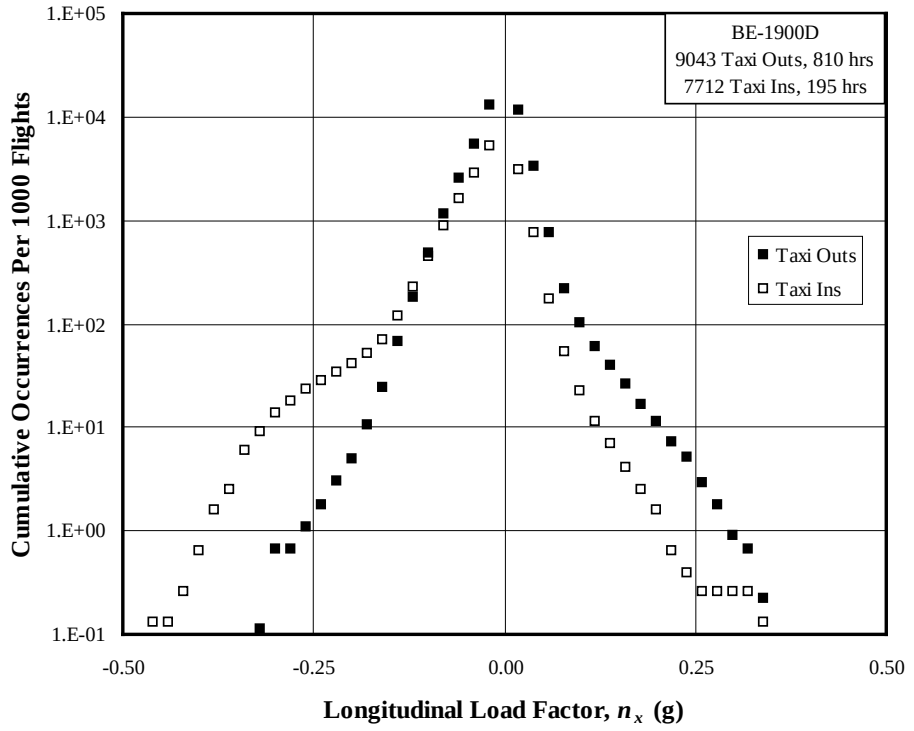

Figure A-60. Cumulative occurrences of longitudinal load factor per 1000 flights during taxi operations

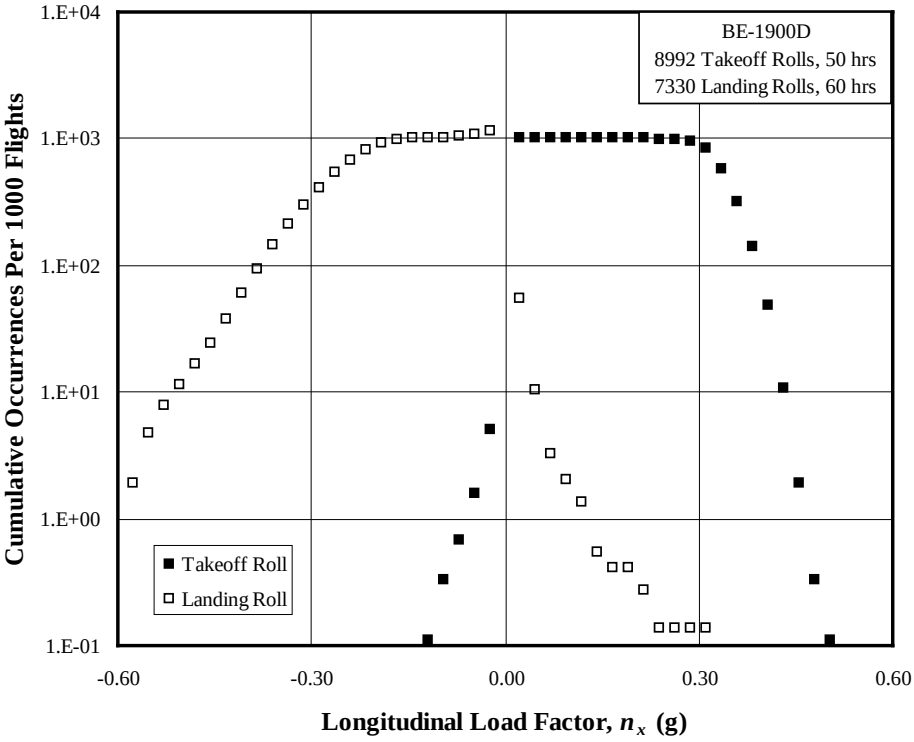

Figure A-61. Cumulative occurrences of longitudinal load factor per 1000 flights during takeoff roll and landing roll

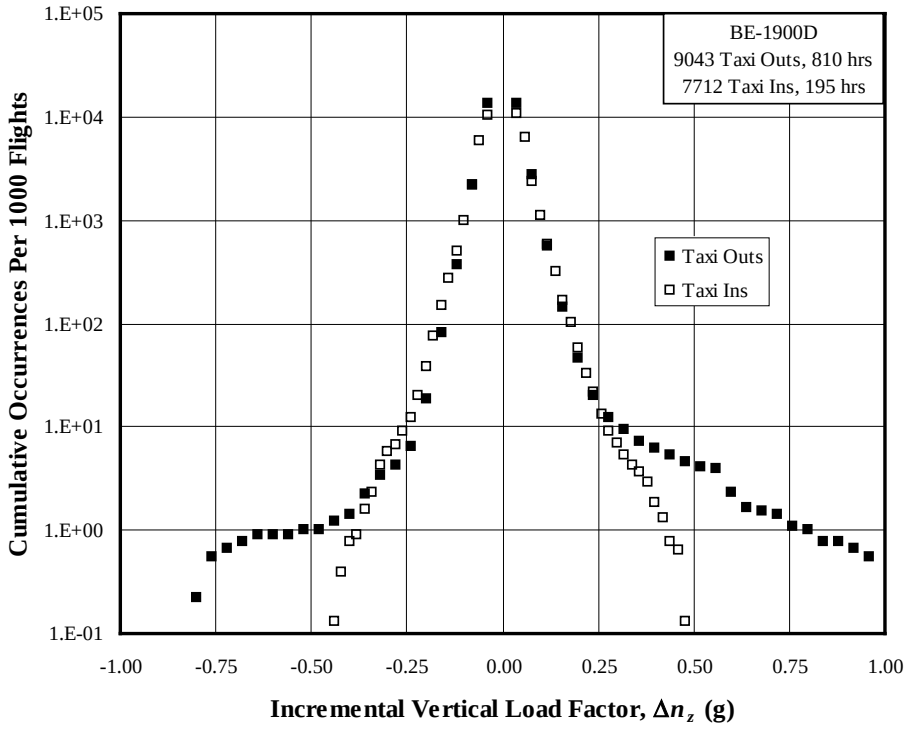

Figure A-62. Cumulative occurrences of incremental vertical load factor per 1000 flights during taxi operations

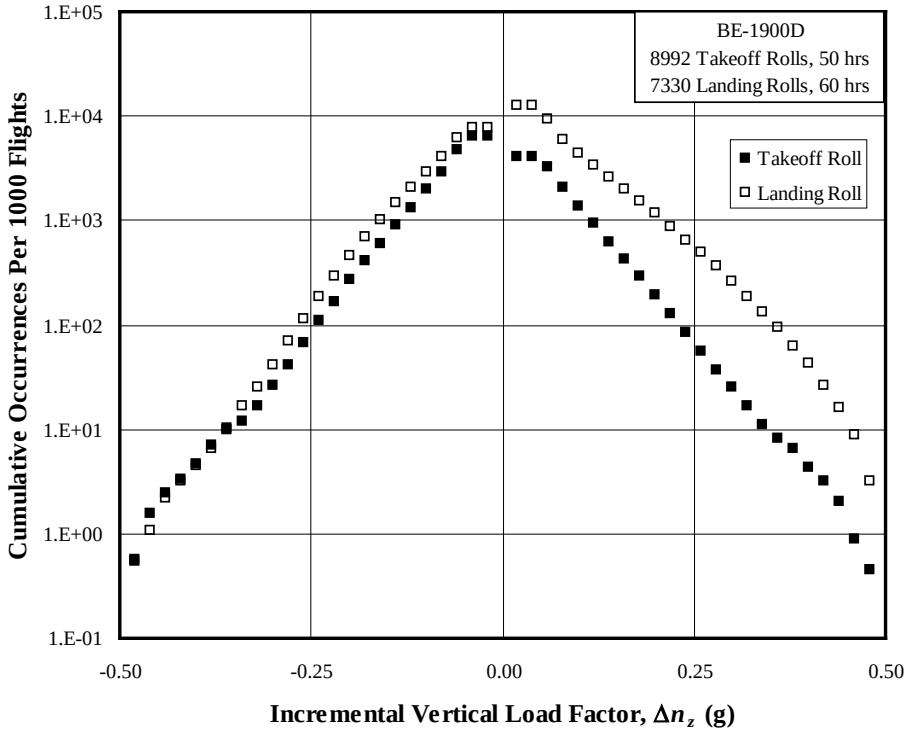

Figure A-63. Cumulative occurrences of incremental vertical load factor per 1000 flights during takeoff roll and landing roll

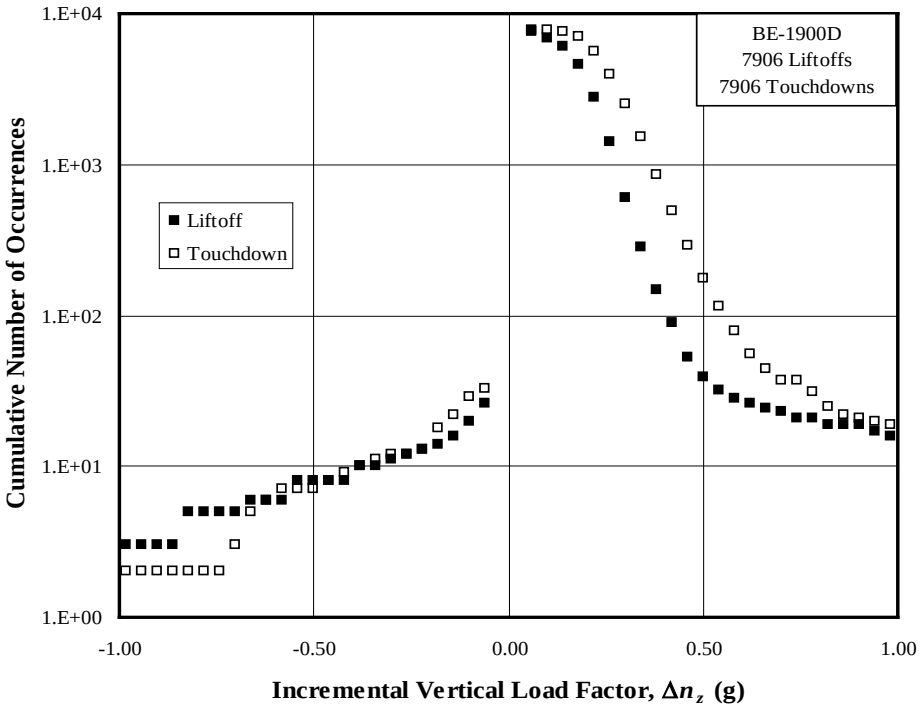

Figure A-64. Cumulative occurrences of incremental vertical load factor per 1000 flights at liftoff and touchdown

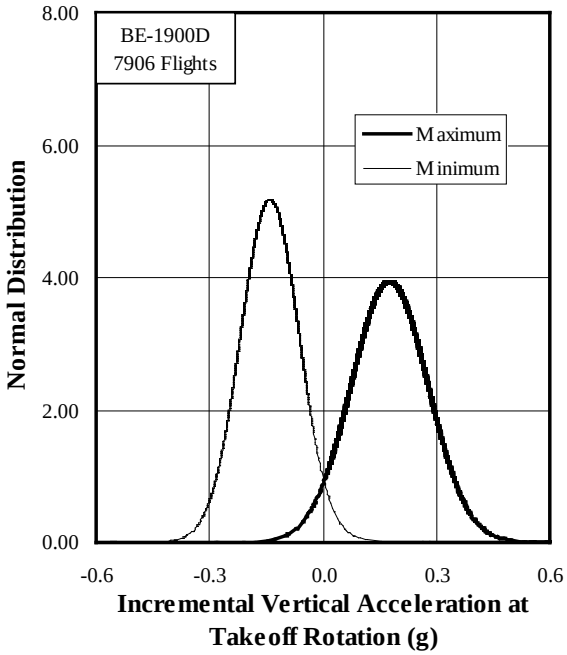

Figure A-65. Normal probability distribution of incremental vertical load factor at takeoff rotation

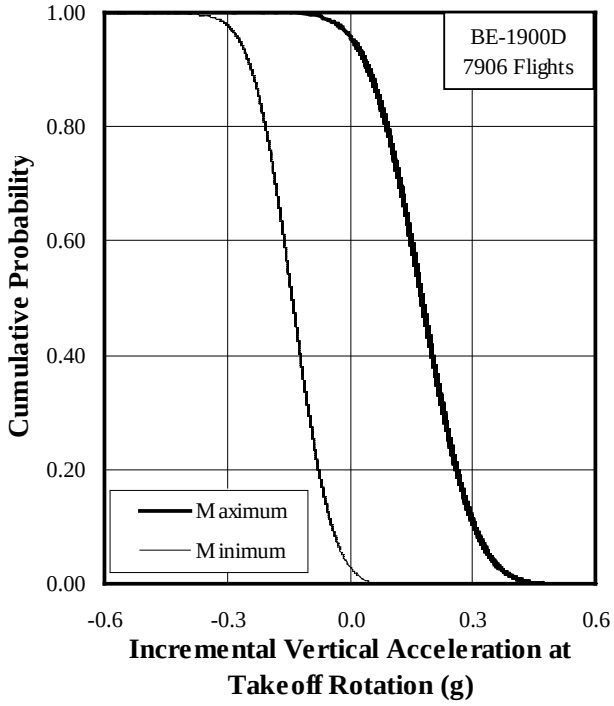

Figure A-66. Cumulative probability of incremental vertical load factor at takeoff rotation

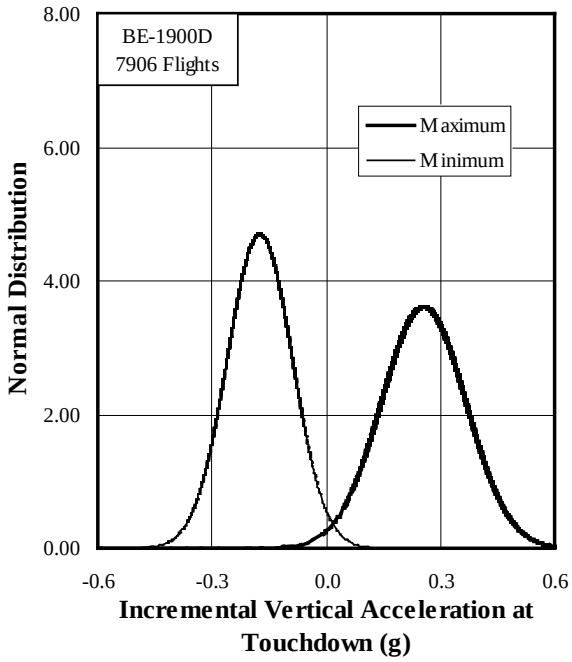

Figure A-67. Normal probability distribution of incremental vertical load factor at touchdown

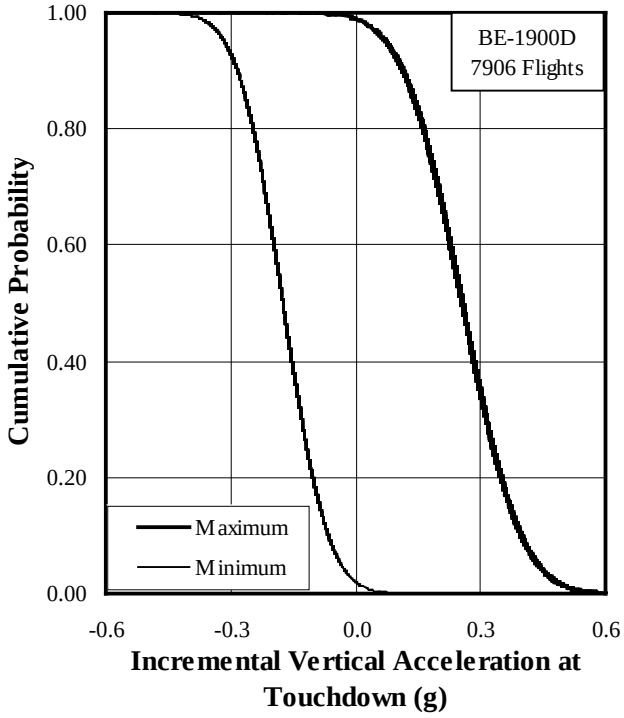

Figure A-68. Cumulative probability of incremental vertical load factor at touchdown

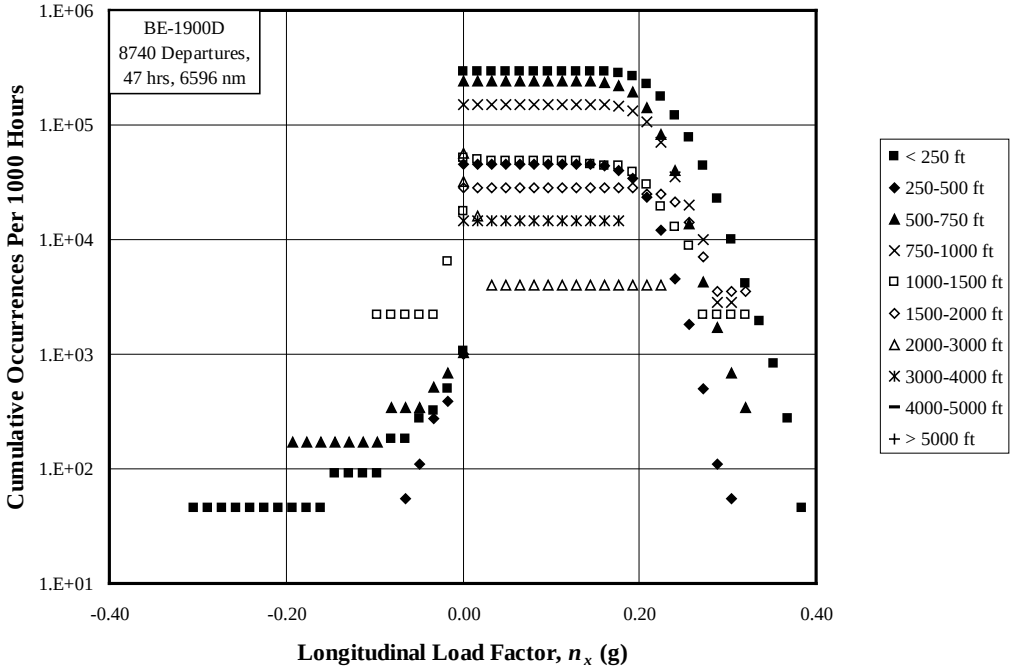

Figure A-69. Cumulative occurrences of longitudinal load factor per 1000 hours for departure phase

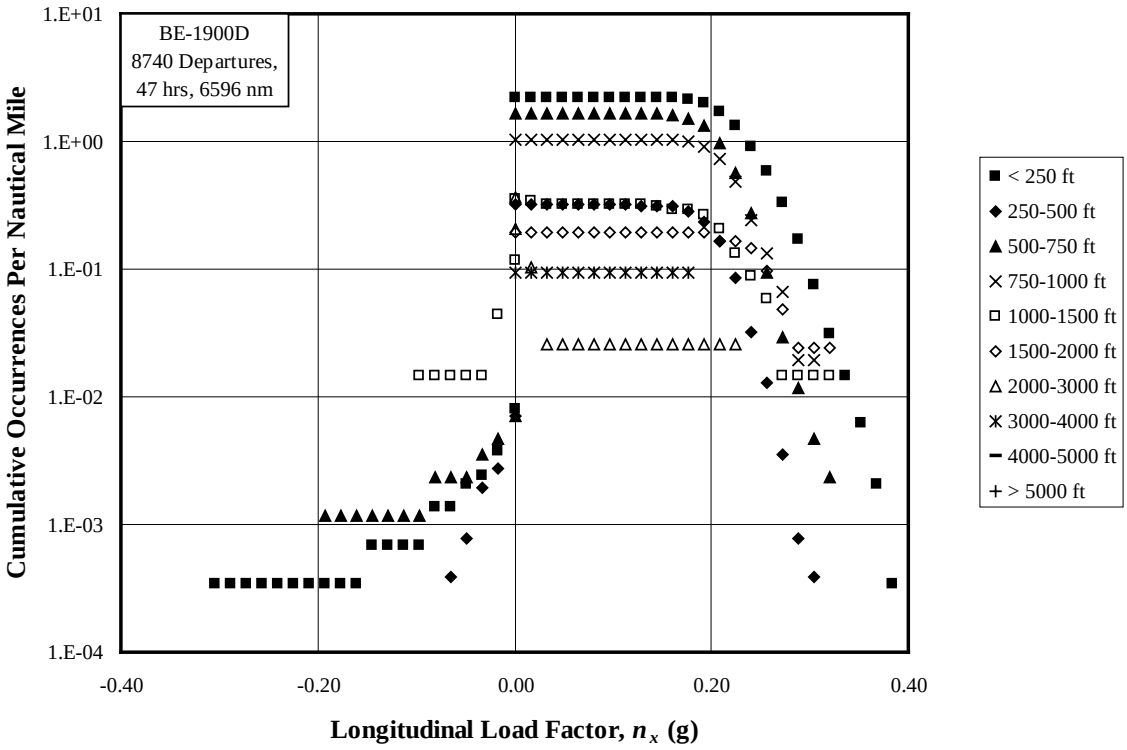

Figure A-70. Cumulative occurrences of longitudinal load factor per nautical mile for departure phase

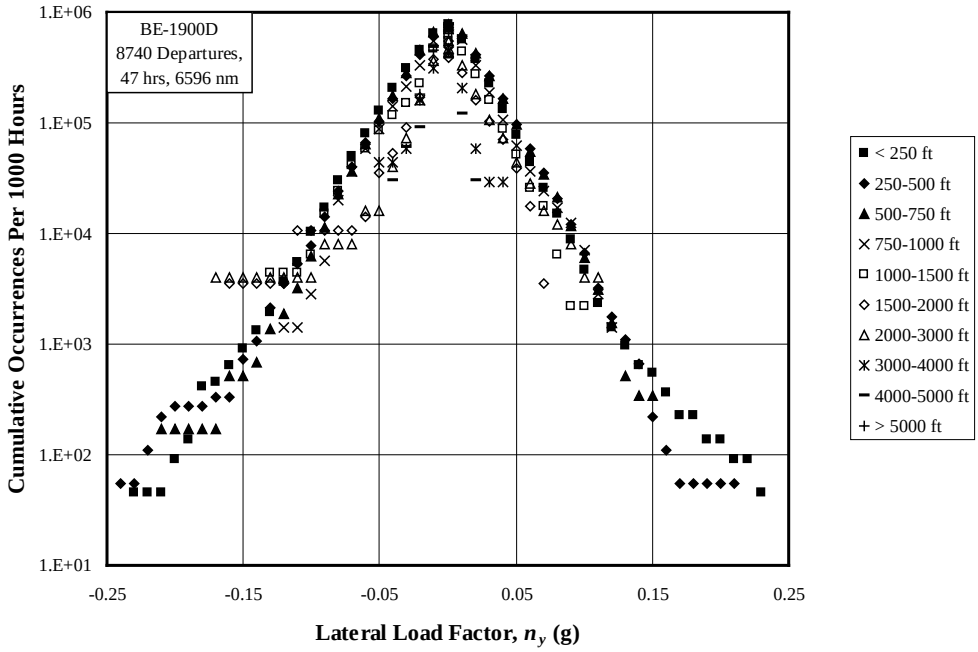

Figure A-71. Cumulative occurrences of lateral load factor per 1000 hours for departure phase

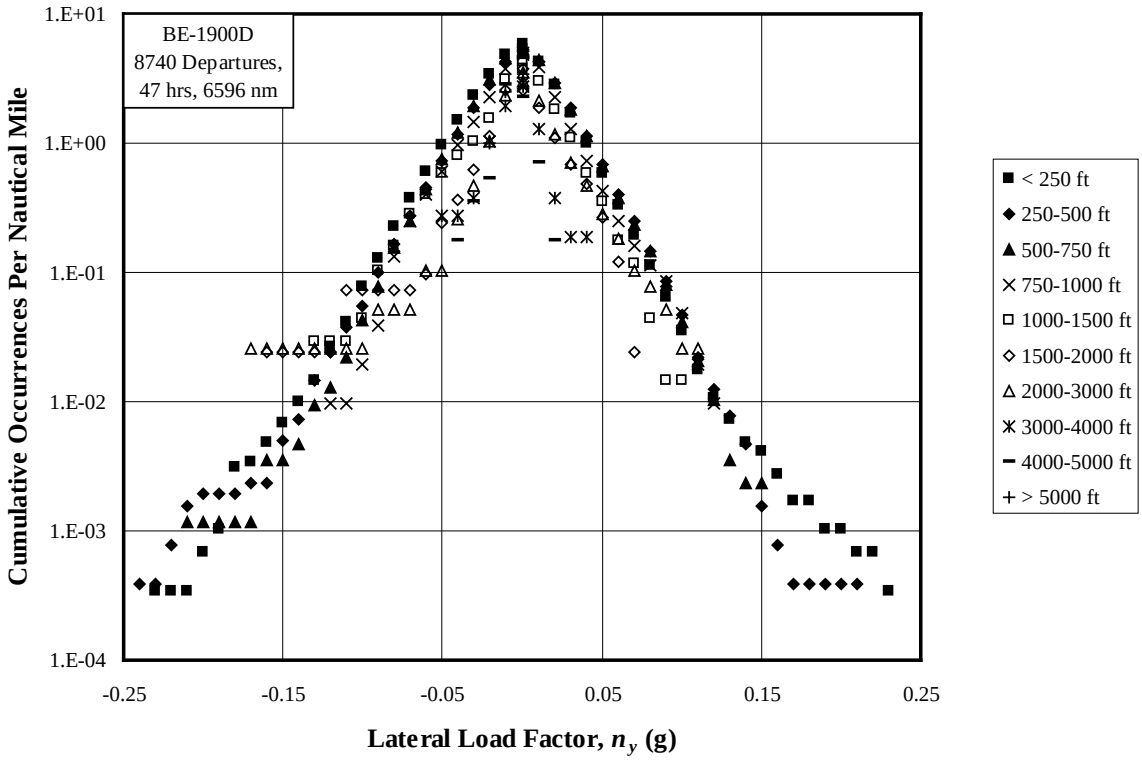

Figure A-72. Cumulative occurrences of lateral load factor per nmi for departure phase

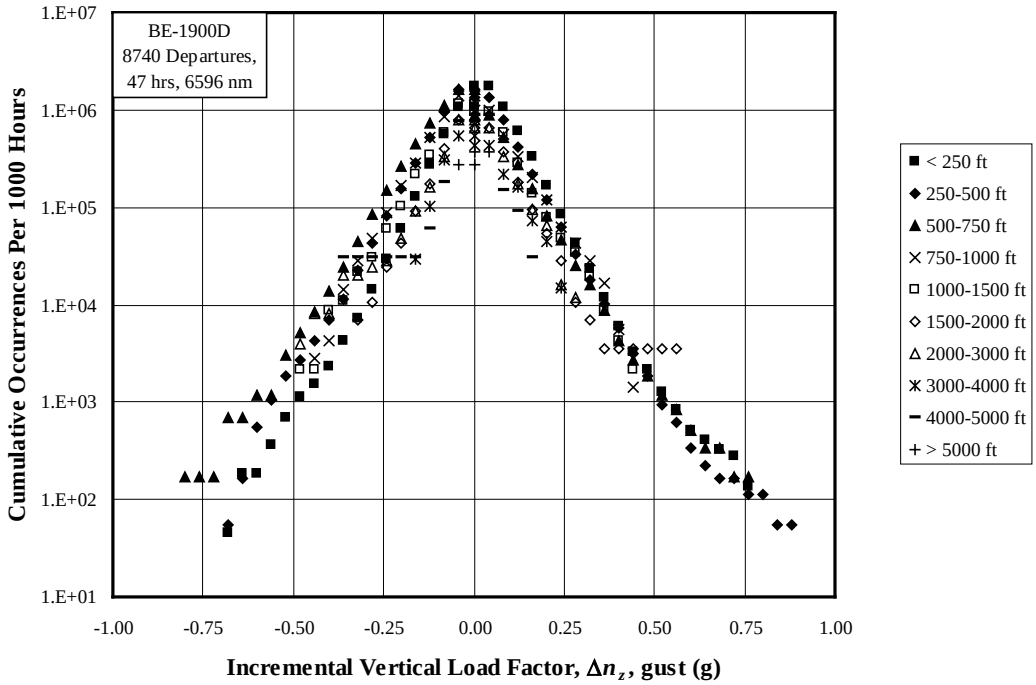

Figure A-73. Cumulative occurrences of incremental gust vertical load factor per 1000 hours for departure phase

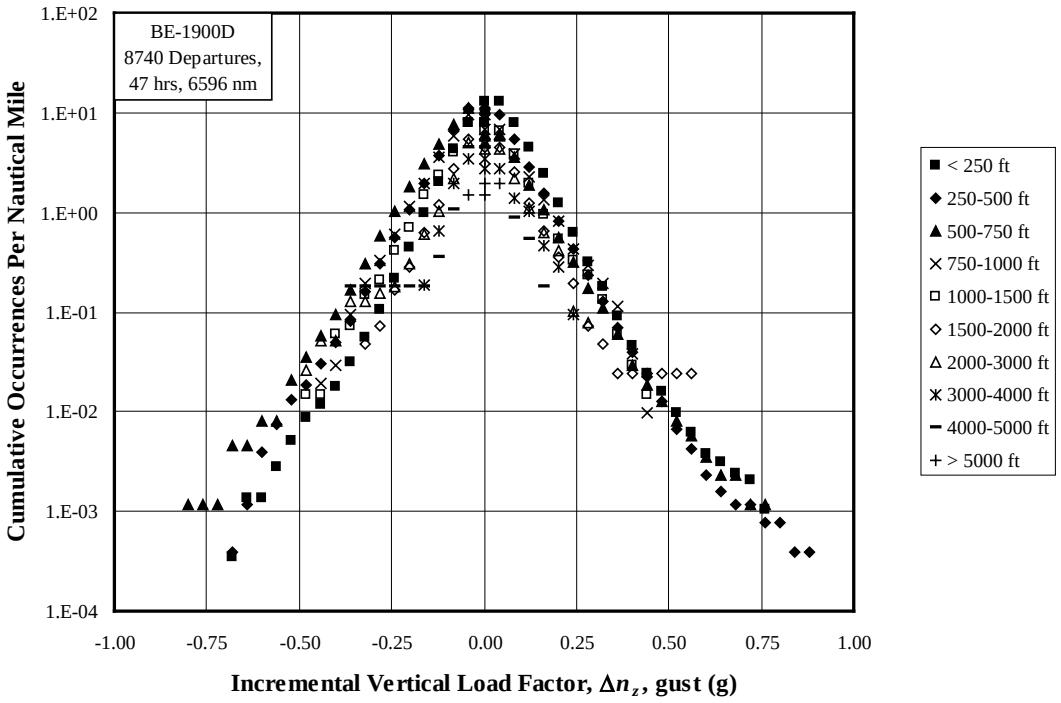

Figure A-74. Cumulative occurrences of incremental gust vertical load factor per nmi for departure phase

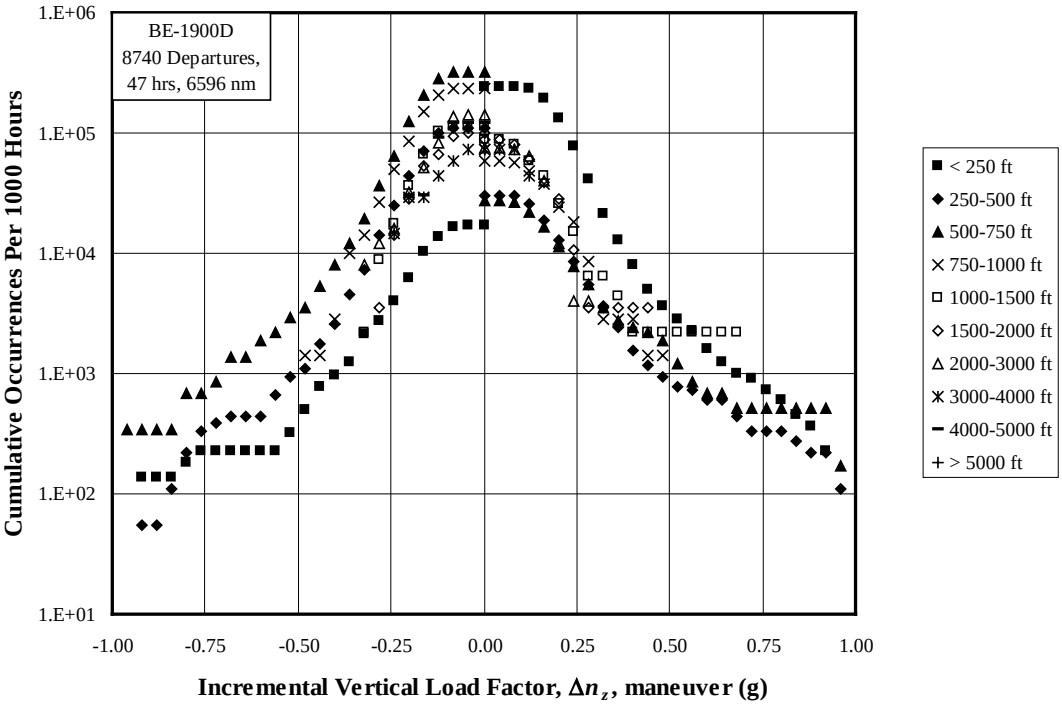

Figure A-75. Cumulative occurrences of incremental maneuver vertical load factor per 1000 hours for departure phase

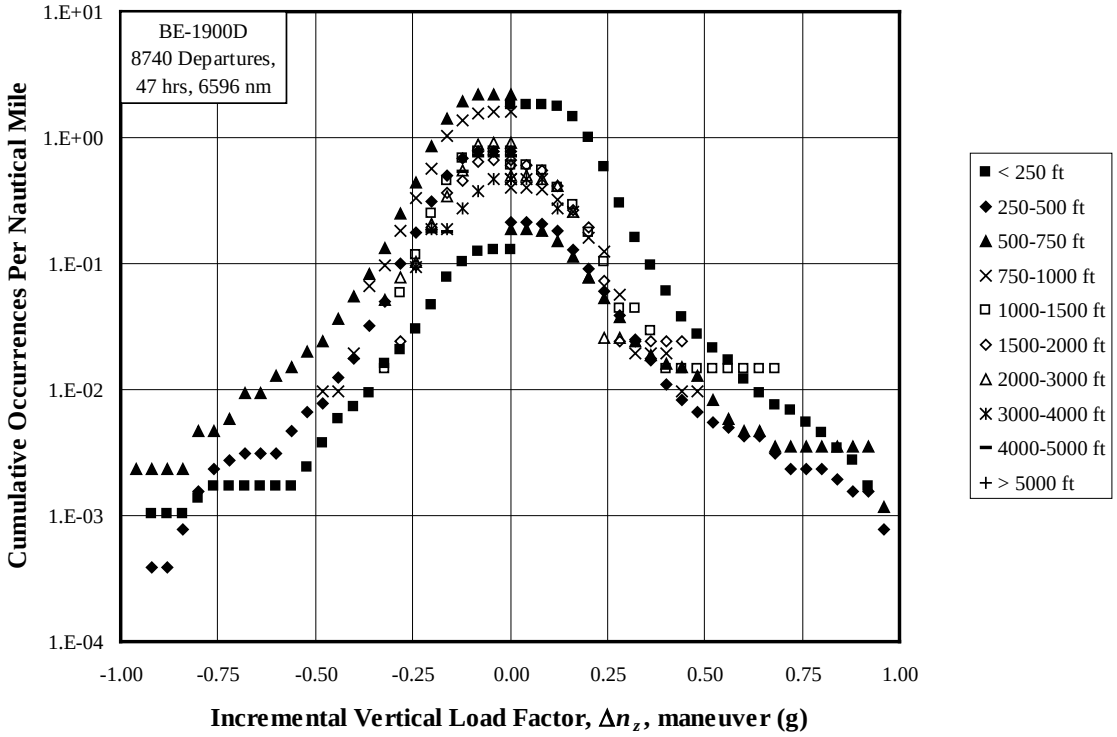

Figure A-76. Cumulative occurrences of incremental maneuver vertical load factor per nmi for departure phase

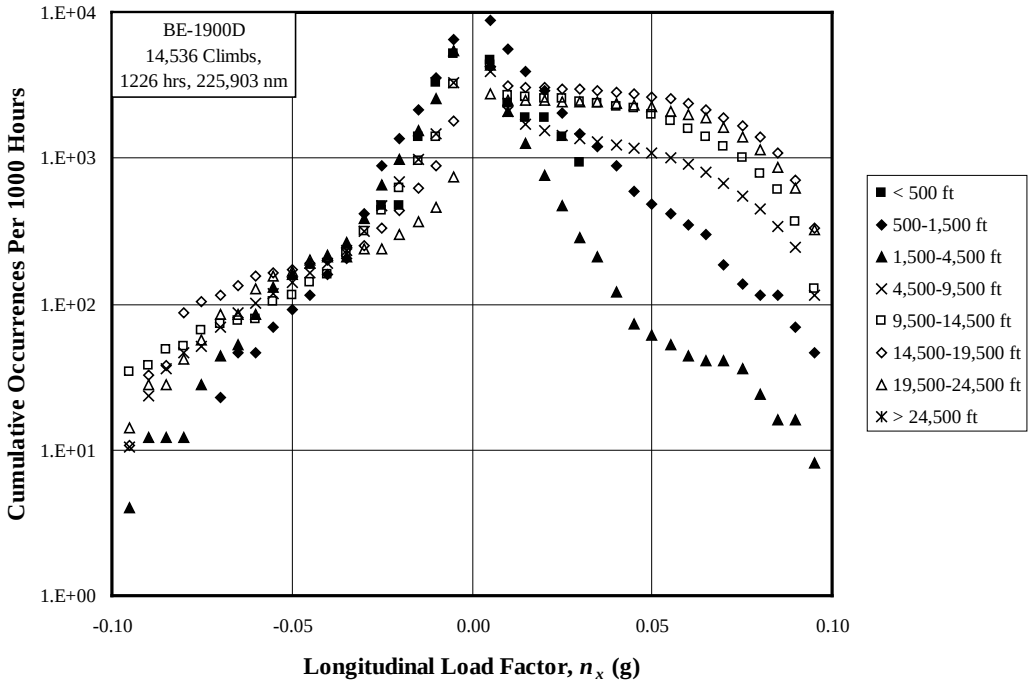

Figure A-77. Cumulative occurrences of longitudinal load factor per 1000 hours for climb phase

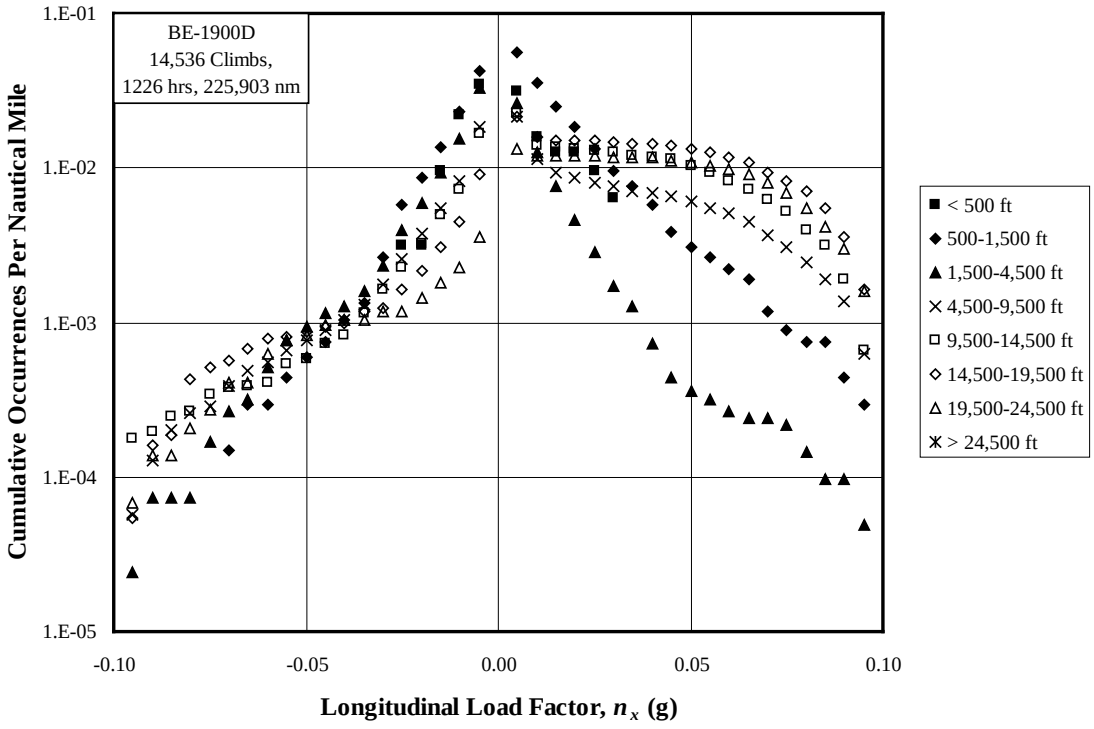

Figure A-78. Cumulative occurrences of longitudinal load factor per nmi for climb phase

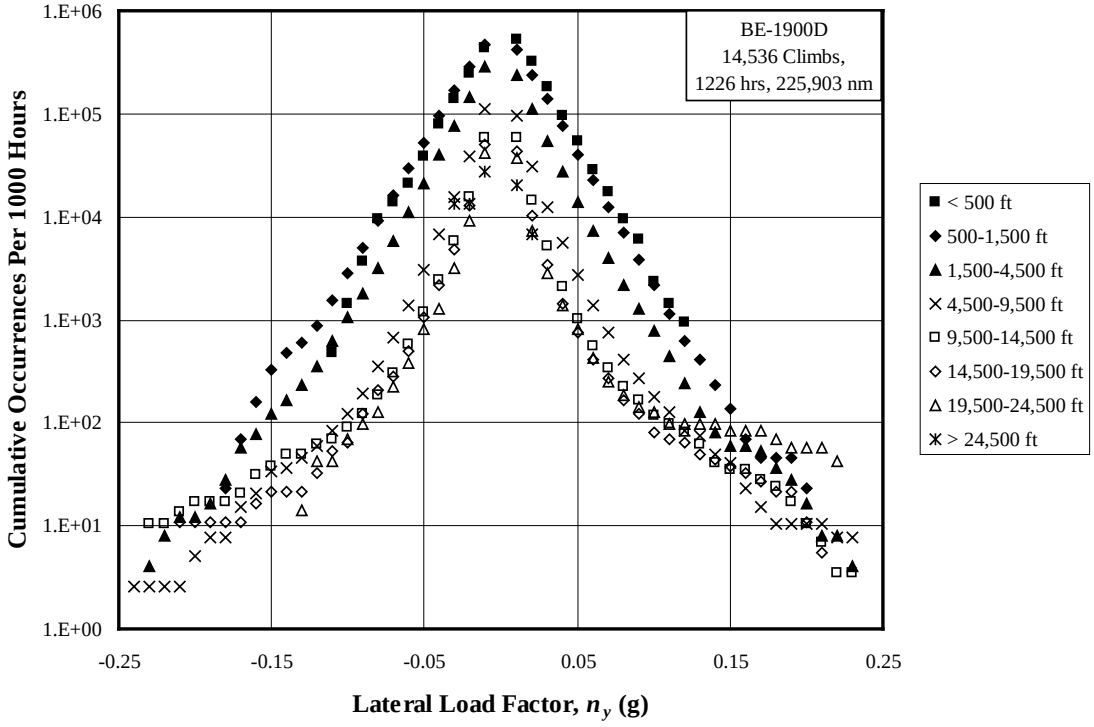

Figure A-79. Cumulative occurrences of lateral load factor per 1000 hours for climb phase

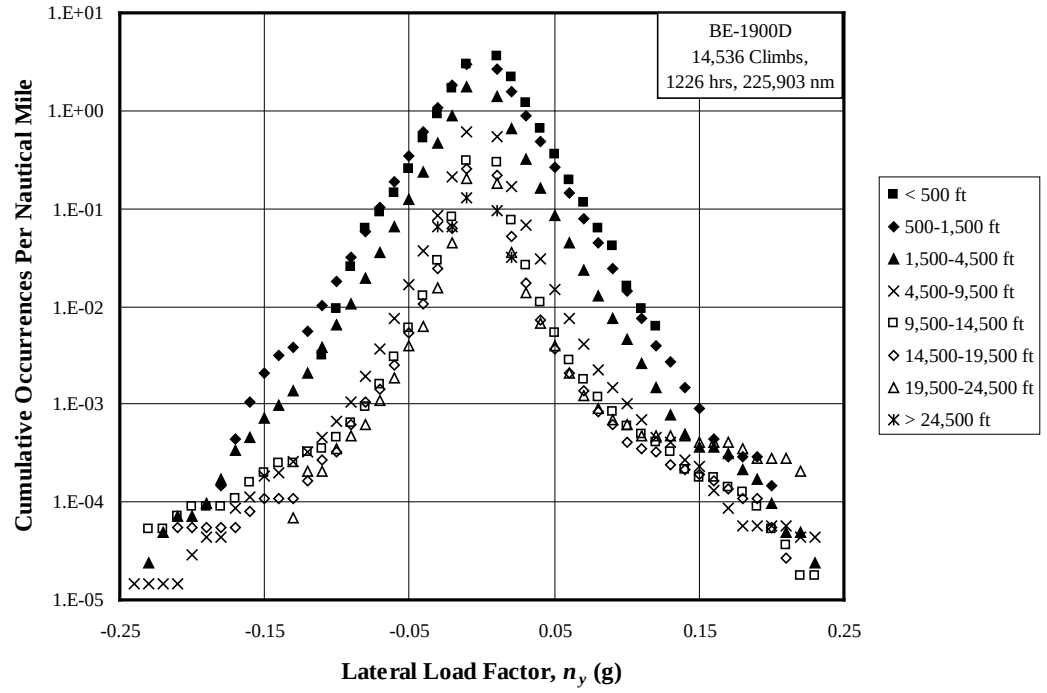

Figure A-80. Cumulative occurrences of lateral load factor per nmi for climb phase

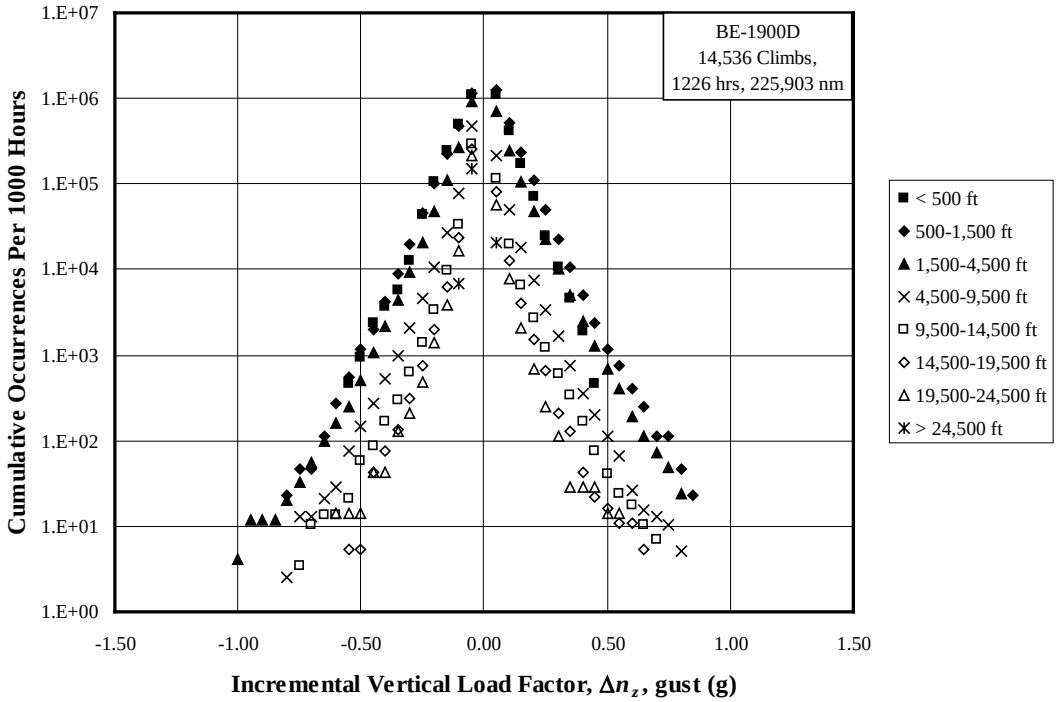

Figure A-81. Cumulative occurrences of incremental vertical gust load factor per 1000 hours for climb phase

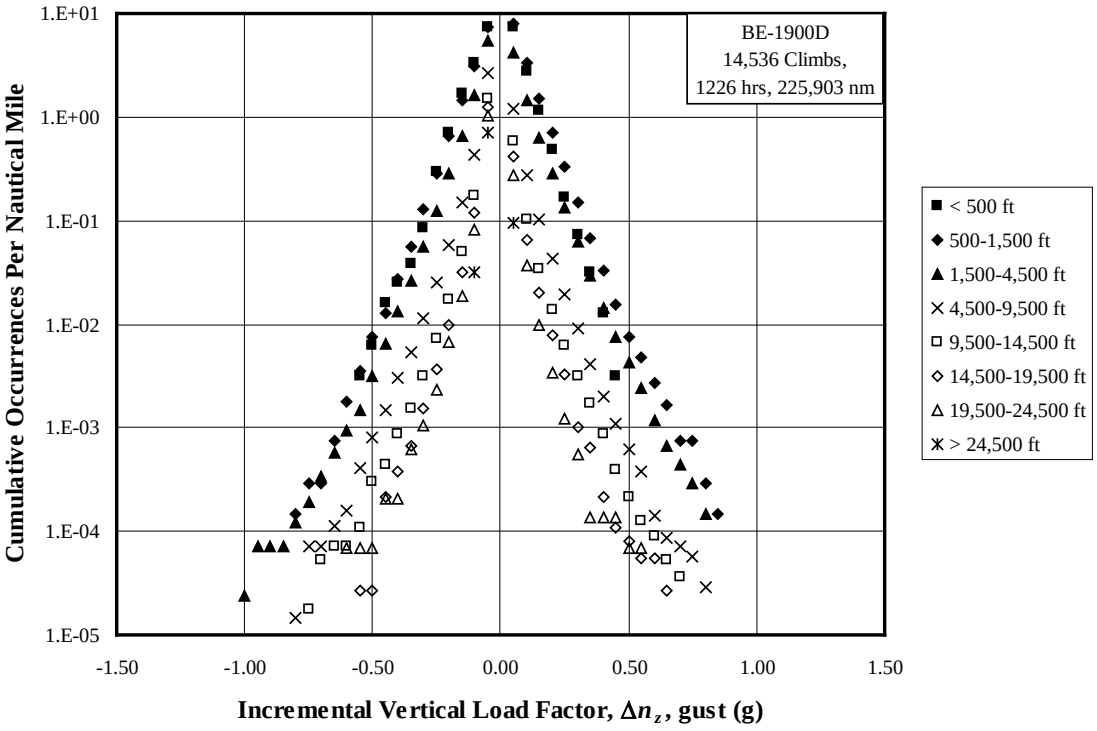

Figure A-82. Cumulative occurrences of incremental vertical gust load factor per nmi for climb phase

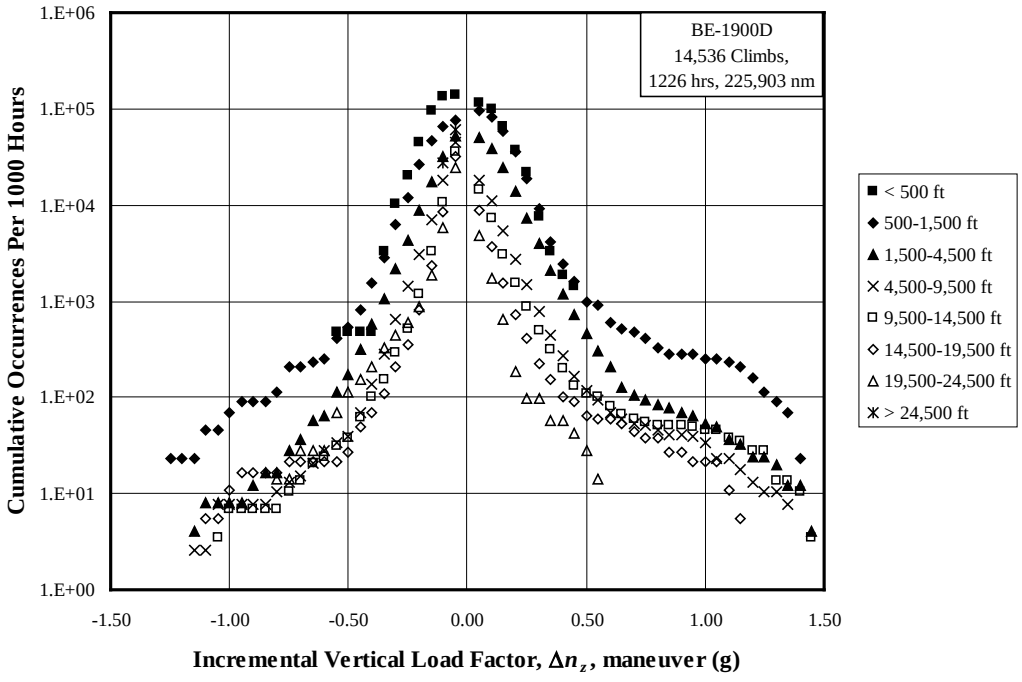

Figure A-83. Cumulative occurrences of incremental maneuver vertical load factor per 1000 hours for climb phase

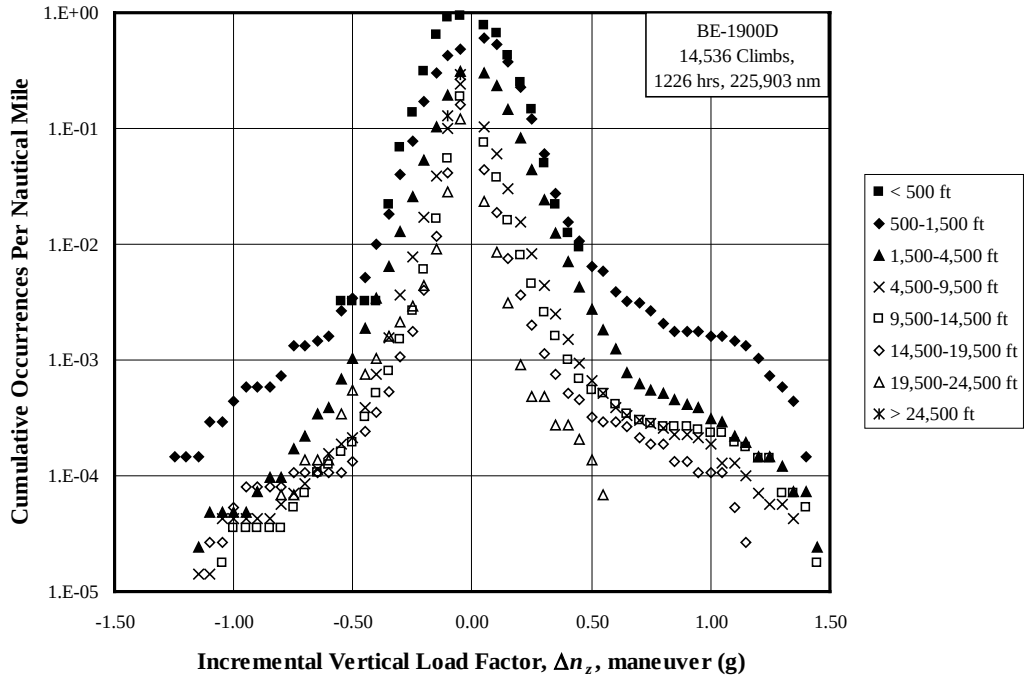

Figure A-84. Cumulative occurrences of incremental maneuver vertical load factor per nmi for climb phase

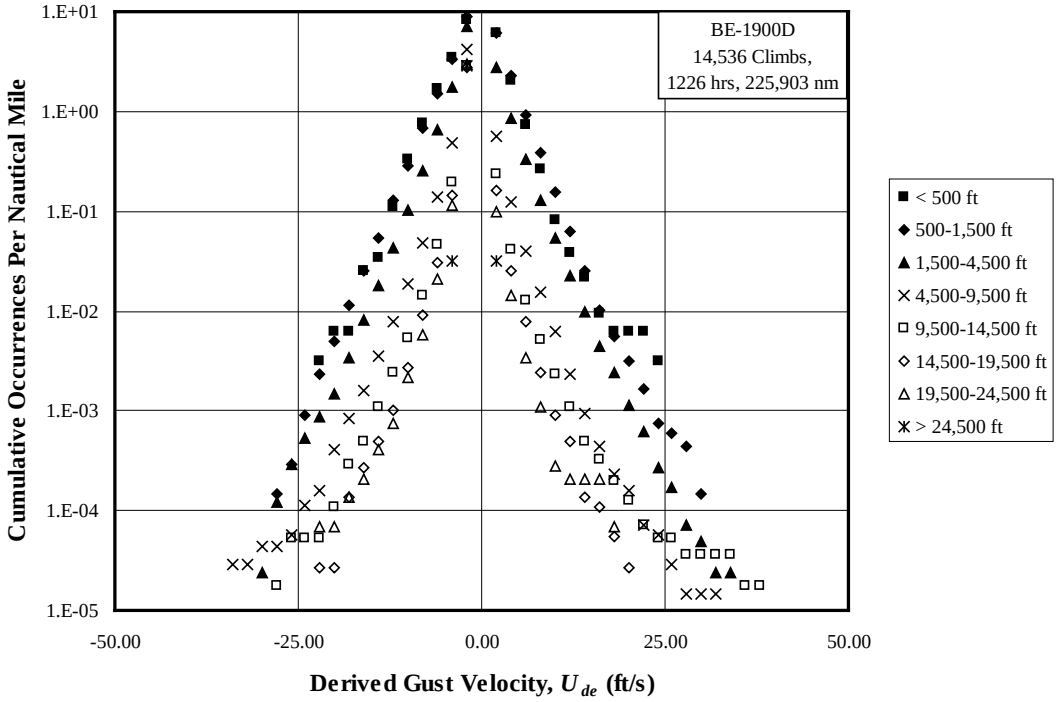

Figure A-85. Cumulative occurrences of derived gust velocity per nmi for climb phase

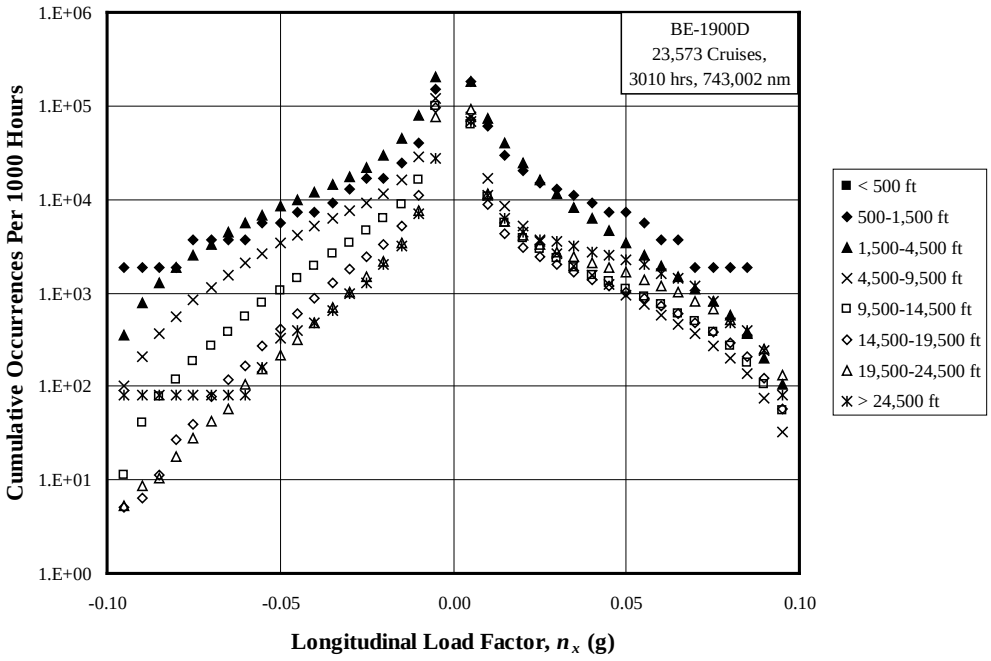

Figure A-86. Cumulative occurrences of longitudinal load factor per 1000 hours for cruise phase

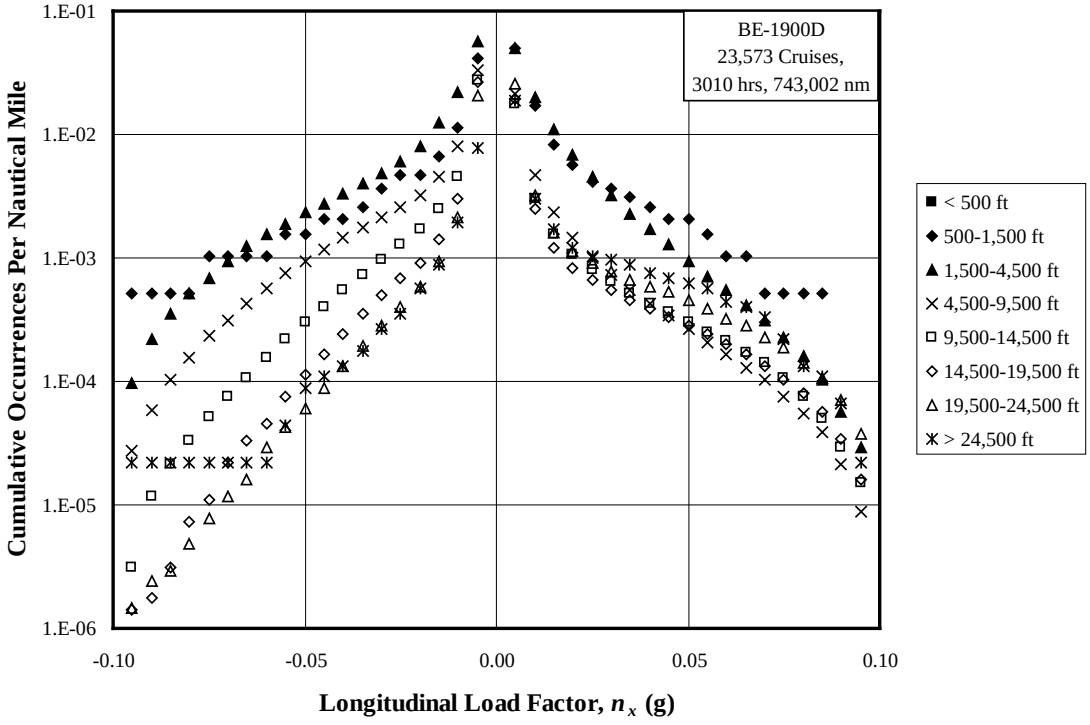

Figure A-87. Cumulative occurrences of longitudinal load factor per nmi for cruise phase

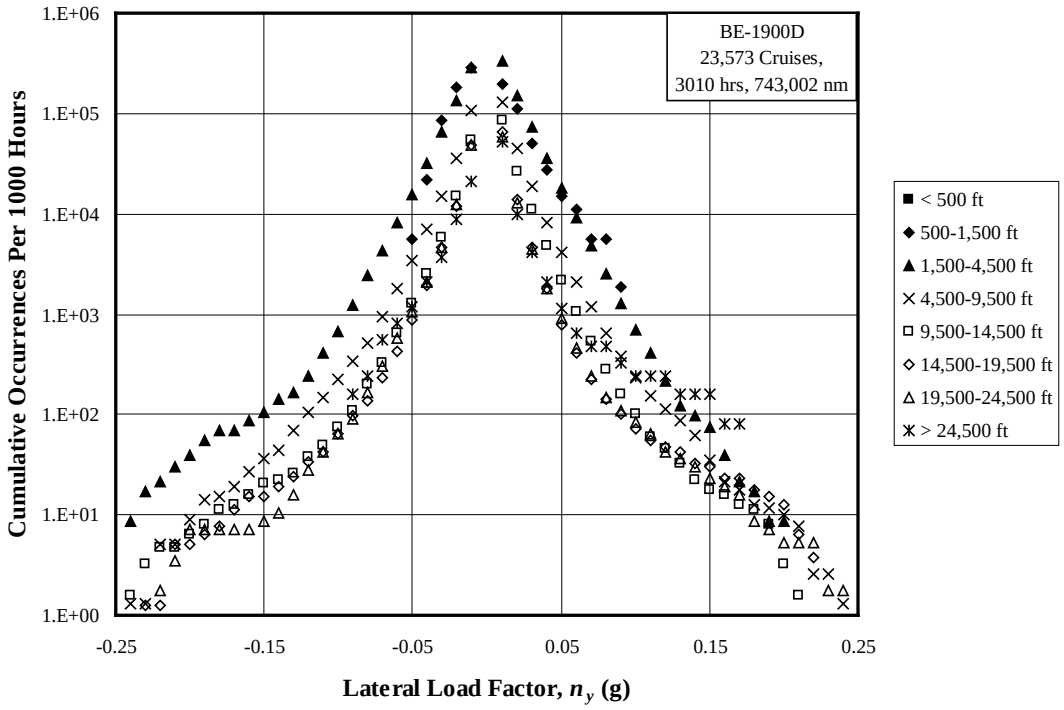

Figure A-88. Cumulative occurrences of lateral load factor per 1000 hours for cruise phase

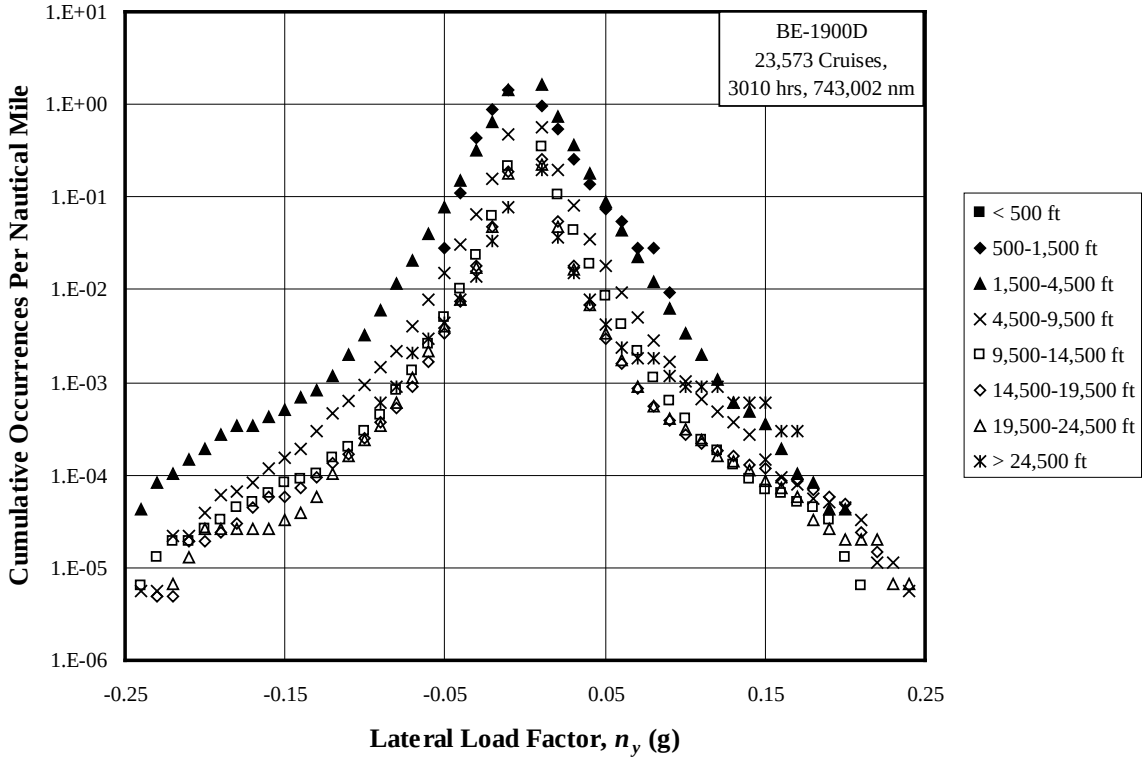

Figure A-89. Cumulative occurrences of lateral load factor per nmi for cruise phase

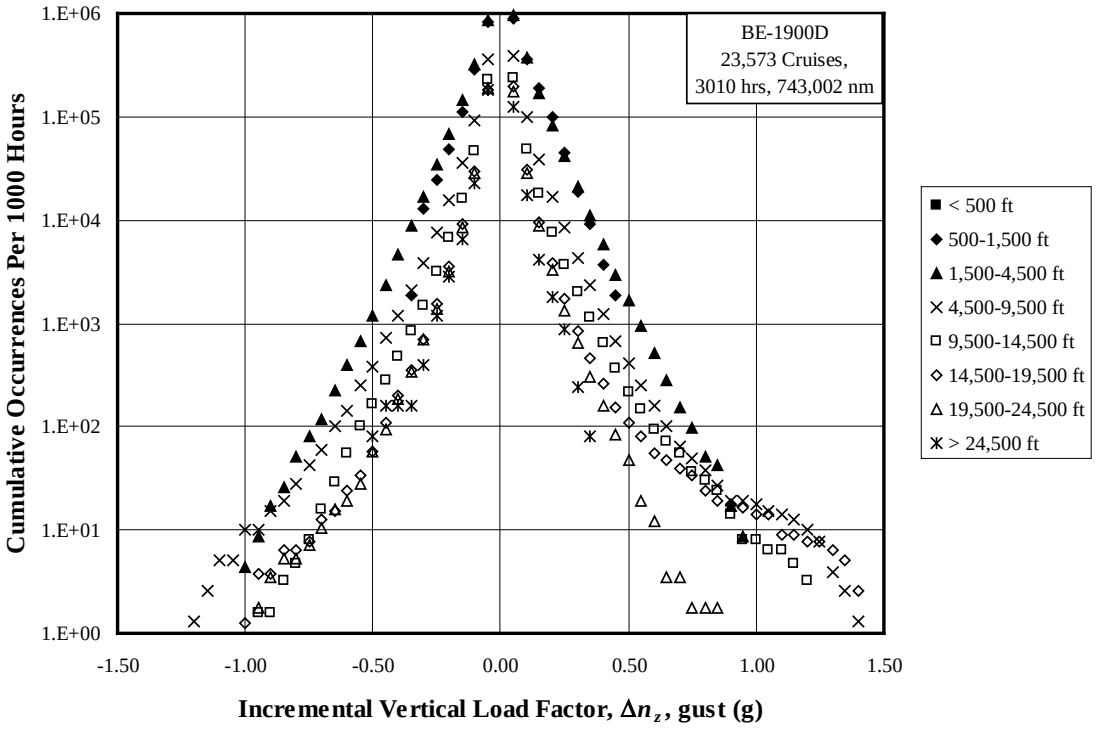

Figure A-90. Cumulative occurrences of incremental gust vertical load factor per 1000 hours for cruise phase

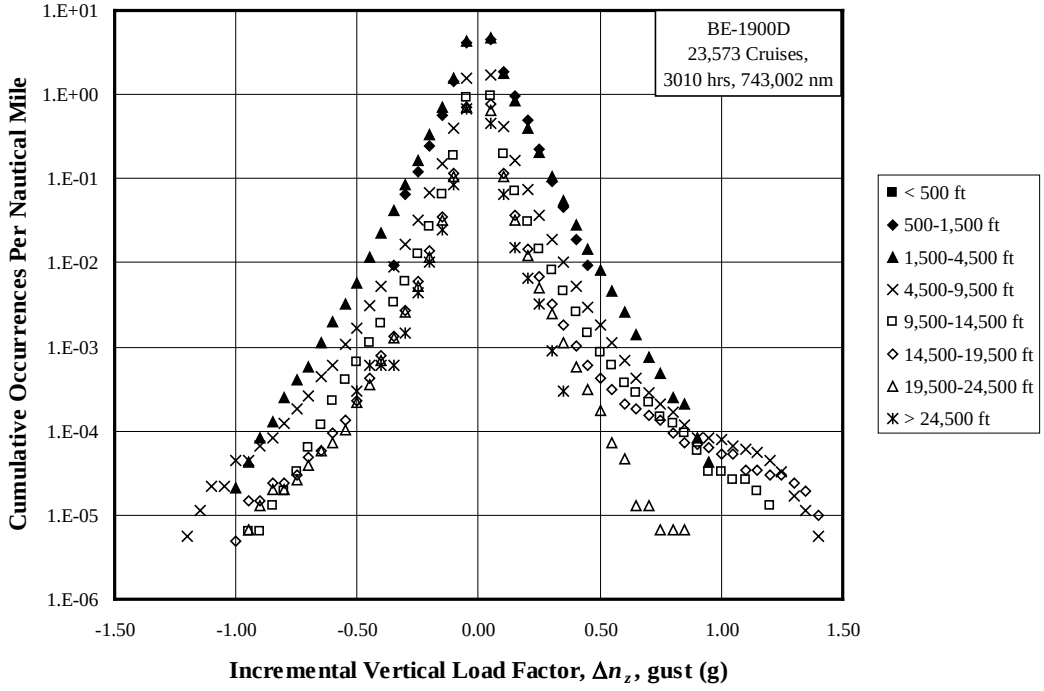

Figure A-91. Cumulative occurrences of incremental gust vertical load factor per nmi for cruise phase

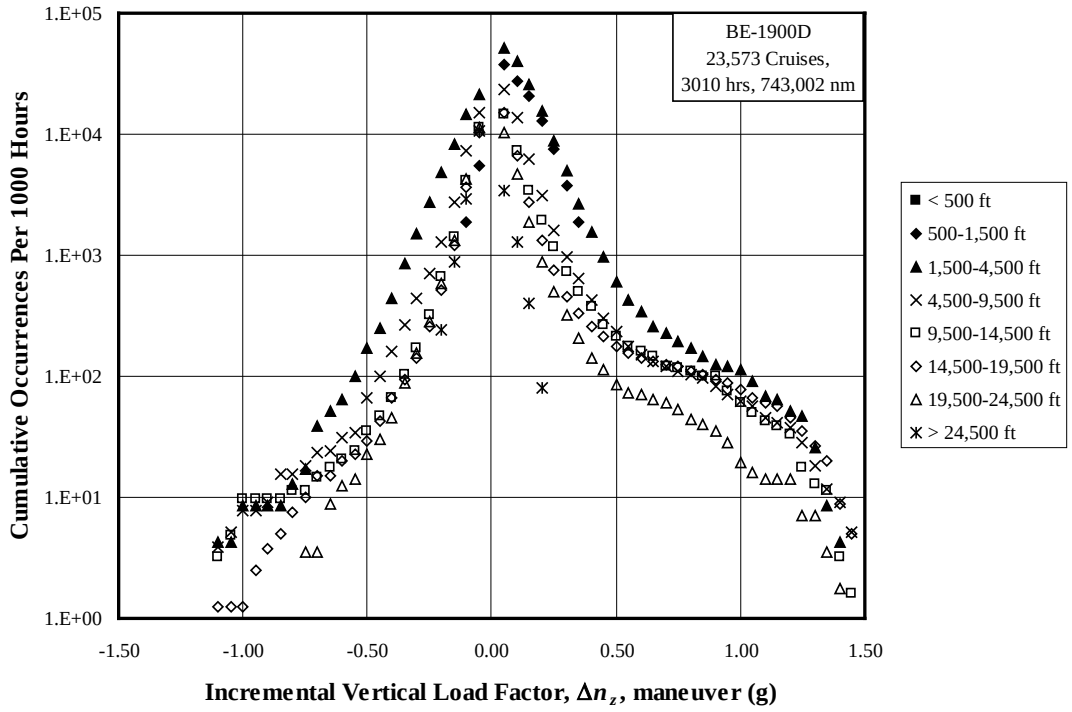

Figure A-92. Cumulative occurrences of incremental maneuver vertical load factor per 1000 hours for cruise phase

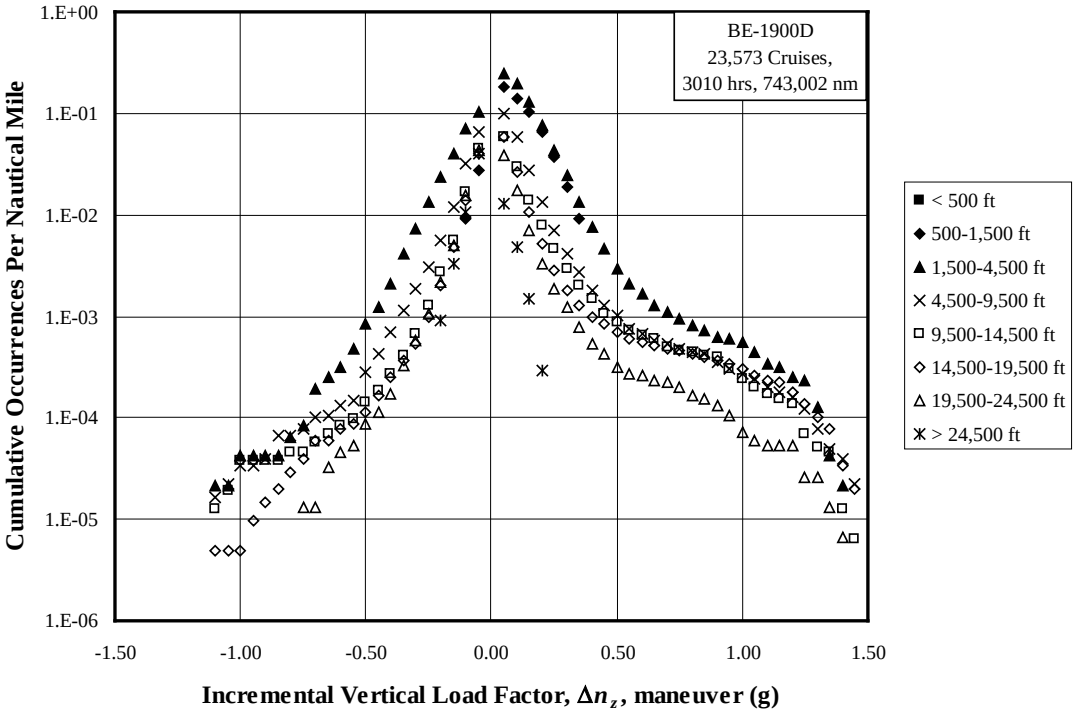

Figure A-93. Cumulative occurrences of incremental maneuver vertical load factor per nmi for cruise phase

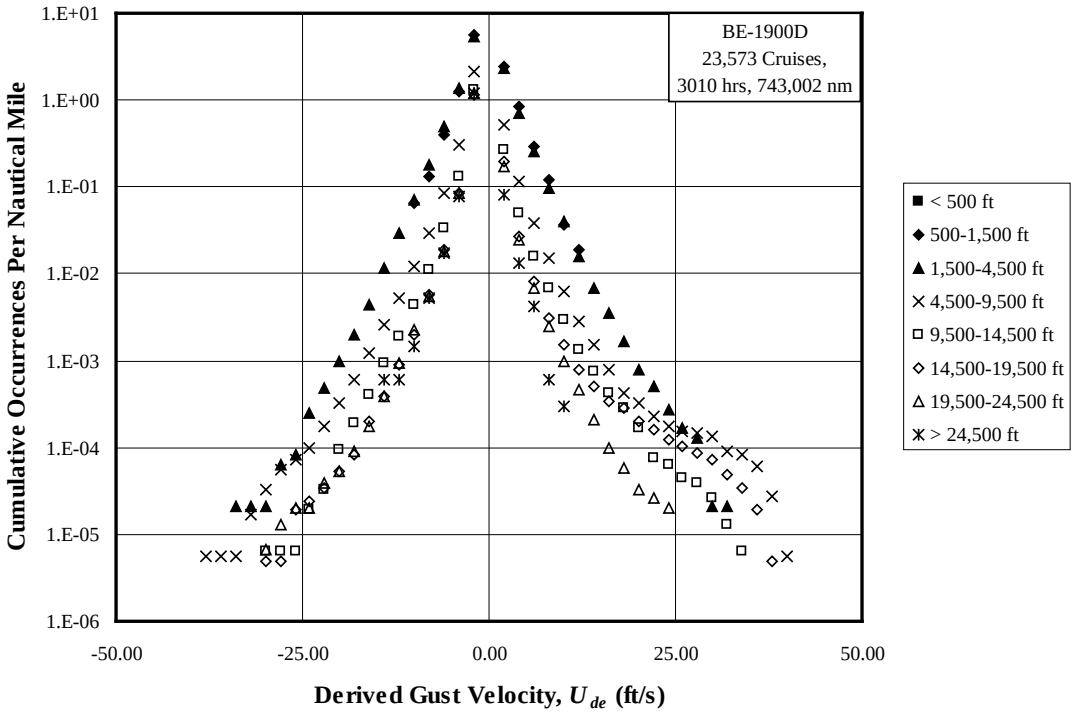

Figure A-94. Cumulative occurrences of derived gust velocity per nmi for cruise phase

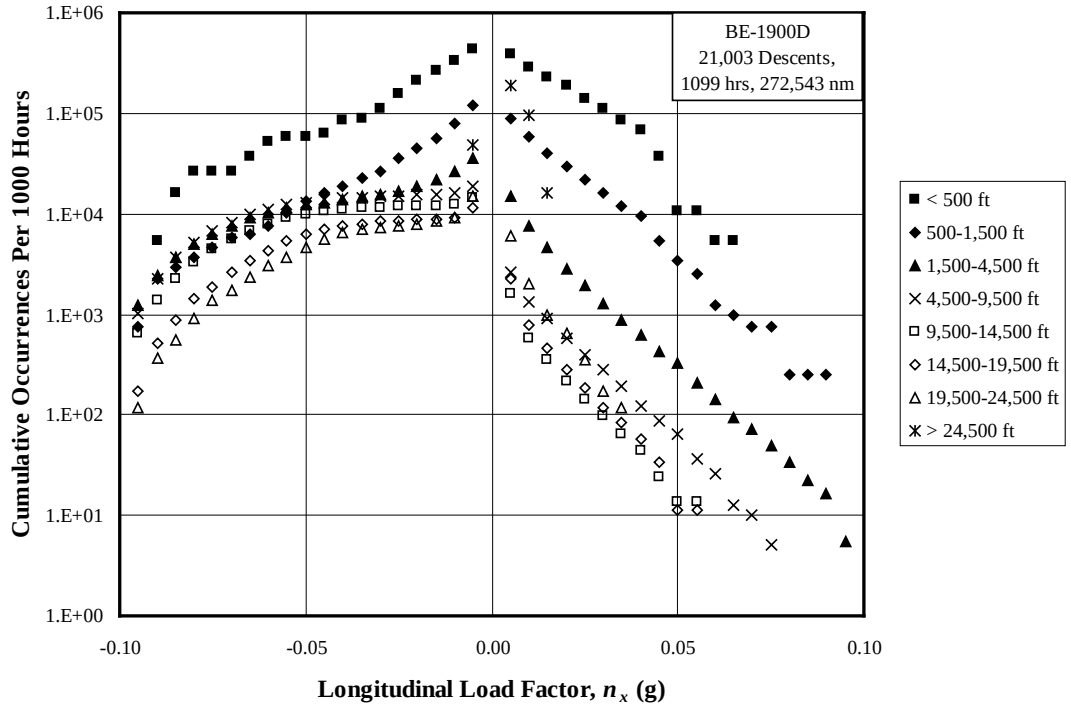

Figure A-95. Cumulative occurrences of longitudinal load factor per 1000 hours for descent phase

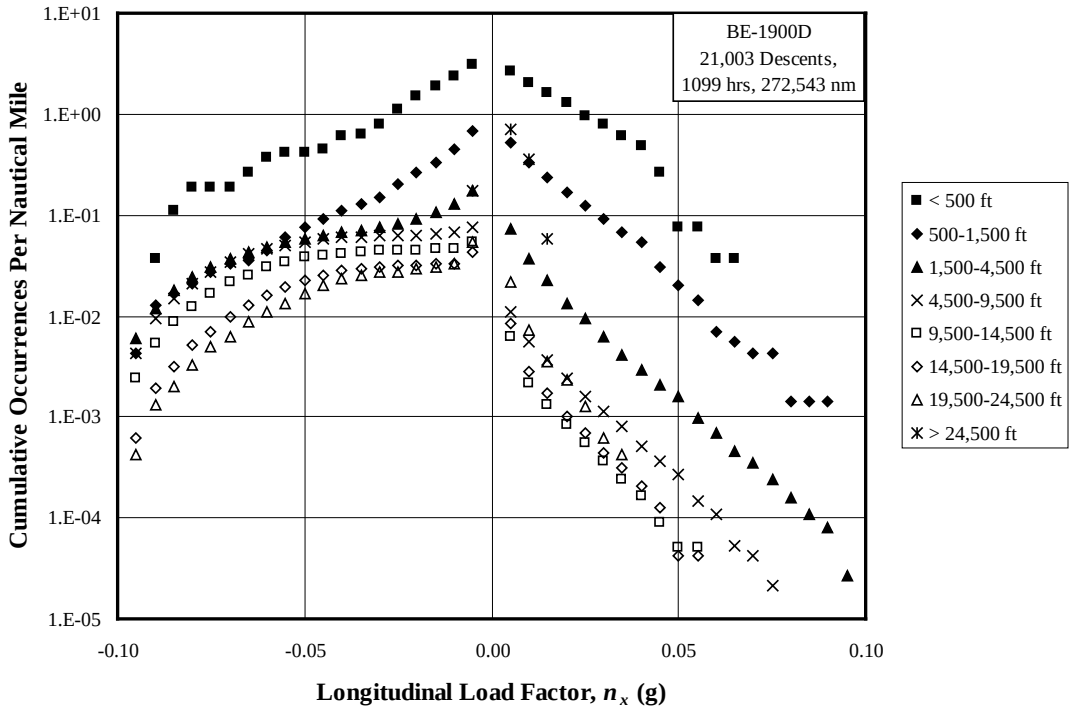

Figure A-96. Cumulative occurrences of longitudinal load factor per nmi for descent phase

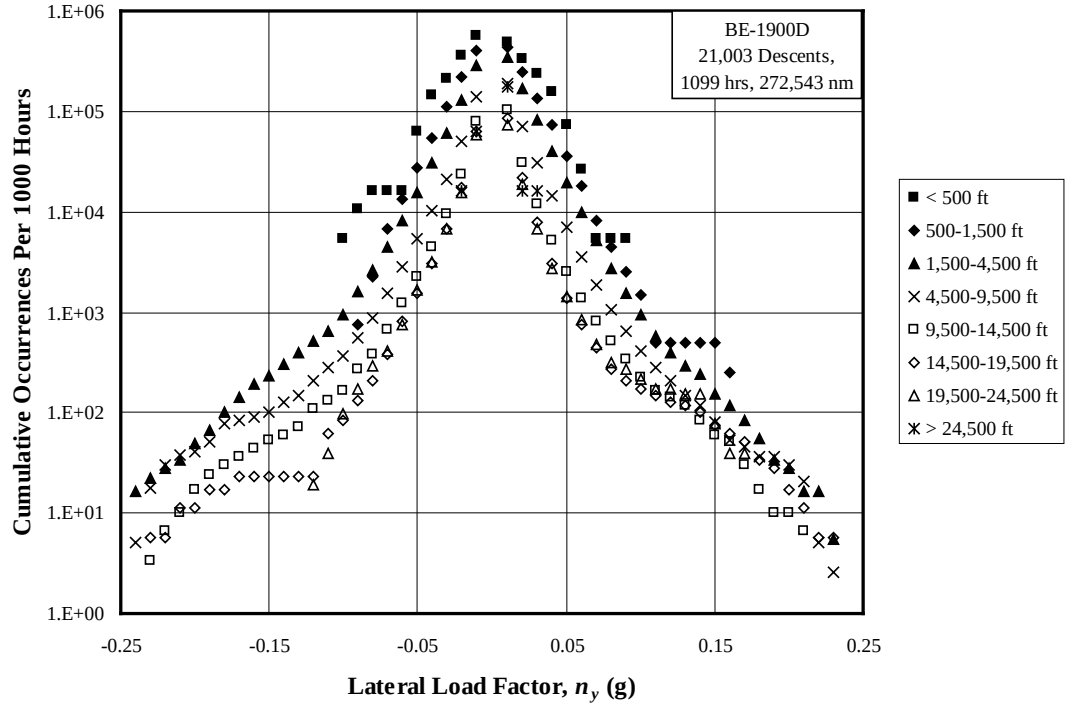

Figure A-97. Cumulative occurrences of lateral load factor per 1000 hours for descent phase

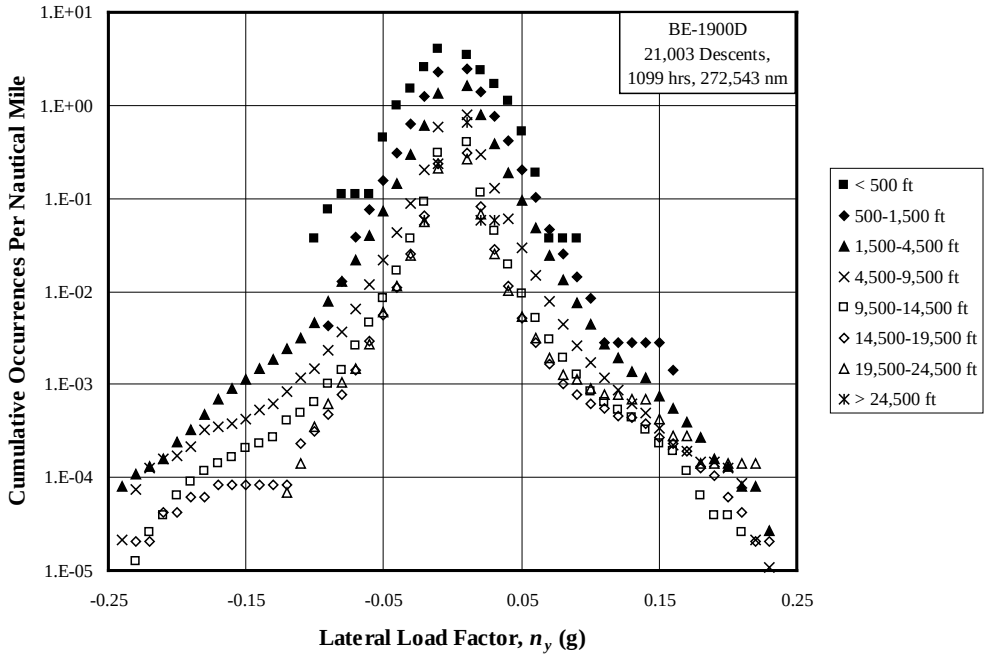

Figure A-98. Cumulative occurrences of lateral load factor per nmi for descent phase

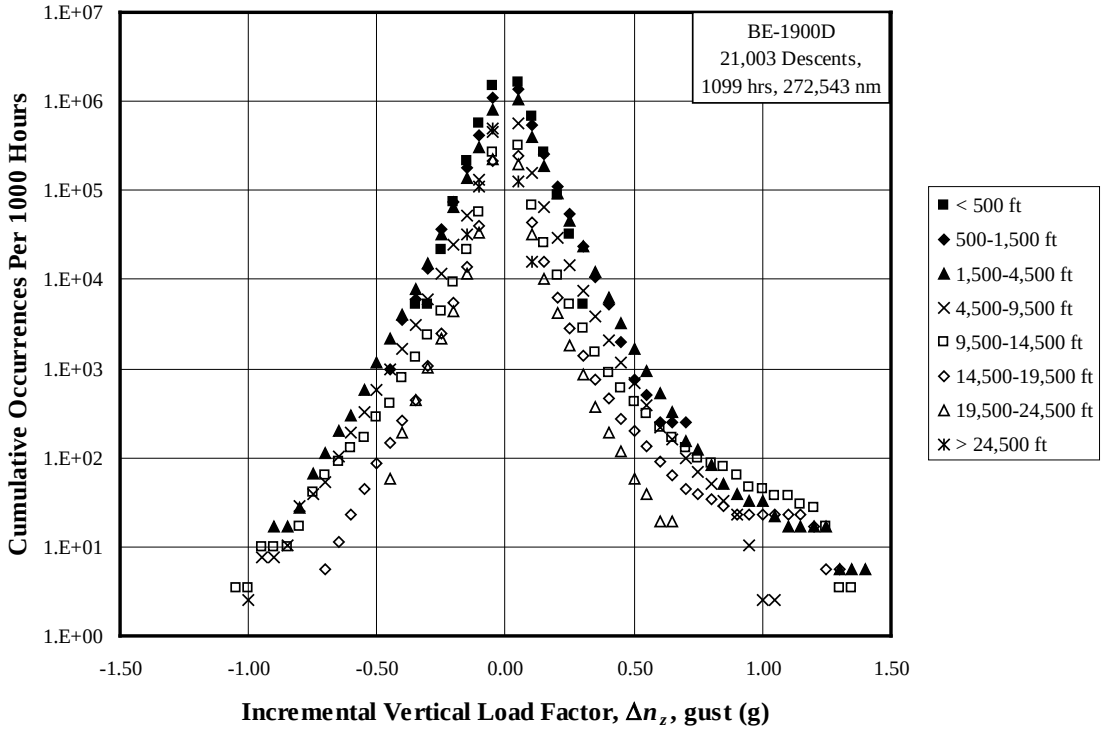

Figure A-99. Cumulative occurrences of incremental gust vertical load factor per 1000 hours for descent phase

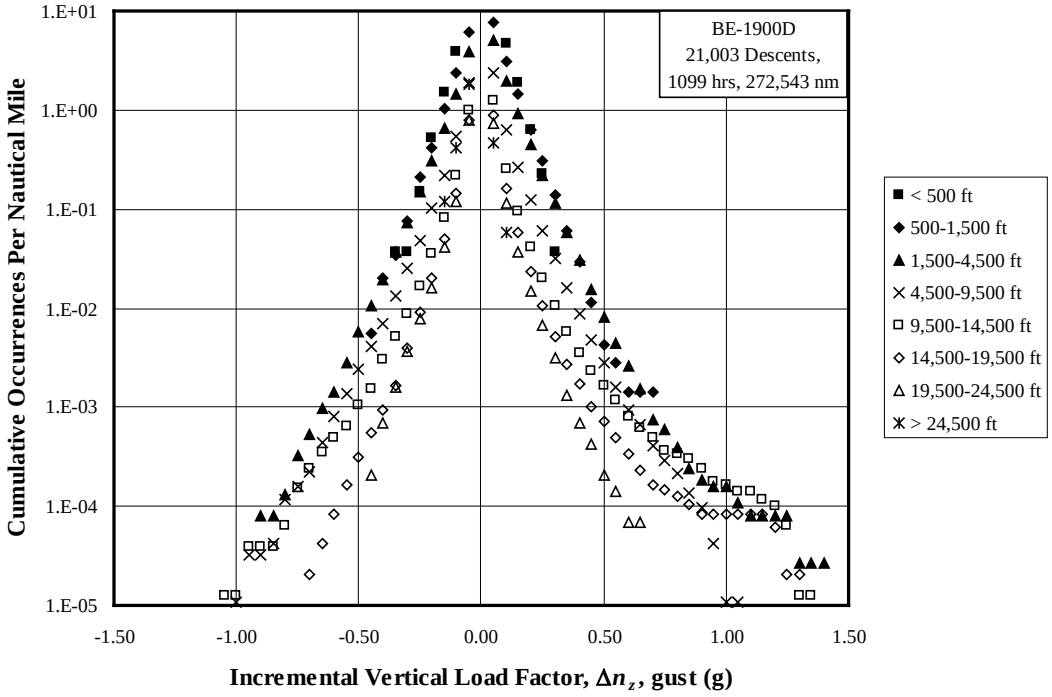

Figure A-100. Cumulative occurrences of incremental gust vertical load factor per nmi for descent phase

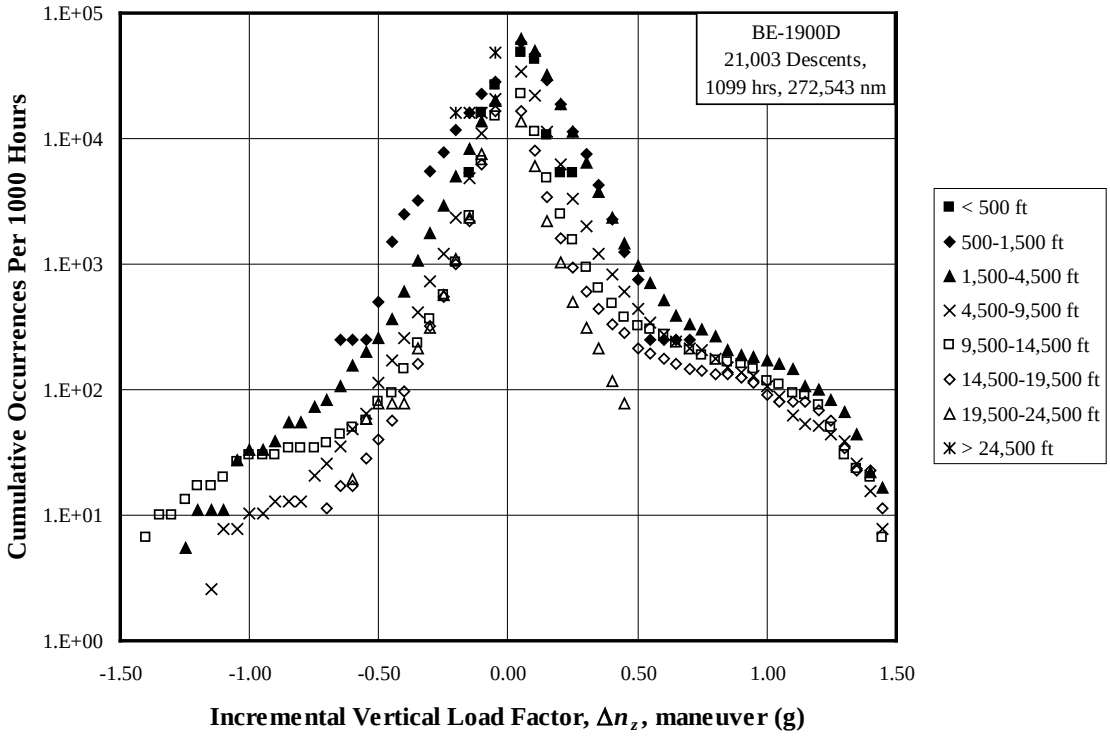

Figure A-101. Cumulative occurrences of incremental maneuver vertical load factor per 1000 hours for descent phase

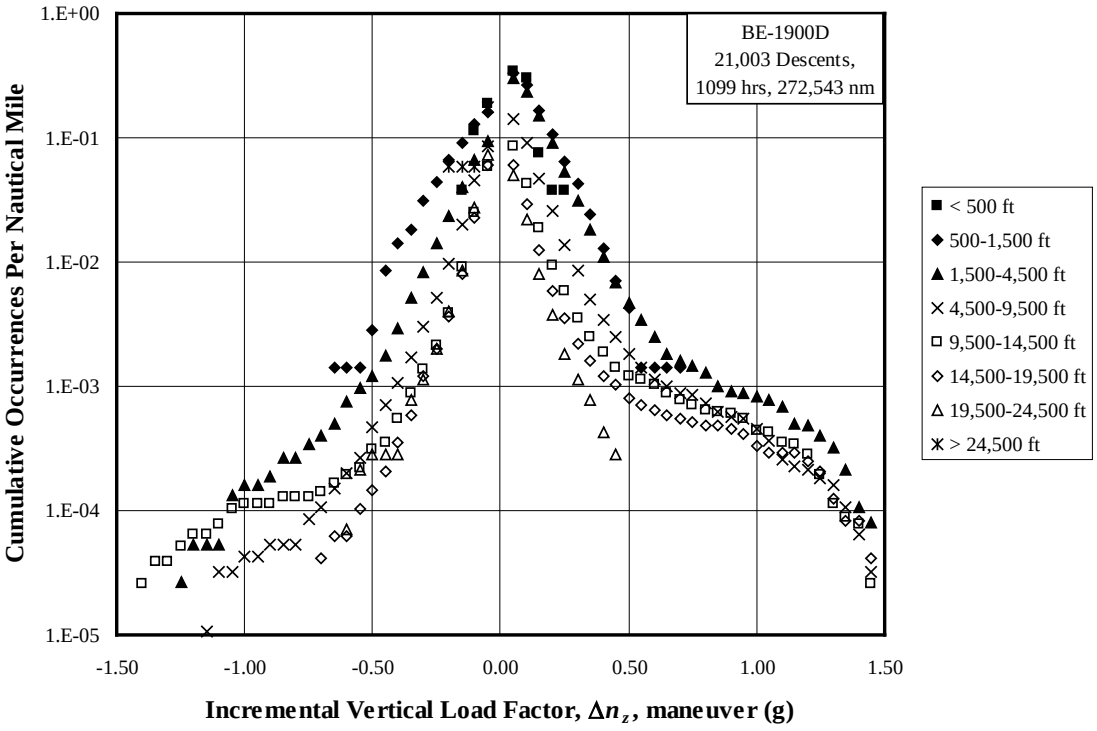

Figure A-102. Cumulative occurrences of incremental maneuver vertical load factor per nmi for descent phase

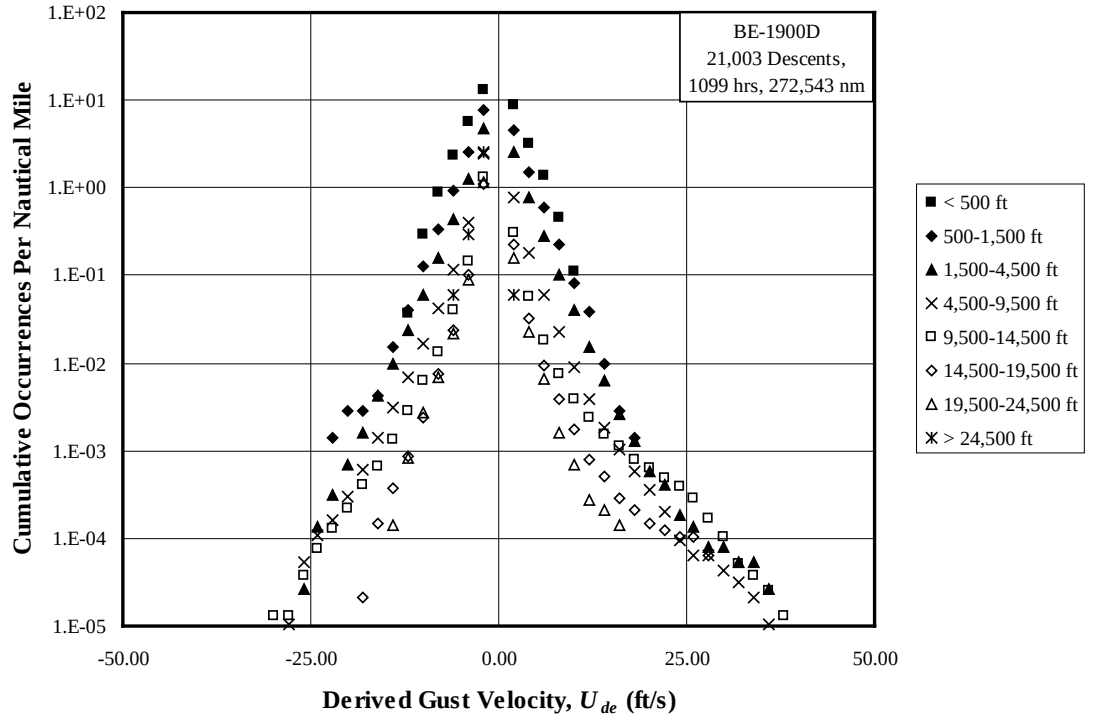

Figure A-103. Cumulative occurrences of derived gust velocity per nmi for descent phase

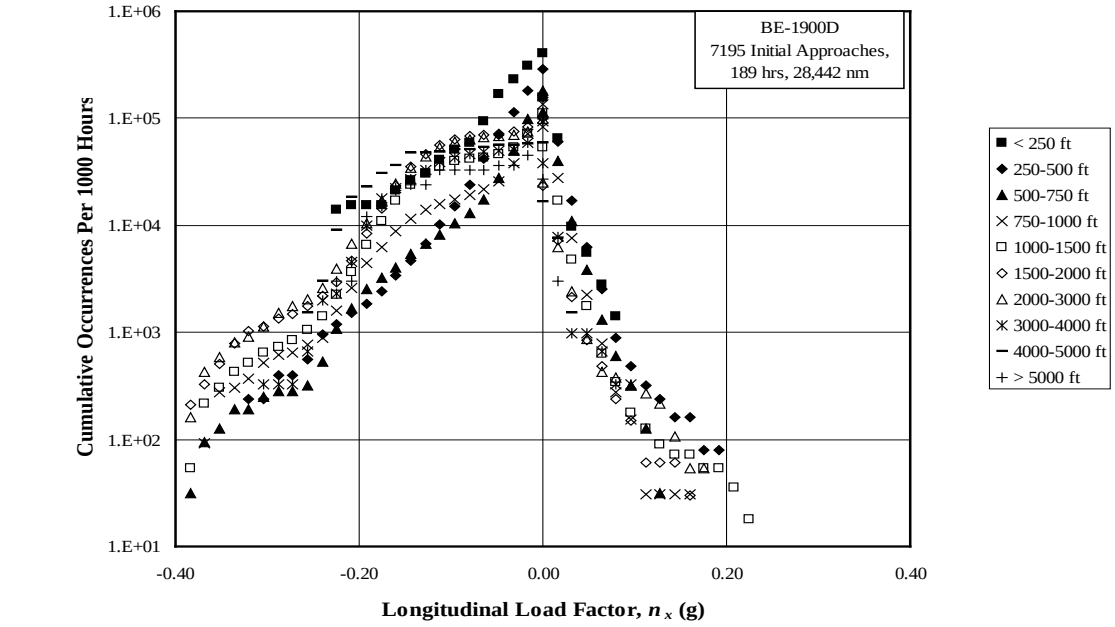

Figure A-104. Cumulative occurrences of longitudinal load factor per 1000 hours for initial approach phase

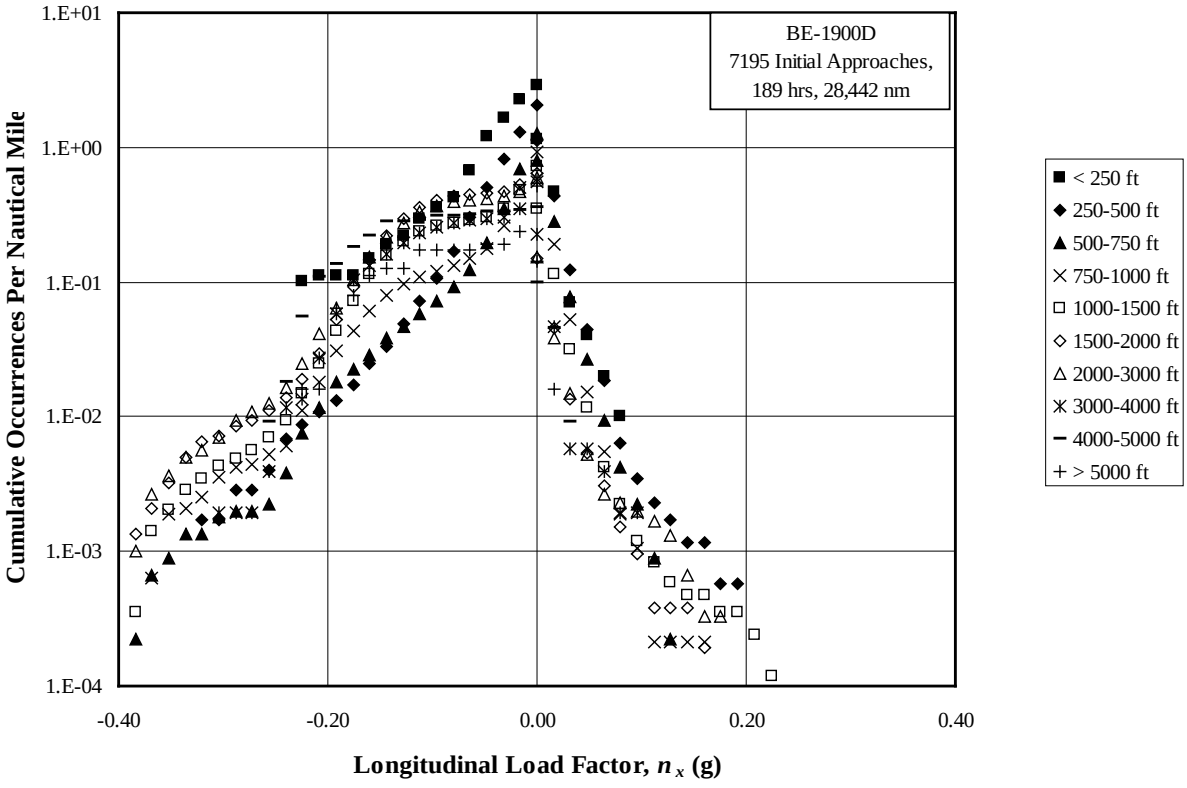

Figure A-105. Cumulative occurrences of longitudinal load factor per nmi for initial approach phase

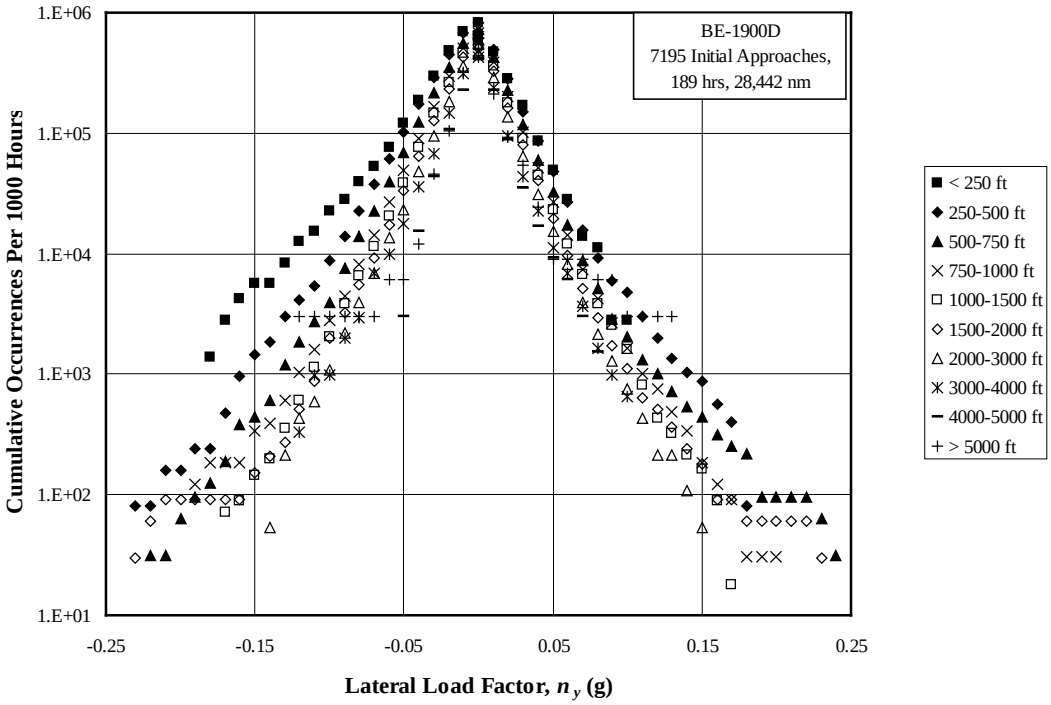

Figure A-106. Cumulative occurrences of lateral load factor per 1000 hours for initial approach phase

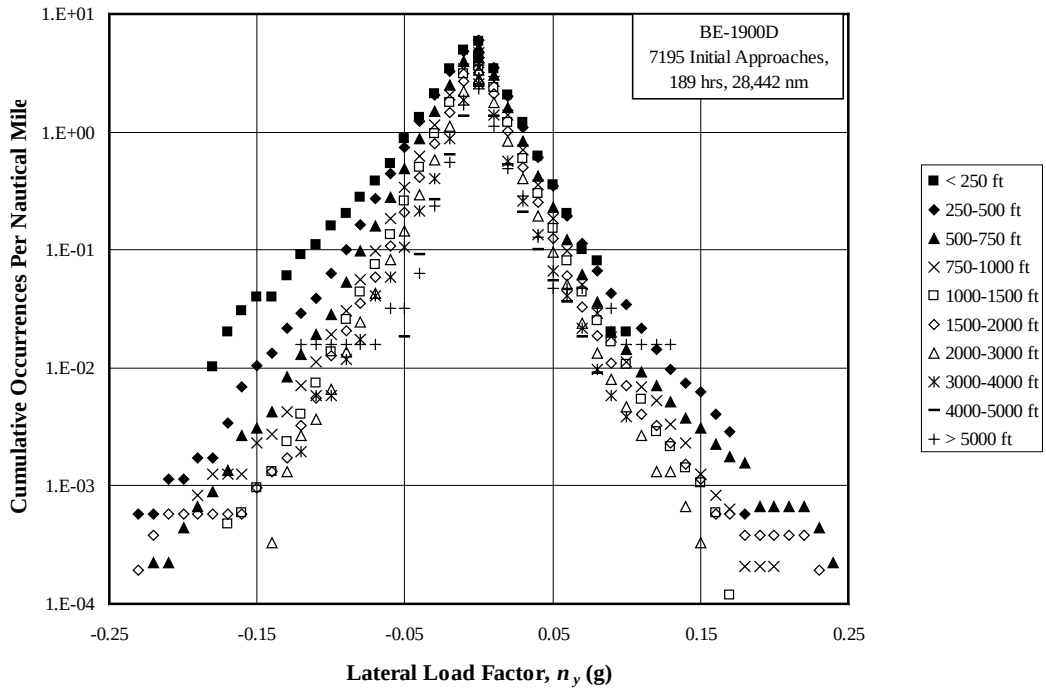

Figure A-107. Cumulative occurrences of lateral load factor per nmi for initial approach phase

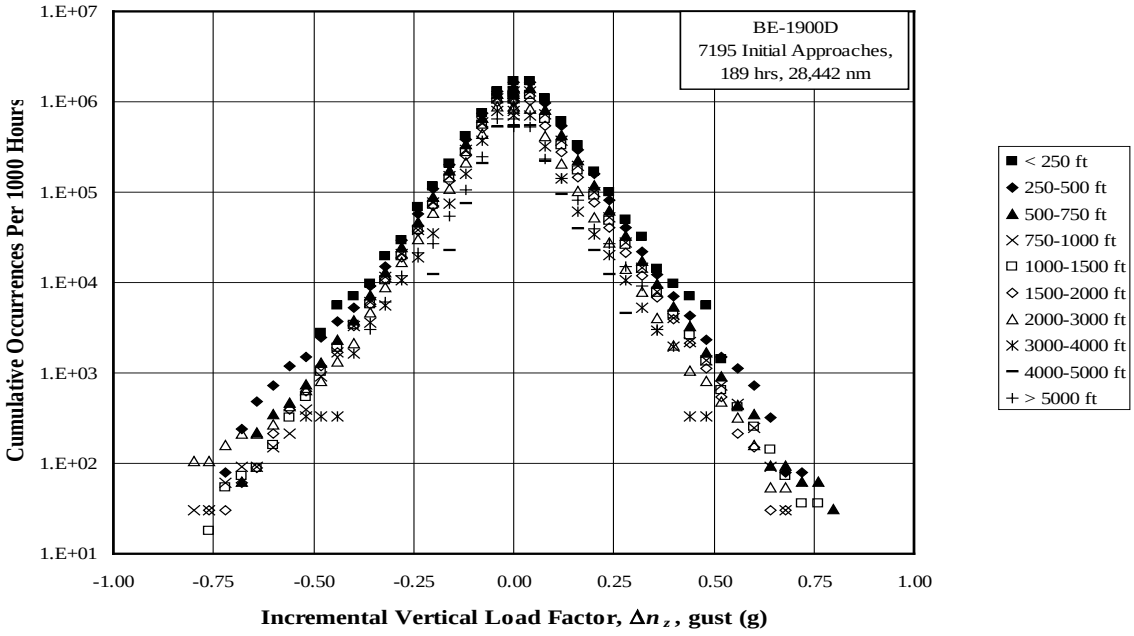

Figure A-108. Cumulative occurrences of incremental gust vertical load factor per 1000 hours for initial approach phase

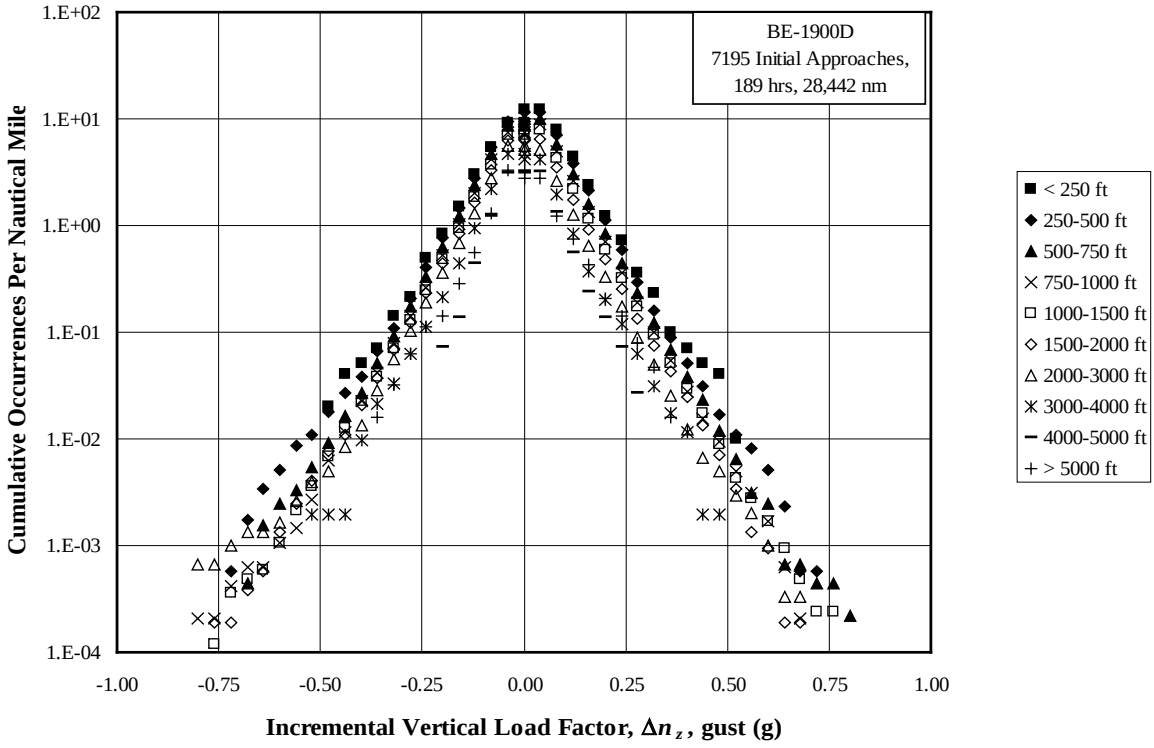

Figure A-109. Cumulative occurrences of incremental gust vertical load factor per nmi for initial approach phase

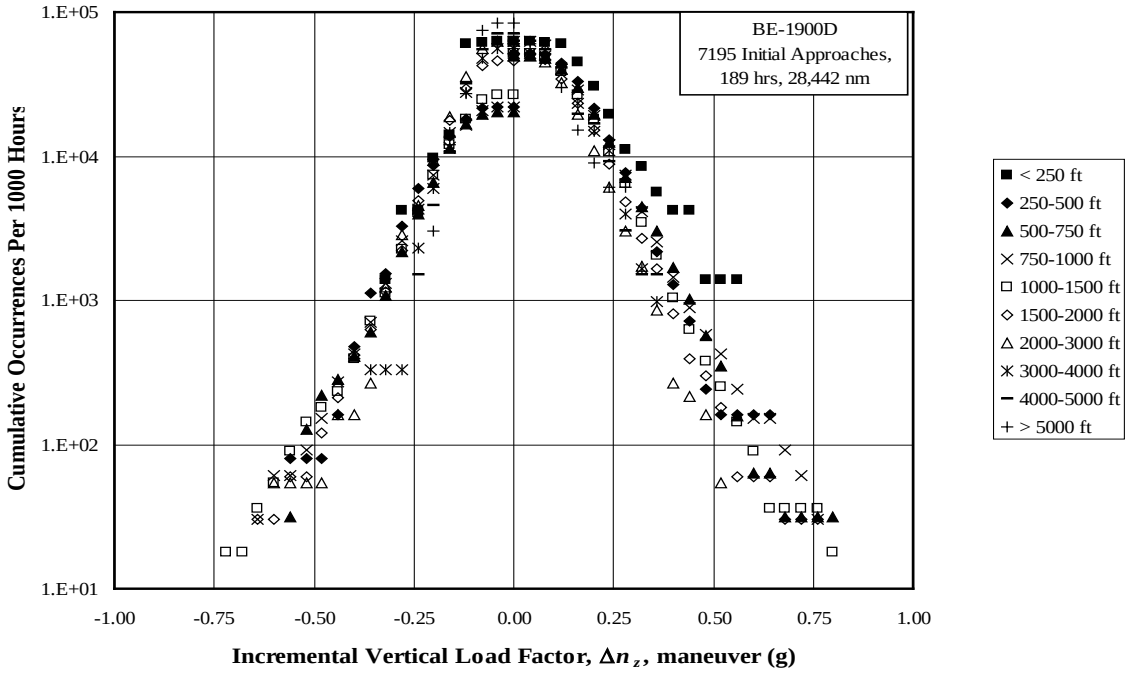

Figure A-110. Cumulative occurrences of incremental maneuver vertical load factor per 1000 hours for initial approach phase

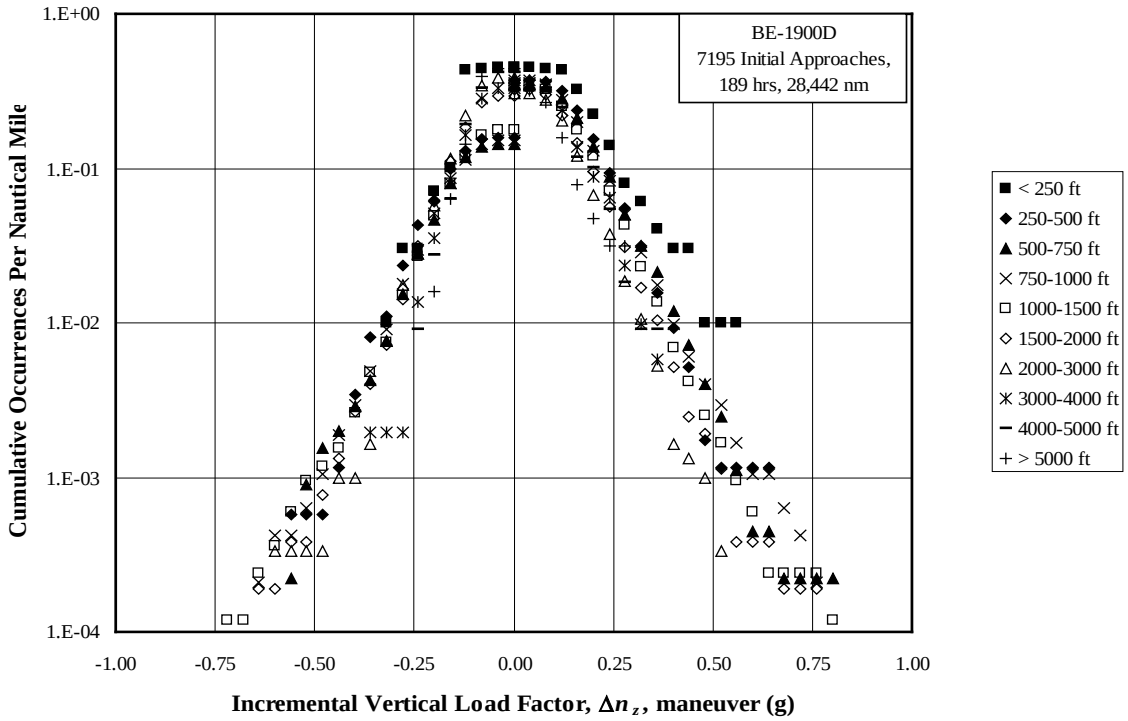

Figure A-111. Cumulative occurrences of incremental maneuver vertical load factor per nmi for initial approach phase

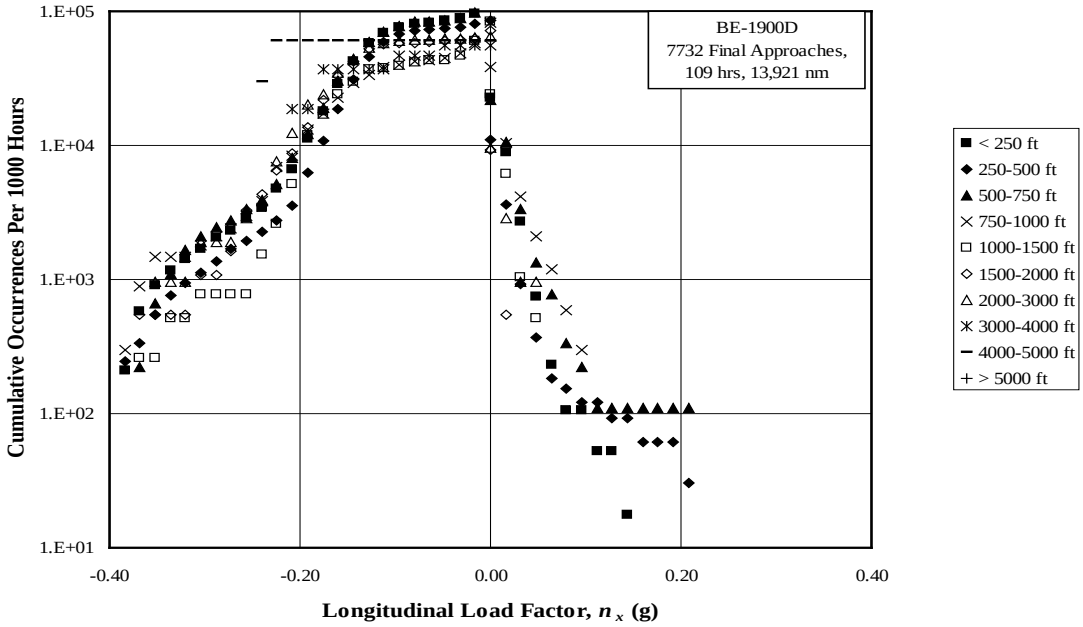

Figure A-112. Cumulative occurrences of longitudinal load factor per 1000 hours for final approach phase

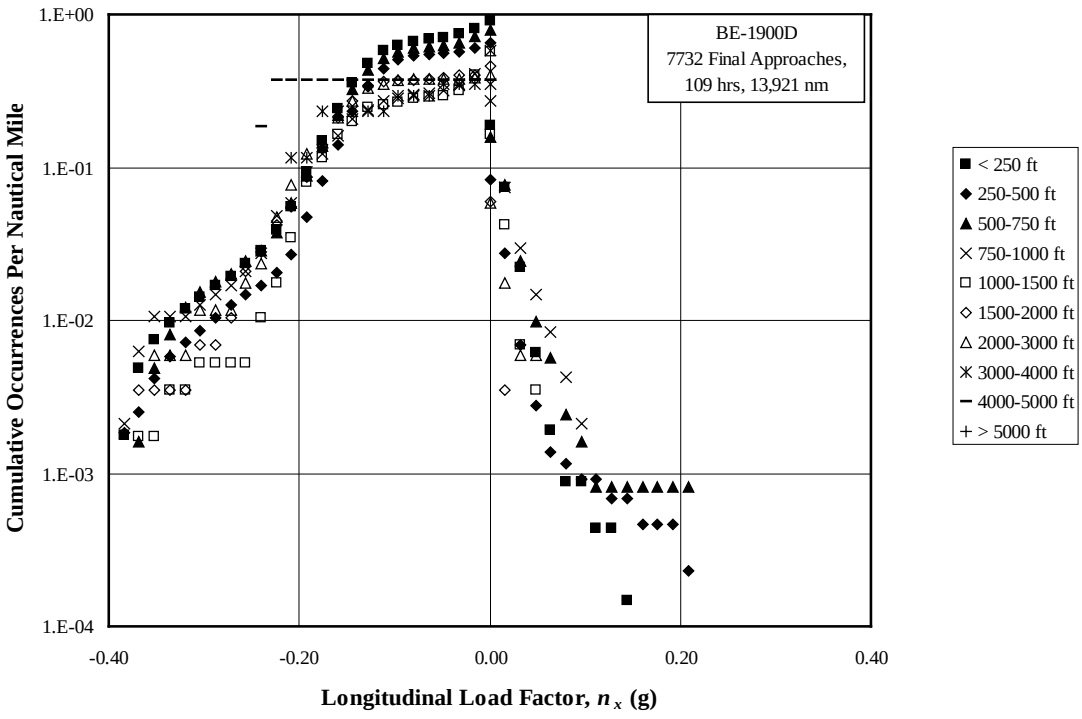

Figure A-113. Cumulative occurrences of longitudinal load factor per nmi for final approach phase

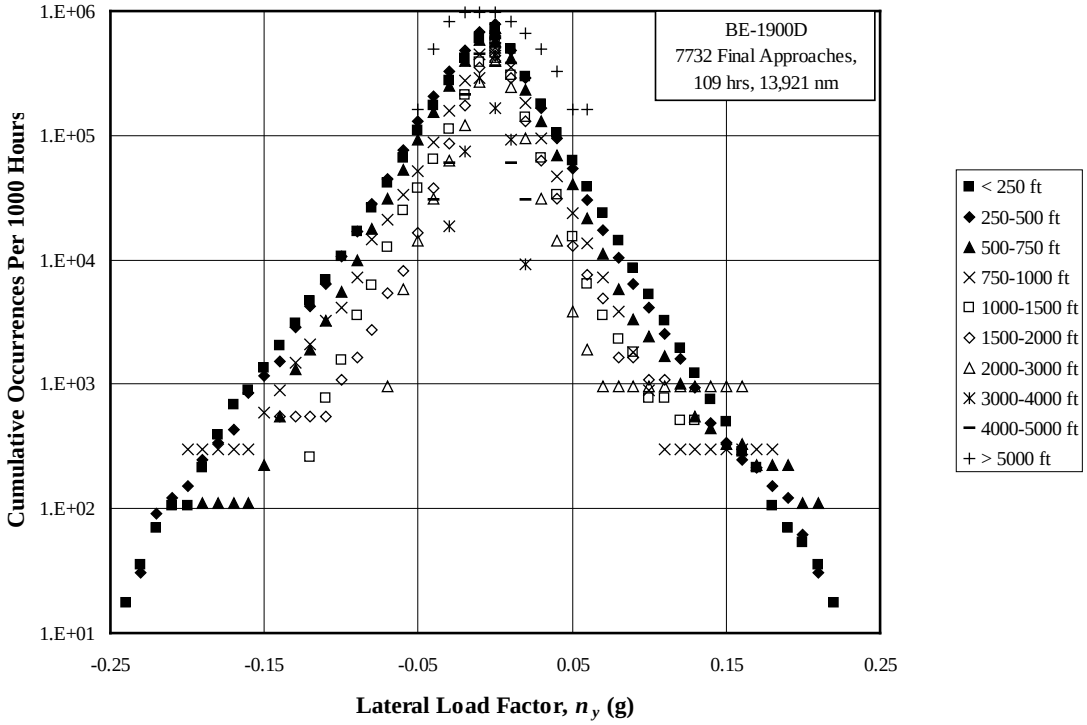

Figure A-114. Cumulative occurrences of lateral load factor per 1000 hours for final approach phase

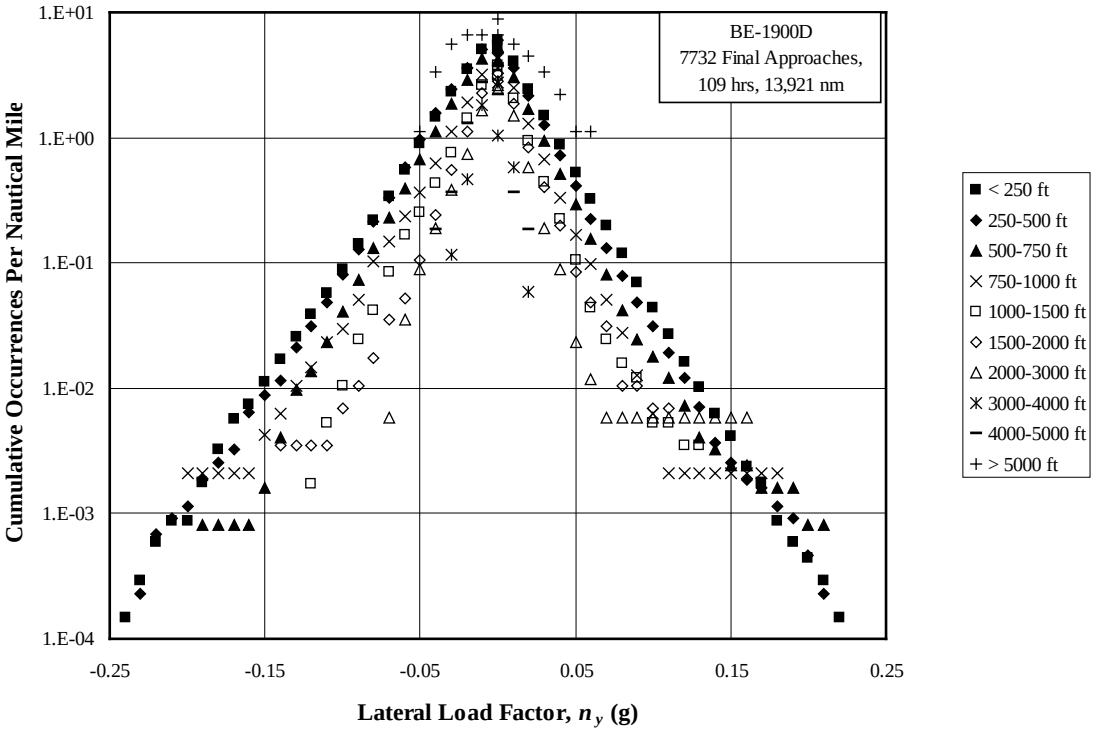

Figure A-115. Cumulative occurrences of lateral load factor per nmi for final approach phase

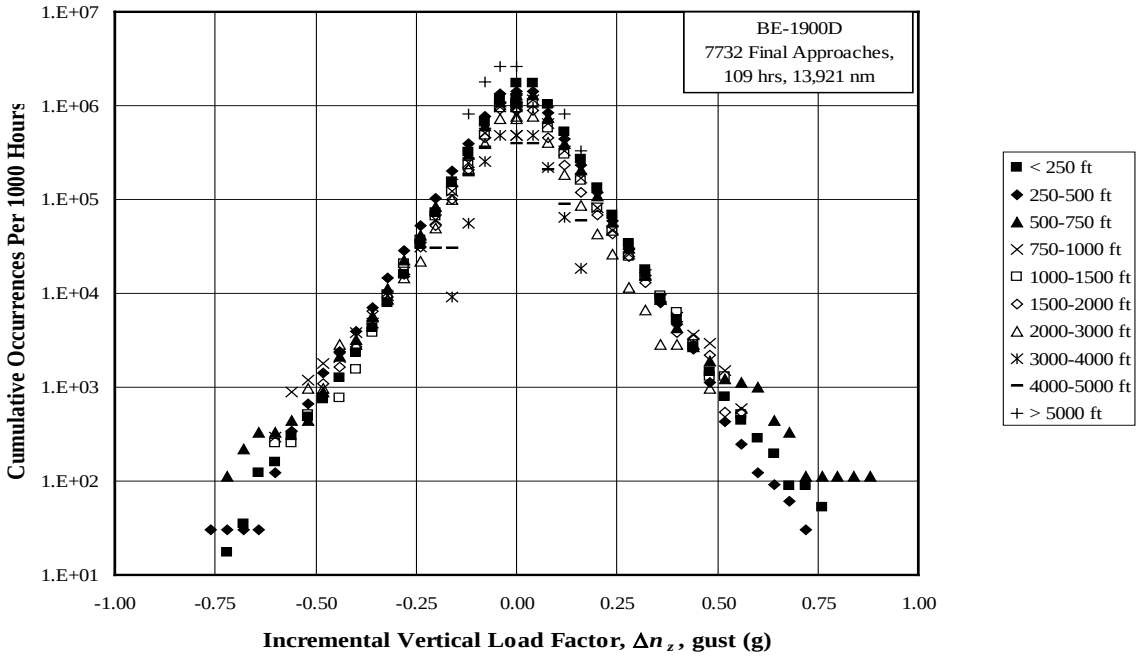

Figure A-116. Cumulative occurrences of incremental gust vertical load factor per 1000 hours for final approach phase

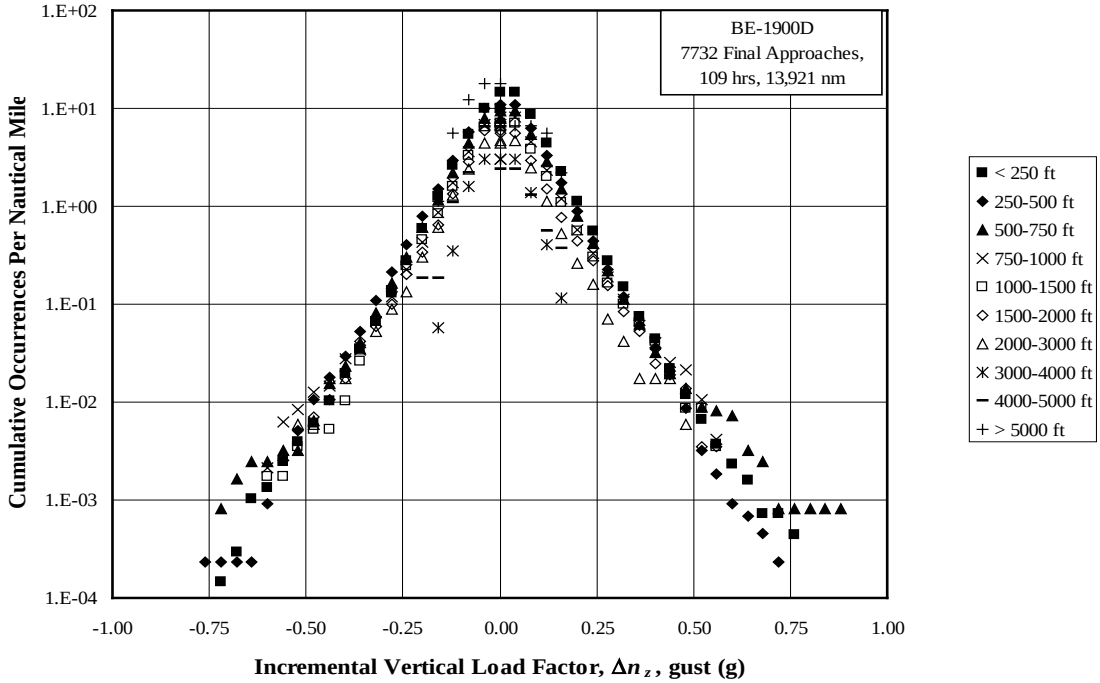

Figure A-117. Cumulative occurrences of incremental gust vertical load factor per nmi for final approach phase

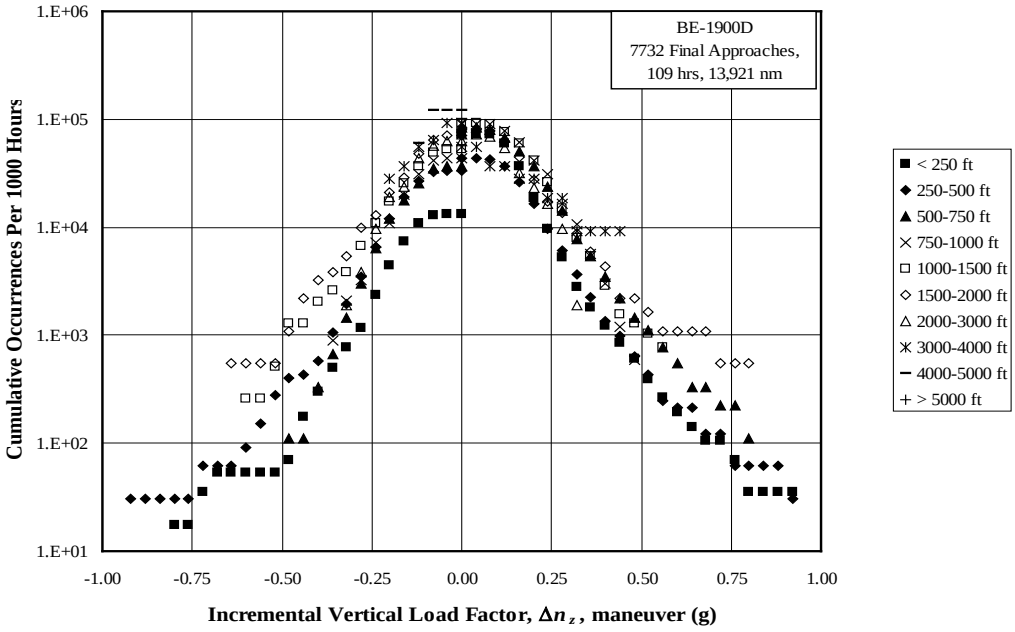

Figure A-118. Cumulative occurrences of incremental maneuver vertical load factor per 1000 hours for final approach phase

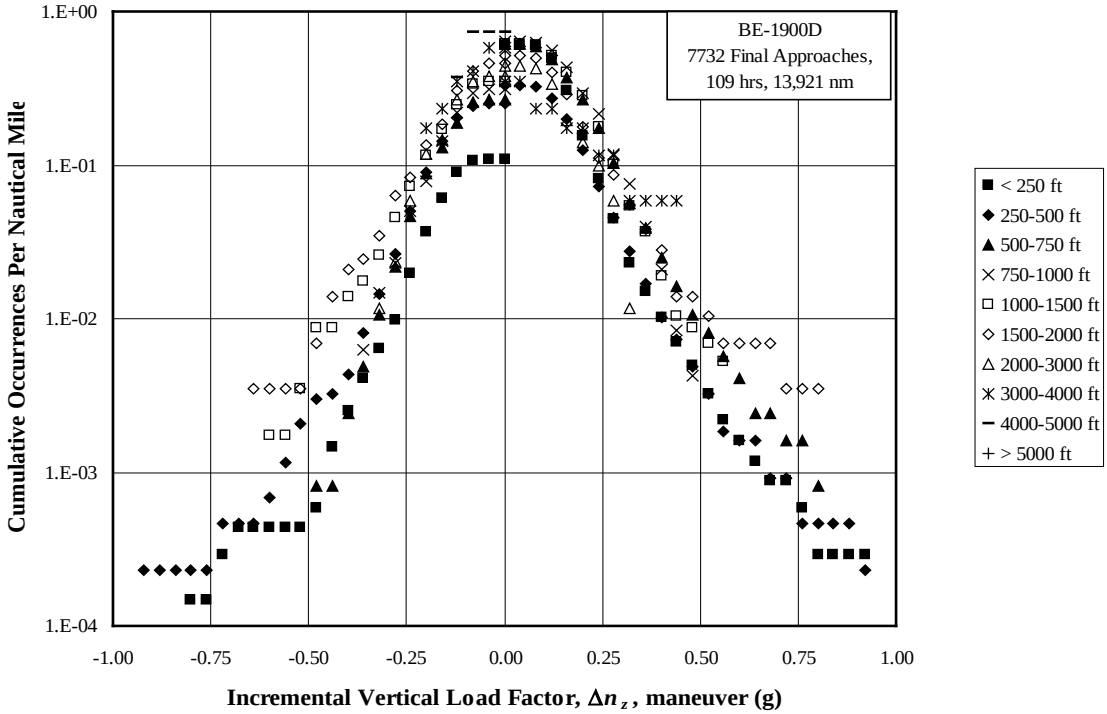

Figure A-119. Cumulative occurrences of incremental maneuver vertical load factor per nmi for final approach phase

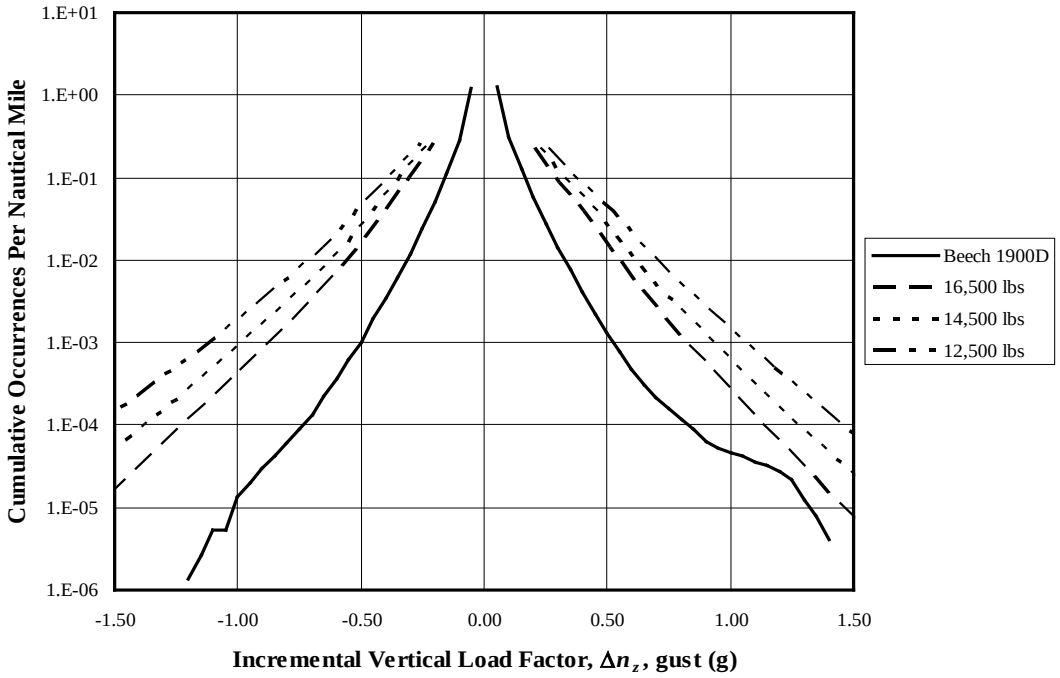

Figure A-120. Comparison of cumulative occurrences of incremental vertical gust load factor per nmi, BE-1900D vs. AC23-13A for cruise

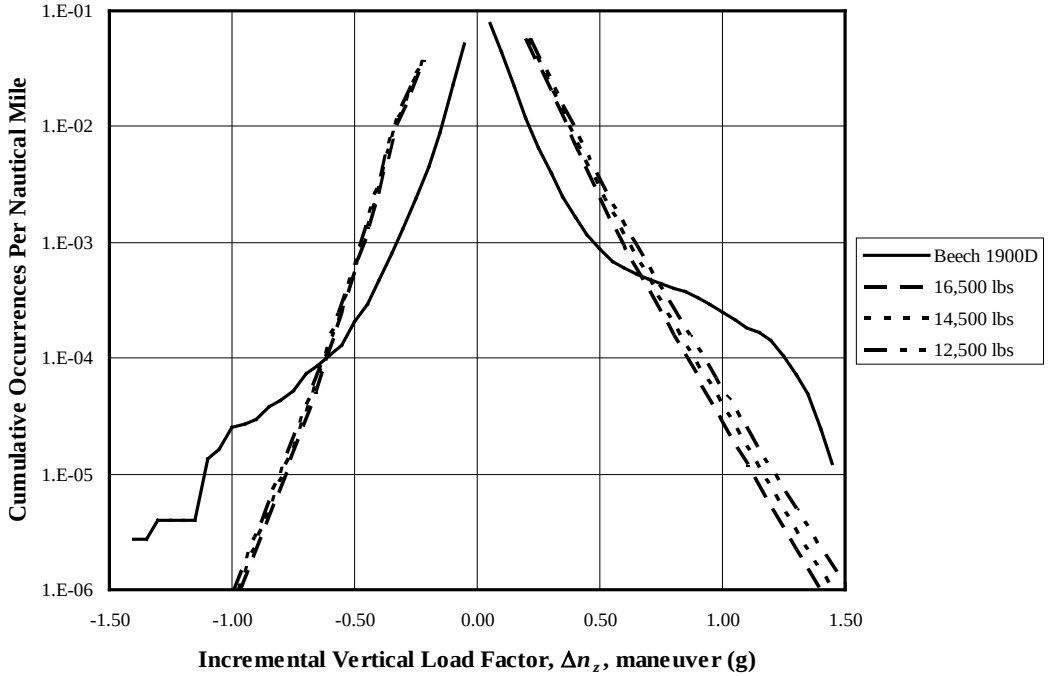

Figure A-121. Comparison of cumulative occurrences of incremental vertical maneuver load factor per nmi, BE-1900D vs. AC23-13A for cruise

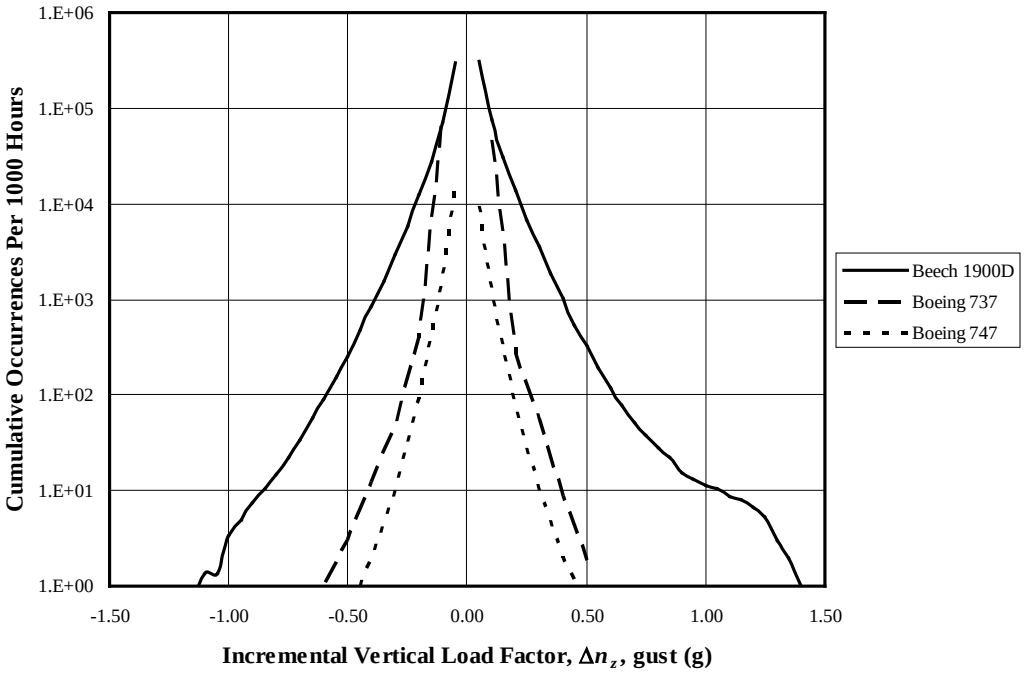

Figure A-122. Comparison of cumulative occurrences of incremental vertical gust load factor per 1000 hours, BE-1900D vs. B-737-400 and B-747-400 for cruise

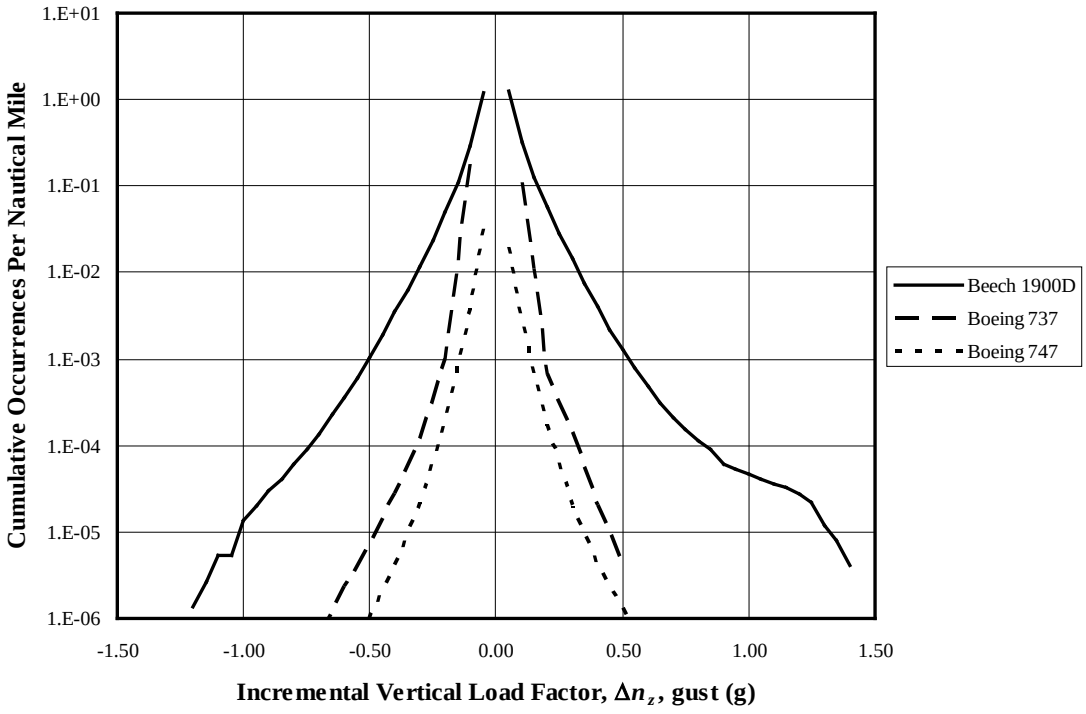

Figure A-123. Comparison of cumulative occurrences of incremental vertical gust load factor per nmi, BE-1900D vs. B-737-400 and B-747-400 for cruise

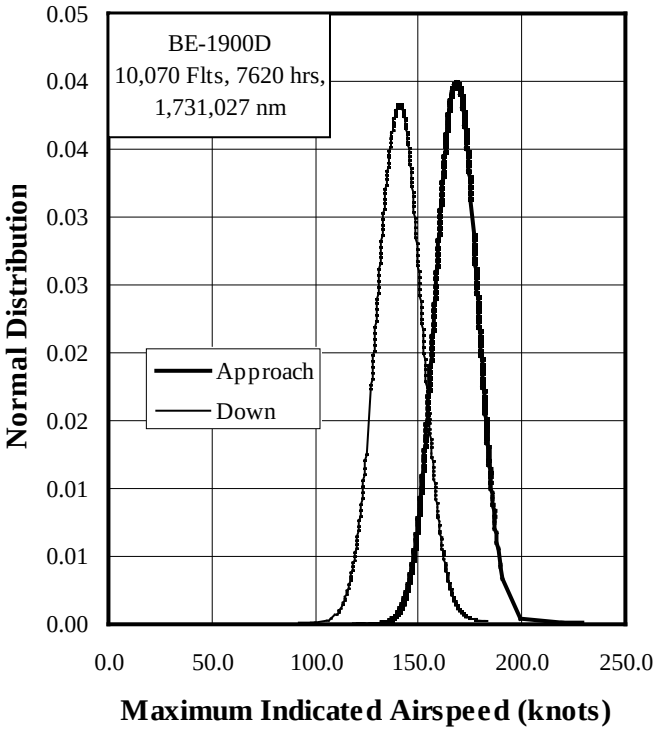

Figure A-124. Probability of maximum indicated airspeed at flap deployment

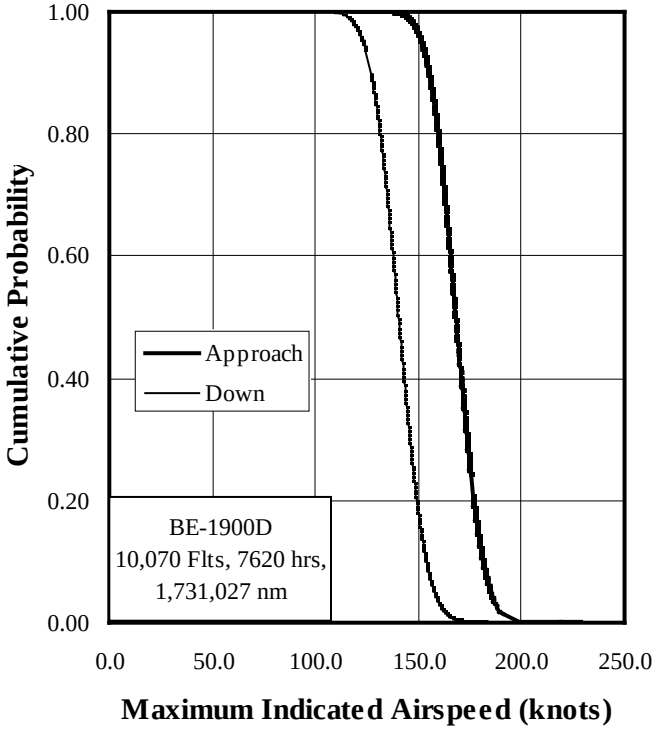

Figure A-125. Cumulative probability of maximum indicated airspeed at flap deployment

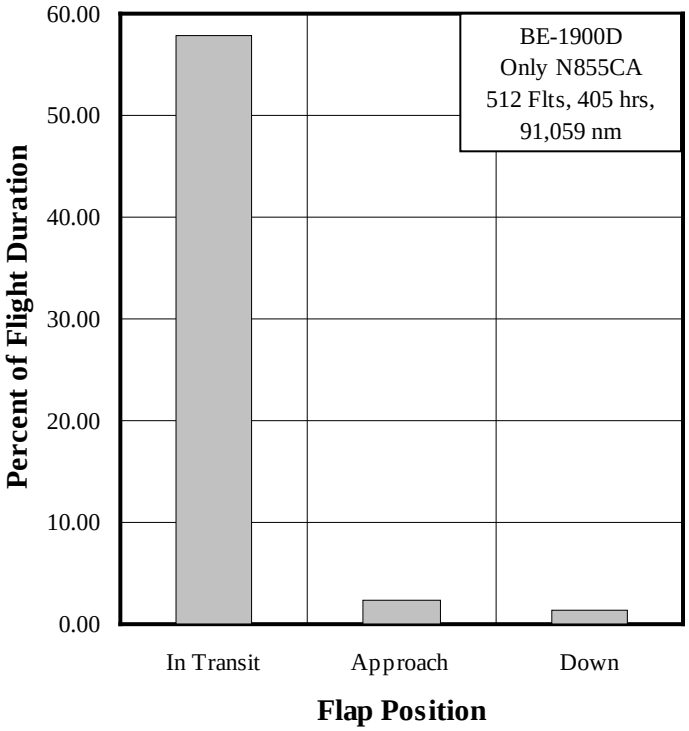

Figure A-126. Percentage of flights with flaps deployed for N855CA

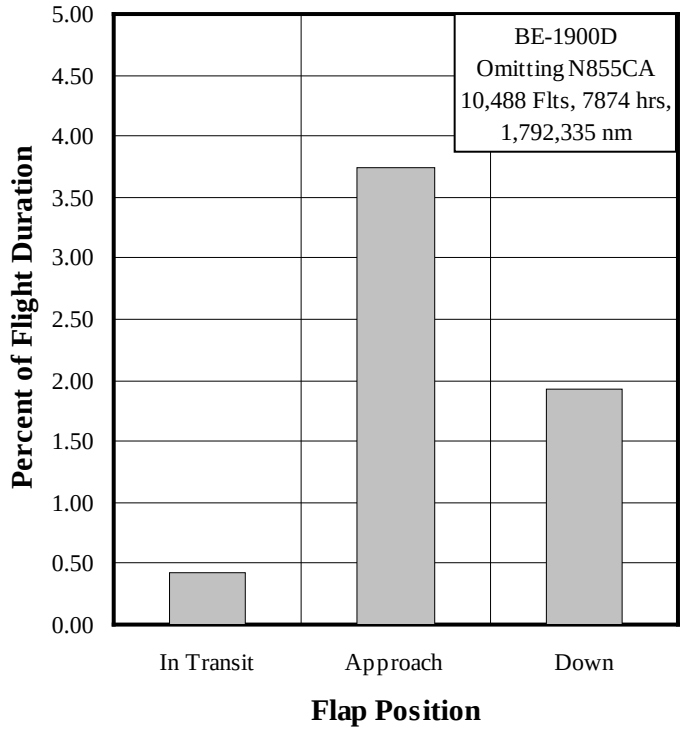

Figure A-127. Percentage of flights with flaps deployed, excluding N855CA